# Chemistry of Some Amphoteric Cations ($Sn^{2+}$; $Pb^{2+}$; $Cr^{3+}$) in Hyper-Alkaline Aqueous Solutions

PhD Theses

**Éva Gabriella Bajnóczi**

Supervisors:
Dr. Pál Sipos
Dr. Gábor Peintler

Doctoral School of Chemistry

Material and Solution Structure Research Group
Department of Inorganic and Analytical Chemistry
Faculty of Science and Informatics
University of Szeged

Szeged

2015

# Contents

# 1 Introduction

The hydrolysis of metal ions is one of the most widely studied field of inorganic solution chemistry, including the structure, the composition and the thermodynamics of the hydroxo complexes formed. Their formation constants, as well as the solubility products of solid hydroxides are summarized in different kinds of databases and textbooks. These studies were usually carried out within the *p*H-range of 2–13. The speciation and the structure of the hydroxo complexes formed in strongly alkaline aqueous solutions are usually unknown because of well-known theoretical and practical/technical difficulties. In concentrated solutions, the ion associations and the effect of the activity coefficients are often inseparable. Technical problems include the effect of impurities, which are readily accumulated because of the high concentrations; therefore the use of high purity chemicals is inevitable. Another problem is that these highly alkaline solutions are quite hygroscopic and aggressive, and during the storage and measurement, they tend to corrode/destroy the equipment and instruments.

In spite of these hurdles, the number of publications dealing with this particular aspect of solution chemistry steadily increases. For obvious reasons, metal ions with reasonable solubility, *e.g.* amphoteric ones, are most intensely studied, including aluminum(III), gallium(III), chromium(III), lead(II) and thallium(I). Besides these, data for metal ions, which are hardly soluble under alkaline conditions have also emerged, *e.g.* copper(II), iron(III) and the actinides.

During my doctoral studies we have decided to study the hydrolysis of tin(II), lead(II) and chromium(III) in highly alkaline aqueous solutions, because relevant data are scarce in the open literature.

Organotin compounds—although they are considered highly toxic—have been investigated extensively, since they are used in synthetic organic chemistry and several industrial fields. The equally important—especially from geochemical and hydrological perspective—inorganic tin species are less well studied, nevertheless, tin is an abundant element in the crust of the Earth, and it has the most isotopes over the whole periodic table. One of its isotopes is $^{126}$Sn, which is a radionuclide produced by nuclear fission, and it is present in radioactive waist, with a half life of $\sim 10^5$ years. Although the environment is protected by several barriers from the contamination, the flowing groundwater, of which *p*H can reach even up to 13.5, is able to transport the soluble species. Lead(II) was also investigated, because it has a similar $d^{10}s^2$

valence electron structure; therefore there are many analogies between the behavior of tin(II) and lead(II).

Chromium compounds are widely used for various industrial purposes like leather tanning, producing several alloys, avoiding corrosion, etc. As a consequence, significant amount of chromium polluted waste is produced. Chromium can exist in several oxidation states, but only chromium(III) and chromium(VI) are proven to be stable, generally. In low concentration, chromium(III) is an important trace element for humans, however, in higher amounts, it can cause kidney and liver failure, dermatitis, etc. The toxicity of chromium(VI) is much higher, it definitely causes teratogenic and mutagenic developments. These facts explain that the chromium removal from contaminated soils and liquids is an important task. One of the frequently used methods to decrease the chromium concentration is to reduce chromium(VI) to chromium(III) and to precipitate it as $Cr(OH)_3$ in slightly alkaline media, since this compound has a very low solubility. Despite the popularity of this procedure, the speciation and kinetic behavior of chromium(III) under alkaline conditions are not adequately described in the literature.

The hydroxide concentrations higher than the environmentally interesting range were also investigated, since these way-out conditions might lead to the formation of new, so far undiscovered hydroxo complexes, or precipitation of solids with peculiar local- and nanostructure.

# 2 Literature review

## 2.1 Tin(II) and lead(II)

### 2.1.1 Tin(II)

The first investigation of tin(II) hydrolysis was performed by Prytz.[1] In this work, solutions of different tin(II) salts were titrated with NaOH, and the concentrations of the hydrogen ion and free tin(II) ion were monitored by hydrogen electrode and tin amalgam electrode, respectively. As a result, the following equilibria were put forward:

$$2Sn^{2+} + H_2O \rightleftharpoons Sn_2O^{2+} + 2H^+ \tag{2.1}$$

$$2Sn^{2+} + 2H_2O \rightleftharpoons Sn_2O_2H_2{}^{2+} + 2H^+ \tag{2.2}$$

Two years later, in 1930, Randall et al.[2] studied the hydrolysis of tin(II) in chloride ion containing media, and $Sn(OH)Cl \cdot H_2O$, a white insoluble solid was found to be precipitated from these solutions. Gorman and his co-workers measured the free hydrogen ion concentration with hydrogen electrode during the titration of $Sn(ClO_4)_2$ solutions with sodium hydroxide.[3] The stability constant of the

$$Sn^{2+} + H_2O \rightleftharpoons Sn(OH)^+ + H^+ \tag{2.3}$$

equilibrium reaction extrapolated to zero ionic strength was found to be $K_1^0 = 0.02$. Garrett and Heiks determined the solubility of SnO in hydrochloric acid, and the existence of $Sn^{2+}_{(aq)}$, $Sn(OH)^+$ and $Sn(OH)_{2(aq)}$ was proposed. The stability constant of $Sn(OH)^+$ was found to be $pK = 2.1$.[4] Next year, in 1942, Gorman et al. carried out nearly the same experiments in perchloric acid.[5] They experienced that there was no difference in the solubility (comparing with the values of Garrett et al.) up to 0.017 M tin(II) and 0.04 M acid concentration; therefore there was no chloro-complex formation in diluted solutions. Supposing only the formation of $Sn(OH)^+$, Vanderzee et al.[6] got $K = 0.02$ at 25°C, which is in good agreement with the values reported previously.

The first mentioning of polynuclear tin(II) complexes goes back to 1954, when Sillén proposed the existence of $Sn_2(OH)_2^{2+}$ and $Sn_3(OH)_4^{2+}$ above 0.002 M tin(II) concentrations, based on potentiometric titrations carried out with hydrogen and/or tin amalgam electrodes.

One of the most comprehensive paper about tin(II) hydrolysis is of Tobias.[7] Potentiometric measurements were performed in the *p*H range of 1.4–3 at two tin(II) concentrations (0.0025 and 0.04 M) and at 3 M ionic strength maintained with $Na(ClO_4)$. The following three equilibria were assumed:

$$Sn^{2+} + H_2O \rightleftharpoons Sn(OH)^+ + H^+ \tag{2.4}$$

$$2\,Sn^{2+} + 2\,H_2O \rightleftharpoons Sn_2(OH)_2^{2+} + 2\,H^+ \tag{2.5}$$

$$3\,Sn^{2+} + 4\,H_2O \rightleftharpoons Sn_3(OH)_4^{2+} + 4\,H^+ \tag{2.6}$$

with the lgK values of –3.9, –4.45, –6.77, respectively. The trinuclear complex was found to be the predominant one. In 1964, the data of Tobias were re-evaluated by Chia-chang et al. with least square analysis and they excluded the formation of $Sn(OH)^+$, and $Sn_2(OH)_3^+$ was proposed instead.[8]

One of the first structural investigations was carried out by Davies et al. in 1968.[9] The Mössbauer spectra of several trihydroxostannates(II) were recorded. From our point of view, the most relevant is $NaSn(OH)_3$, with $\delta = 0.60$ mm/s and $\Delta = 2.29$ mm/s relative to $\alpha$-tin. Other alkaline earth trihydroxostannates have isomer shifts and quadrupole splittings similar to this. According to their paper, the isomer shift values were the lowest, while the quadrupole splitting values were the largest, ever observed for tin(II) compounds. It is also mentioned that the chemical shift of trihydroxostannates follows the same trend as those of the trifluorostannates. The effective 5s electron density is reduced in the complexes by both covalent bonding and electrostatic crystal field effects, since the polarization ability of the hydroxide ion is similar to that of the fluoride ion. The $Sn(OH)_3^-$ ion has a pyramidal structure in all the investigated salts.

Solution X-ray scattering was measured in 3 M tin(II) perchlorate solutions at different acidic *p*H values by Johansson and Ohtaki.[10] In strongly acidic solutions, there are 2–3 water molecules around the tin(II) ion in 2.3 Å average distance. In the more hydrolyzed solutions, a polynuclear complex was found, most probably the already proposed $Sn_3(OH)_4^{2+}$, as the average frequency of the Sn–Sn distances was 1.5 at 3.6 Å. This can be considered as a structural confirmation of the equilibria suggested by Sillén and Tobias.

Nearly the only one hydrolysis study at the alkaline end of the *p*H region was performed by Mark in 1977.[11] Alkaline (initial $OH^-$ concentration was varied between 0.1–0.2 M) tin(II) perchlorate solutions were titrated with perchloric acid at constant 3 M ionic strength adjusted with $NaClO_4$. The concentration of the free tin(II) ions was followed by a tin amalgam electrode.

There were attempts to use hydrogen or glass electrode, but these were failed. During the fitting of the observed titration curves, the existence of either $Sn(OH)_4^{2-}$ or $Sn(OH)_2^0$ was excluded in the concentration ranges applied. The formation constant belonging to the

$$Sn^{2+} + 3\,OH^- \rightleftharpoons Sn(OH)_3^- \tag{2.7}$$

reaction was found to be $\lg\beta = 24.58 \pm 0.04$. It is also noted that this value agrees well with that of Smrz obtained from polarographic measurements.[12]

One citation classic in the field of tin(II) hydrolysis is the paper of Pettine et al. from 1981.[13] They used differential pulse anodic stripping voltammetry to determine the formation constant of the hydrolysis products in various ionic media such as $NaNO_3$, NaCl and artificial seawater. The formation of the chloro, bromo, and sulfato complexes were also investigated. In 0.5 M $NaNO_3$ solution, the $\lg\beta$ values were the followings: $\beta_1 = -3.8 \pm 0.2$, $\beta_2 = -9.9 \pm 0.2$ and $\beta_3 = -17.7 \pm 0.2$, while they were $-3.1 \pm 0.2$, $-8.2 \pm 0.2$ and $-17.8 \pm 0.2$ in 0.5 M NaCl solution, respectively. They concluded that there were no mixed complexes at $p\mathrm{H} > 12$, the only species is the $Sn(OH)_3^-$, even in 0.5 M NaCl solution based on the distribution diagram calculated from the stability constants.

The Sn K-edge X-ray absorption spectra of a 3 M $Sn(ClO_4)_2$ solution was recorded and analyzed by Yamaguchi et al.[14] They also re-evaluated the X-ray diffraction measurements made by Johansson and Ohtaki. It was found that there were three to four strongly bonded water molecules around the tin(II) at a distance of 2.25–2.34 Å. The lone electron pair of tin(II) is stereochemically active and the interaction with water molecules is not significant in aqueous solutions.

The crystal structure of $Na_4[Sn_4O(OH)_{10}]$ and $Na_2[Sn_2O(OH)_4]$ was obtained in 1983 by Von Schnering et al.[15] A fundamental building block of these compounds is the $Sn(OH)_3^-$ ion as it is seen in Figure 2.1. Every tin(II) ion is surrounded by three oxygens in a pyramidal geometry with an Sn–O distance of 2.08 Å.

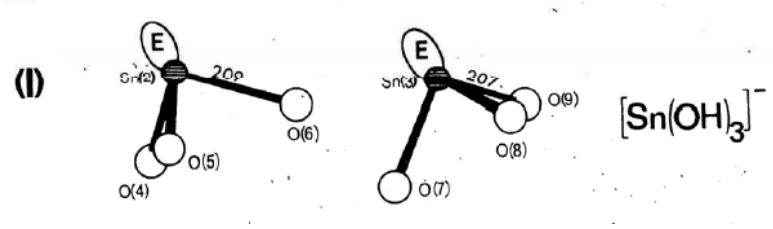


**Figure 2.1.** One of the fundamental building blocks of $Na_4[Sn_4O(OH)_{10}]$ and $Na_2[Sn_2O(OH)_4]$ according to Von Schnering et al. The figure is taken from Ref. 15

At the beginning of the 1990-s, the formation of $Sn_2(OH)_2^{2+}$ and $Sn_3(OH)_4^{2+}$ was experimentally confirmed by potentiometric titrations,[16] while the dimer complex was refused four years later.[17]

An unambiguous structural evidence was given for the existence of $Sn_3(OH)_4^{2+}$ by Donaldson et al. on the basis of single crystal X-ray diffraction, Raman and Mössbauer spectroscopy of $Sn_3(OH)_4(NO_3)_2$.[18] The ion consists of three approximately equidistant tin(II) atoms in a plane with three of the hydroxide groups on one side of the plane and one hydroxide group on the other. The three tin(II) sites are quite similar, thus the $^{119}$Sn Mössbauer spectrum consists of three unresolvable subspectra with $\delta = 3.48$ mm/s relative to $BaSnO_3$ and $\Delta = 1.85$ mm/s.

An extensive review on the thermodynamic data for inorganic tin species appeared in the Geochimica et Cosmochimica Acta in 2001.[19] There is an overall table in which the hydrolysis equilibrium constants and solubility products of tin(II) are summarized, for the details see ref. 19. The Pourbaix diagram of tin clearly shows the redox instability of tin(II) especially in neutral and alkaline media. Halide complexes have to be considered below $p\mathrm{H} = 4$ and at halide ion concentration greater than 0.001 M.

In 2012, Cigala and his co-workers also investigated the hydrolysis of tin using voltammetry.[20] Regarding the stability constants, their results agree well with those of Pettine et al.[13] They draw attention to the preferred formation of different carbonate complexes over the hydroxo and halide complexes.

Another extensive summary of the thermodynamic data of tin is available from 2012 in the Chemical Thermodynamics series.[21]

### 2.1.2 Lead(II)

The solubility of all three lead(II) oxides, red (litharge), yellow (massicot) and black, in alkaline media were investigated by Randall and Spencer[22] and Garrett et al.[23] They both found that the dominant lead-bearing species in the solution were $[Pb(OH)_2]^0$ and $[Pb(OH)_3]^-$ for all crystal forms.

In 1954, Vlcek confirmed this observation by polarographic measurements.[24] Nearly the same speciation was found by Akselrud four years later, except he proposed the existence of a trinuclear anionic complex under alkaline conditions.[25] On the contrary, Johnson et al. found by ultracentrifugation of lead(II)-containing alkaline solution that the dominating complex was mononuclear, and its charge was –2; thus it can be either $[Pb(OH)_4]^{2-}$ or $[PbO_2]^{2-}$.

In the 1960s, Olin and his co-workers studied the hydrolysis of lead(II). Their first publication in this field is about the hydrolysis of lead(II) in perchlorate-containing solutions in the $p$H range of 5–8 at 25℃ and at constant 3 M or 0.3 M ionic strength.[26] The lead(II) concentration was varied between 0.040 and 0.080 M and both glass and lead-amalgam electrodes were used to monitor the $H^+$ and the free lead(II) concentration, respectively. It was found that several polynuclear complexes were formed in the equilibria listed below:

$$Pb^{2+} + H_2O \rightleftharpoons [PbOH]^+ + H^+ \tag{2.8}$$

$$4\,Pb^{2+} + 4\,H_2O \rightleftharpoons [Pb_4(OH)_4]^{4+} + 4\,H^+ \tag{2.9}$$

$$3\,Pb^{2+} + 4\,H_2O \rightleftharpoons [Pb_3(OH)_4]^{2+} + 4\,H^+ \tag{2.10}$$

$$6\,Pb^{2+} + 8\,H_2O \rightleftharpoons [Pb_6(OH)_8]^{4+} + 8\,H^+ \tag{2.11}$$

The $-\lg\beta$ values at 3 M ionic strength were determined to be 7.9, 19.25, 22.87, 42.14 for the 1:1, 4:4, 3:4 and 6:8 complexes, respectively. They obtained almost identical values at lower ionic strength. These findings are more or less in agreement with those of Pedersen[27] ($[PbOH]^+$, $[Pb_2(OH)]^{3+}$ and $[Pb_4(OH)_4]^{4+}$) and Faucherre[28] ($[PbOH]^+$ and $[Pb_4(OH)_4]^{4+}$). Note that the potentiometric measurements of Pedersen were performed in $Pb(NO_3)_2$ solutions, while Faucherre worked in $Pb(ClO_4)_2$.

Measurements were carried out at one order of magnitude higher lead(II) concentrations (1.490, 0.990 and 0.500 M) and at $OH^-$/Pb(II) ratio equals to 0.15[29] to account for the unexplained deviations obtained at the beginning of the hydrolysis. Under these conditions $[Pb_4(OH)_4]^{4+}$ and $[Pb_2(OH)]^{3+}$ complexes were found with $-\lg\beta = 6.45$ for the latter one.

Still in the same year Carell and Olin performed some measurements up to 0.5 M hydroxide concentration with the use of the following cell

$$\text{Pb (in Hg)} \mid B\,\text{M } Pb(ClO_4)_2,\ A\,\text{M NaOH},\ (I\text{-}A)\,\text{M } Na(ClO_4) \mid \text{ref.}$$

where $B$ is the total concentration of Pb(II) and $A$ is the total concentration of $OH^-$, $I = 3$ M.[30] According to their measurements only simple mononuclear complexes are formed, namely $[Pb(OH)_2]^0$ and $[Pb(OH)_3]^-$ with $\log\beta$ values of 10.90 and 13.66, respectively. Despite of the varying experimental conditions, these values agree quite well with those of Heyrovsky,[31] Lingane[32] and Goward,[33] all three based on polarographic measurements. They also excluded the existence of $[Pb(OH)_4]^{2-}$.

Electromotive force measurements at 1.45 M lead(II) concentration and 4.35 M ionic strength adjusted with $Mg(ClO_4)_2$ or $Ba(ClO_4)_2$ were also taken by Pajdovsky and Olin.[34] These experiments led to the same conclusion as the potentiometry at high lead(II) concentrations, i.e. $[Pb_4(OH)_4]^{4+}$ and $[Pb_2(OH)]^{3+}$ were found to be present in the solutions.

The formation enthalpy and entropy of the 4:4, 3:4 and 6:8 complexes were also determined by calorimetric titrations.[35]

Olin and Johansson performed the first solution X-ray diffraction measurements[36] on these topic. Lead(II) perchlorate solutions with lead(II) concentration of 1.5 M were investigated at different $OH^-$/Pb(II) ratios. If this ratio was $\sim$1, the tetrahedral arrangement of the lead(II) ions was found, suggesting the existence of the $[Pb_4(OH)_4]^{4+}$ complex. At higher ratio ($\sim$1.33),

they got a quite similar diffractogram, to that obtained by Spiro (according to ref. 36 it is based on private communication) for $Pb_6O(OH)_6(ClO_4)_4$. It can be considered as an evidence for the $[Pb_6(OH)_8]^{4+}$ complex.

In 1973, the existence of the $[Pb(OH)_4]^{2-}$ complex was proposed again with $-\log\beta = 38.32$ by Pokric, based on light scattering measurements.[37] The results obtained until 1976 are summarized in the book of Baes and Mesmer.[38]

A detailed potentiometric investigation was carried out by Sylva and his co-workers in 1980 at low ($1{\cdot}10^{-4}$–$2{\cdot}10^{-3}$ M) lead(II) concentrations. The ionic strength was adjusted to 0.1 M with $KNO_3$.[39] They tried to fit several models to simulate the titration curves, the best one included the $[PbOH]^+$, $[Pb_3(OH)_4]^{2+}$, $[Pb_3(OH)_5]^+$, $[Pb_4(OH)_4]^{4+}$ and $[Pb_6(OH)_8]^{4+}$ complexes with $-\log\beta$ values of 7.86, 23.90, 31.75, 20.40 and 43.38, respectively. This is the first mention of the $[Pb_3(OH)_5]^+$ species. The formation constants for the other complexes are in good agreement with the ones determined by Olin.

Cruywagen et al. used the same model as Sylva to evaluate their potentiometric measurements, and basically got the same $\lg\beta$ values at 1 M ($NaClO_4$) ionic strength.[40] The results were exactly the same in 1 M $KNO_3$, which excluded the nitrato complex formation. Although, the accessible concentration range is restricted for the nitrate, since the solubility of $Pb(NO_3)_2$ is limited.

A standalone result was published by Ferri et al. in 1989.[41] They performed potentiometric titrations up to 4.2 M free hydroxide concentration using a lead-amalgam electrode. The existence of the $[Pb(OH)q^{(2-q)}]$ species was proposed where $q \leq 6$ but $q \neq 5$.

At elevated temperatures, 100℃, the number of the hydrolyzed species is lower, only the $[PbOH]^+$ and $[Pb_4(OH)_4]^{4+}$ complexes are present.[42]

The most recent study is the paper of Perera et al.[43] A combined UV-vis spectrophotometric and potentiometric titration was performed at very low (10 $\mu$M) lead(II) concentration up to 5 M hydroxide. Only mononuclear complexes were found: $[PbOH]^+$, $[Pb(OH)_2]^0$, $[Pb(OH)_3]^-$ and $[Pb(OH)_4]^{2-}$ with $-\log\beta$ values of 7.2, 16.1, 26.5 and 38.0, respectively (see Figure 2.2).

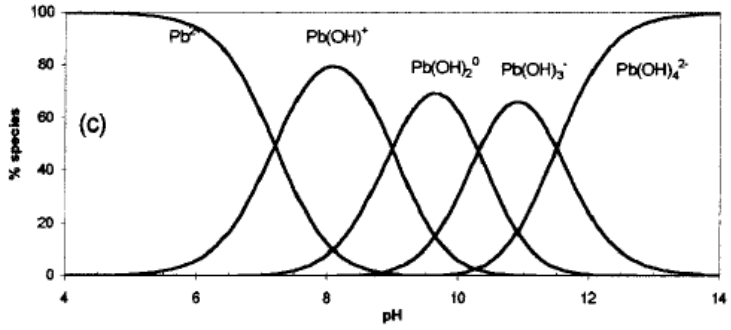


**Figure 2.2.** Lead(II) speciation at I = 1 M and 25℃ as a function of $p$H, according to Perera et al. The figure is taken from Ref. 43

They also tried to give some structural evidence for these complexes with the help of $^{207}$Pb NMR and Raman spectroscopies. At the highest hydroxide concentrations the existence of $[PbO_2]^{2-}$ was suggested from the Raman spectrum of an alkaline solution containing lead(II).

## 2.2 Chromium(III)

### 2.2.1 Behavior in alkaline medium

In 1924, von Fricke et al. investigated the solubility of $Cr_2O_3$ in 0–17.5 M sodium hydroxide solutions. It was suggested by potentiometric measurements that $[Cr(OH)_4]^-$ was formed above 10 M sodium hydroxide.[44] The observations were exactly the same in potassium hydroxide. This and some other studies carried out in acidic or slightly alkaline media are summarized in the work of Baes and Mesmer.[38] In alkaline aqueous solutions they assume only mononuclear hydroxo complexes, the last member being the $[Cr(OH)_4]^-$. Bradley et al. found that this complex was formed only above $[OH^-]$:[Cr(III)] = 4:1 ratio, and the complex had octahedral geometry.[45] At higher ratios, the $[CrO_4Cr_{12}(OH)_{24}(H_2O)_{12}]^{7+}$ polyoxocation was also proposed based on gel permeation chromatography measurements. Only monomer complexes (with varying deprotonation degree) were found in the 3.5–14.5 *p*H-range by Rai et al.[46] The equilibration was monitored over a period of 130 days. On the contrary, fast dimerization and tetramerization of $[Cr(OH)_4]^-$ were also reported.[47] It must be mentioned, however, that the oligomerization is observed to be completed within 100 seconds, while all the other references claim that this process requires days if not weeks. The existence of polynuclear species is still uncertain. For example Beverskog et al. reported revised Pourbaix diagrams of chromium, and the dominant species in alkaline medium was considered as an unknown.[48] During the calculations, only $[Cr(OH)_4]^-$ was assumed; however, it is mentioned that sometimes it can be misleading as the polynuclear species might exist.

Only two further studies were found in the literature at *p*H>14, the earlier one is the work of Torapava et al.[49] In this paper, the hydrolysis of chromium(III) was investigated in strong alkaline media (up to 10 M) with UV-vis spectroscopy and Extended X-ray Absorption Spectroscopy (EXAFS). They proposed the existence of an oligomeric species $[Cr(\mu{-}OH)_2(OH)_2]_n^{n-}$ with a Cr−O mean distance of 2.00 Å and a Cr−Cr distance of 2.98 Å in 10 M NaOH. The structure of this complex was suggested applying analogies with the slightly acidic systems.[50]

A more recent publication in this field is the paper of Zydorczak et al.[51] The solubility of $Cr_2O_3$ was investigated in concentrated sodium hydroxide solution with the molality of 6 mol/kg. An unexpected observation was found and carefully confirmed. The solution phase contained only chromium(VI) as $CrO_4^{2-}$ along the whole investigation time, and there was no chromium(III) detectable. The UV-vis spectra of a $CrCl_3$ solution containing 6 mol/kg sodium

hydroxide were also investigated as a function of time. The spectrum of the freshly prepared solution belongs to $[Cr(OH)_4]^-$ only and it had two absorption maxima at 426 nm and 594 nm. A new absorption peak appeared at 374 nm after a few days, belonging to chromate. As the experiments were carried out in cautiously deoxygenated solutions and with the exclusion of light, it is probable that chromium(III) was oxidized to chromium(VI) directly by the water (or by the hydroxide ion) in a highly alkaline media like this.

This result is quite surprising since this redox reaction was not mentioned earlier at all. Careful reinvestigation of the literature, however, explored a few signs to support this observation. Von Fricke and Windhausen have already observed that the color of alkaline chromium(III) solutions turned to yellow on heating, and it can be related to the formation of chromate.[44] Alkaline chromium solutions were aged by Baloga et al. and their observations can completely be explained by the reaction of chromium(III) and water[52] (see Figure 2.3).

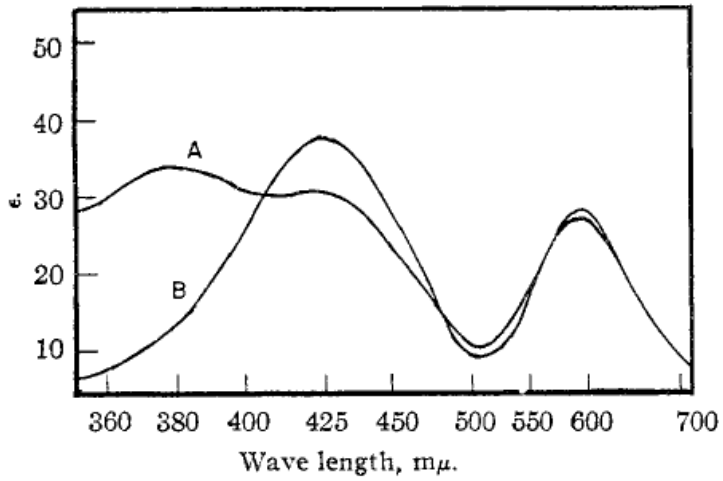


**Figure 2.3.** The spectral change of an alkaline chromium(III) solution. Spectrum $A$ was measured after an aging period of 4 days, while spectrum $B$ was measured after 5 minutes after mixing. The spectra are taken from Ref. 52

Zhao et al. also mentioned that the UV-vis spectra of the alkaline chromium(III) solutions were not stable in time, and if the solutions were acidified with perchloric acid, the color turned into greenish, instead of the expected blueish $[Cr(H_2O)_6]^{3+}$.[47] The oxidation of chromium(III) to chromium(VI) has already been used in a cycle producing hydrogen and oxygen in alkaline media, although under very different conditions.[53] The reaction with $H_2O_2$ also supports the stability of chromium(VI) in alkaline solutions, since $H_2O_2$ oxidizes chromium(III) at high $p$H, while it reduces chromium(VI) to chromium(III) at low $p$H.[52,54]

### 2.2.2 Behavior in acidic medium

The first hydrolysis study of chromium(III) dates back to 1907, when Niels Bjerrum published his results on this issue.[55] The hydrolysis of both the green and the blue chromic chloride was investigated. While the first one is the chloro-complex of the chromium, the latter is the hexa-aqua form. According to conductivity and hydrogen electrode potentiometric measurements, the equilibrium constant was found to be $0.89 \cdot 10^{-4}$ at 25 °C for the following reaction

$$[Cr(H_2O)_6]^{3+} \rightleftharpoons [Cr(H_2O)_5OH]^{2+} + H^+ \tag{2.12}$$

Lamb and his co-workers studied the same equilibrium using five different experimental methods, and they obtained the average value of $K = 1.58 \cdot 10^{-4}$ with 5 % deviation.[56] They reject the idea of any dimer formation.

The paper of Schaal and Faucherre gives a detailed description of their experiments carried out in $Cr(NO_3)_3$ solutions. A given fraction of the total chromium(III) (0.25, 0.5 and 0.75) was 'neutralized' by added hydroxide at 0.1 and 0.01 M total chromium(III) concentration. Some precipitate appeared when the hydroxide stock solution was added, but it was dissolved within a few hours. The *p*H of the solutions with different total chromium(III) concentrations but with identical $c_{Cr(III)}/c_{OH^-}$ ratio was nearly the same at the beginning. After that the one's with higher chromium(III) concentration decreased faster, the maximum difference between the *p*H-s of the solutions was 0.6, at approximately 50 hours after the mixing. The solutions reached their final *p*H after four or ten days, depending on their initial chromium(III) concentration. An original graph from this paper can be seen in Figure 2.2.2, in which the main observations are summarized.

It is also mentioned that this aging time also depends on the concentration of the $KNO_3$, used to maintain constant the ionic strength. Regarding the change of the *p*H as a function of the dilution of the solutions, they concluded that there was a dimer complex in these solutions, and its formation was quite slow.

A decade later Charreton performed basically the same experiment in $Cr(ClO_4)_3$ solution, but the *p*H was measured nearly immediately after (within 30 s) the addition of the alkaline solution to eliminate the effect of the previously proposed dimer formation.[58] The $[CrOH]^{2+}$ complex was found to be formed instantly with a K value of $10^{-4.4}$.

The first combined spectrophotometric and *p*H measurements also supported the existence of the $[Cr(OH)_2]^+$ complex in 1959.[59] The decrease of the *p*H with time (–0.09 *p*H units after four hours) was also observed by them. The deprotonation constants obtained were $0.8 \cdot 10^{-4}$ and $1.09 \cdot 10^{-}6$ for $[CrOH]^{2+}$ and $[Cr(OH)_2]^+$, respectively.

The degree of polymerization was also investigated by spectrophotometry by Morrow et al.[60] The shift of the first peak in the visible spectra of $Cr(ClO_4)_3$ solution at around 408 nm

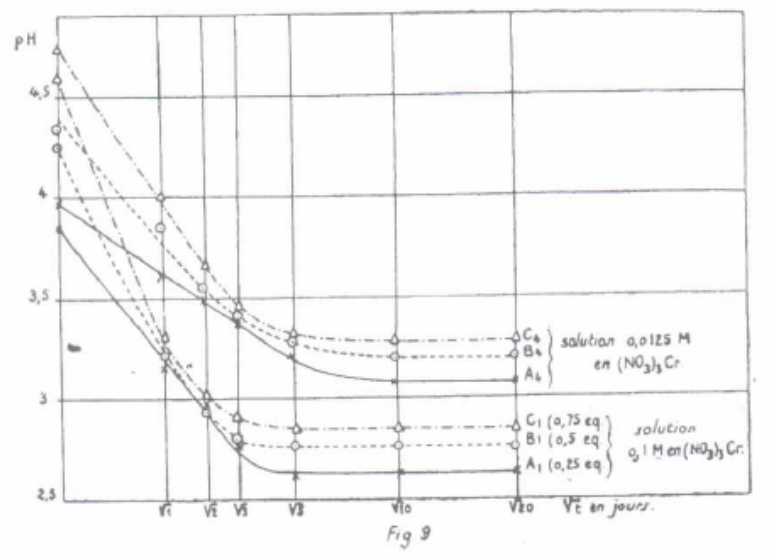


**Figure 2.4.** The observations of Schaal and Faucherre on the $p$H change of $Cr(NO_3)_3$ solutions as a function of time. The graph is taken from Ref. 57

was followed as a function of $T_{OH^-}/T_{Cr(III)}$ ratio, where $T$ stands for the total concentrations. The spectra were taken when the equilibrium was considered to be reached (no more than $\pm 0.01$ $p$H unit change within two weeks). The assumption of dimer as the largest species was sufficient to describe their observations.

The hydrolysis kinetics of chromium perchlorate in aqueous solution was studied by Rich et al.,[61] and the following rate constants were obtained: $k_1 = 1.4{\cdot}10^5\,\mathrm{s}^{-1}$, $k_{-1} = 7.8{\cdot}10^8\,\mathrm{M}^{-1}\mathrm{s}^{-1}$, for the

$$[Cr(H_2O)_6]^{3+} \underset{k_{-1}}{\overset{k_1}{\rightleftharpoons}} [Cr(H_2O)_5OH]^{2+} + H^+ \tag{2.13}$$

reaction.

A new set of equilibrium constants were reported by Meyenburg for the $[CrOH]^{2+}$ and $[Cr(OH)_2]^+$ complexes: $p\mathrm{K}_1 = 4.15$ and $p\mathrm{K}_2 = 6.5$ at 20 °C and 0.1 M ionic strength. The possible formation of the dimer and its deprotonation was also mentioned.

Later, a new polymeric complex was proposed by Finholt et al. based on freezing point depression and ion-exchange chromatography measurements.[62] A symmetrical triangular structure was put forward, but the formation constant of the $[Cr_3(OH)_4]^{5+}$ was not determined, since the results were not reproducible.

Longer polymers are also mentioned in the literature, even up to hexameric one. The first six members of the series of the hydrolytic products were separated from $Cr(ClO_4)_3$ solutions with different alkalinity ($< 1$ equivalent) on a Sephadex SP C-25 column, eluted with $NaClO_4$ and $LiClO_4$ solutions containing acid in variable concentrations.[63] The polymers were assigned by their UV-visible spectra (however, there were tiny shifts in the spectra between each species, up to 5 nm), and their acidity constants were determined by potentiometry. The acid content

of the eluent was varied systematically to elute the complexes in their fully protonated form. This continuous change in the *p*H, together with the poorly defined UV-visible spectra make the existence of these multinuclear complexes at least questionable. The authors also proposed structures for the trimer and the tetramer with three- or fourfold times bonded oxygens (!) in the center of them, respectively. This article was the first part of a twelve member series of publication with the title of "Early stages of the hydrolysis of chromium(III) in aqueous solution." In the sequels, they investigated the formation kinetics, the different forms (singly or doubly bonded) of the dimer, the stability constants, the cleavage of the trimer and the tetramer, as well as, the formation kinetics of the hexamer in detail.[64–74]

# 3 Objectives

The aims of my PhD work were the followings:

- Identification and characterization of hydroxido complexes of tin(II), lead(II) and chromium(III), which are formed at *p*H higher than 13, up to 16–20 M hydroxide concentration.
- The solution structure of these complexes has not been described in the literature; therefore it was one of our aims to determine the solution-state structures in these systems by direct means.
- Determining if any multinuclear complex formation or dehydration takes place at higher metal ion concentrations under the most water deficient conditions.

More specifically, the following issues were addressed:

- For tin(II) and lead(II), the existence or non-existence of the $[Sn(OH)_4]^-$ and $[Pb(OH)_4]^-$ became the main question, respectively. In both cases, there were some assumptions regarding these complexes; however, without unequivocal thermodynamic or structural evidences.
- Recent literature data indicated that chromium(III) tended to turn to chromium(VI) under strongly alkaline conditions. Accordingly, we decided to perform a broader range of experiments, and to accumulate experimental evidence for proving the reaction between chromium(III) and its solvent (including the effect of the counter ion and the mechanism of this reaction).
- As our results on the structure of the alkaline chromium(III) complexes seemed to be in contradiction with the previously proposed ones, which were invoked on the basis of analogies with complexes forming in acidic solutions. Therefore, the hydrolysis of chromium(III) in slightly acidic aqueous solutions was re-investigated.

# 4 Experimental part

## 4.1 Tin(II)- and lead(II)-containing systems

### 4.1.1 Materials and solution preparation

#### Preparation of the concentrated and carbonate-free NaOH and KOH stock solutions

Analytical grade sodium hydroxide (ANALR NORMAPUR) was dissolved in distilled water in 1:1 mass ratio, with intense stirring and cooling to prepare the stock solutions. This way ∼50% (w/w) (∼19 M) NaOH solution is achievable, in which the sodium carbonate is precipitated. After the filtration on an alkali-resistant, polysulphonate Nalgene filter, the solution can be considered as carbonate free.[75] The exact concentration was calculated from the density of the solution, determined by a pycnometer at 25℃, according to the literature procedure.[76] The stock solution was stored in caustic resistant Pyrex bottle with tightly fitting screw-top. Its dilutions were carried out by weight.

For some measurements concentrated potassium hydroxide stock solution was also prepared, its concentration was about 14 M. The preparation and treatment method was basically the same as for the sodium hydroxide, except the carbonate was removed as $CaCO_3$ by adding 2 g/l CaO into the saturated KOH solution in this case.

#### Preparation of the acidic tin(II)-containing stock solutions

As tin(II) is much less sensitive to aerial oxidation in acidic media than in alkaline one, all the stock solutions prepared were strongly acidic.

Different preparation methods were used depending on the requirements of the applied experimental method.

For the stock solution with $c_{\mathrm{Sn(II)}} \approx 0.5\,\mathrm{M}$ and $c_{\mathrm{acid}} \approx 1\,\mathrm{M}$, tin(II) oxide powder, SnO (Sigma Aldrich), was dissolved in oxygen-free atmosphere in dilute (1:1 volume ratio) analytical grade hydrochloric or perchloric acid (Sigma Aldrich). The purity of SnO was checked with powder X-ray diffraction, and was found to contain less than ca. 2 % $SnO_2$. This kind of stock solution

was used for the X-ray absorption, Raman, and $^{119}$Sn Mössbauer spectroscopy measurements (in the latter case only for the alkaline samples).

The tin(II) stock solution for the potentiometric titrations ($c_{\mathrm{Sn(II)}} \approx 0.6\,\mathrm{M}$ and $c_{\mathrm{HCl}} \approx 1.5\,\mathrm{M}$) was prepared under oxygen-free conditions by dissolving analytical grade metallic tin (Reanal) in diluted analytical grade hydrochloric acid. This process took about four days, and the temperature was kept at 50°Cduring this time. A practically tin(IV)-free solution could be prepared this way, as the continuously evolving hydrogen gas secured reducing conditions and any further oxidation of formed tin(II) was not possible. The solution was filtered under nitrogen atmosphere. The same kind of stock solution was used for the $^{117}$Sn NMR measurements.

The exact concentration of tin(II) was determined by standard iodometric titration procedure[77] in both cases according to the following reactions:

$$\mathrm{Sn^{2+} + I_2 \longrightarrow Sn^{4+} + 2\,I^-} \tag{4.1}$$

$$\mathrm{I_2 + 2\,S_2O_3^{2-} \longrightarrow 2\,I^- + S_4O_6^{2-}} \tag{4.2}$$

$$\mathrm{6\,H^+ + IO_3^- + 5\,I^- \longrightarrow 3\,I_2 + 3\,H_2O} \tag{4.3}$$

The concentration of hydrochloric acid was determined by $p$H potentiometric titration with sodium hydroxide.

For the $^{119}$Sn Mössbauer spectroscopy measurements, we needed $^{119}$Sn enriched acidic samples also. For this purpose, $\mathrm{Sn(ClO_4)_2}$ in $\mathrm{HClO_4}$ solution was prepared according to the procedure described in the literature,[7,78] using purified metallic tin and Cu(II) perchlorate under argon atmosphere. The redox reaction is quantitative,[7] and it yields tin(II) perchlorate solution. The metallic Sn and Cu (i.e., Cu grains covered with Sn) was then separated from the solution. With this method, approximately 0.05–0.10 M Sn(II) concentrations could be prepared in ca. 0.1–0.5 M $\mathrm{HClO_4}$.

### Preparation of the acidic lead(II) nitrate stock solutions

The lead(II) stock solution ($c_{\mathrm{Pb(II)}} = 1\,\mathrm{M}$ and $c_{\mathrm{HNO_3}} = 0.05\,\mathrm{M}$) was prepared by dissolving analytical grade lead(II) nitrate, $\mathrm{Pb(NO_3)_2}$ (Sigma Aldrich), in analytical grade nitric acid, in order to avoid the hydrolysis of the lead(II) ions when diluted by distilled water.

### Preparation of the alkaline tin(II)- and lead(II)-containing samples

The alkaline tin(II) and lead(II) samples were prepared by adding the calculated amount of the M(II) (M = Sn, Pb) stock solution dropwise to the NaOH solution, in a small Pyrex bottle, for which a custom-made screw-top was fabricated with two small holes for the argon gas in- and outlet, and a bigger one for the addition of the M(II) stock solution. The calculated amount of the freshly prepared M(II) stock solution was added dropwise to 25 ml of the appropriately

diluted NaOH solution with continuous and intense argon bubbling through the sample, and stirring. The NaOH solutions were diluted by weight from the concentrated stock solution, and argon gas was bubbled through it for at least 15 minutes before adding the metal ion stock solution.

### 4.1.2 Instrumentation and computational methods

#### Potentiometric titrations

The *p*H potentiometric titrations were carried out using a Metrohm 888 Titrando instrument equipped with $H_2$/Pt electrode. The experimental setup used for these measurements was the same as described in the literature.[79,80] The full electrochemical cell contained a platinized hydrogen electrode and a Ag|AgCl reference electrode.

$$H^+/H_2(Pt) \mid \text{test sol., I} = 4\,\text{M (NaCl)} \parallel 4\,\text{M NaCl} \parallel 4\,\text{M NaCl, Ag/AgCl}$$

The behavior of the electrode was found to be Nernstian, with the slope of $59.2 \pm 0.2$ mV/decade. The electrode performance was regularly checked via calibrations using strong acid – strong base titrations in the concentration range employed during the measurements. All the titrations were performed in an externally thermostatted home-made cell and the temperature was kept at $25.00 \pm 0.04$ °C by circulating water from a Julabo 12 thermostat. The ionic strength was kept constant, I = 4 M, with analytical grade NaCl (Prolabo).

#### Raman spectroscopy measurements

Raman spectra were recorded on a BIO-RAD Digilab Division dedicated FT-Raman spectrometer equipped with liquid nitrogen-cooled germanium detector and $CaF_2$ beam splitter The excitation line was provided by a Spectra Physics T10 106C Nd:$YVO_4$ laser at 1064 nm. The spectra were recorded in the range of 3600–100 $cm^{-1}$ with 4 $cm^{-1}$ optical resolution. 4096 scans were collected and averaged for each spectrum. The excitation power was 280 mW at the sample position. The spectrometer was controlled by using BIO-RAD Win IR 3.3 software. The samples were placed in a 1 cm path length quartz cuvette. Spectra were recorded at room temperature. Data were processed by the SpekWin32 software, and fitting of the Lorentzian curves were performed with QtiPlot. Attempts to collect infrared spectra for these solutions in ATR mode were unsuccessful, most probably due to insufficient signal-to-noise ratio.

#### X-ray absorption spectroscopy measurements

The X-ray absorption spectra for tin were collected at the bending magnet beamline Samba at the Soleil synchrotron facility, Paris, France, operating at 2.75 GeV and a maximum current of 400 mA. The Samba beamline covers the energy range of 4–42 keV. The maximum flux on

the sample at 10 keV was $1\times10^{12}$ photon/s/0.1% bandwidth. The energy scale of the X-ray absorption spectra were calibrated by assigning the first inflection point of the tin K-edges of metallic tin foil to 29200.0 eV.[81] For recording the spectrum of the tin(II)-containing solutions, 15 ml sample was placed in a cubic polyethylene sample holder with a tightly fitted screw-top.

The X-ray absorption spectra for lead were collected at the wiggler beamline I811 at MAX-lab, Lund University, Sweden, using the MAX II storage ring operating at 1.5 GeV and a maximum current of 250 mA. The maximum flux on the sample is $5\times10^{11}$ at 9 keV on a $(0.5\,\mathrm{mm})^2$ surface area. The measurements were performed in fluorescence mode at the lead $L_3$-edge. The energy scales of the X-ray absorption spectra were calibrated by assigning the first inflection point of the lead $L_3$-edges of metallic lead foil to 13038.0 eV.[81] The samples were measured in cells, made of a 1.5 mm Teflon spacer and 6 $\mu$m polypropylene X-ray film held together with titanium frames.

The analysis of the data was performed with the EXAFSPAK[82] and FEFF7[83] program packages, allowing the determination of the structural parameters of the local coordination around the absorber ions.

In the followings I am going to give a brief review of X-ray absorption spectroscopy, focusing on the parts, which are important for our work,[84,85] as it is not a technique used day by day. (It also holds for the Mössbauer spectroscopy, which is introduced in the following section.)

The absorption of the X-rays is based on the photoeffect, as the energy of the radiation kicks out a bonded electron from one of the inner shells. The absorption coefficient of the X-rays decreases with the increasing photon energy until it reaches the bonding energy (so called threshold energy) of an inner electron. At this point a sharp peak appears in the spectrum. The decay of the absorption coefficient above the edge has a fine structure up to 1000 eV.

An X-ray absorption spectrum can be divided into three regions which hold different information. The first part is the pre-edge region, just before the absorption edge. Its structure can refer to the bonding character, the oxidation state and the coordination geometry of the observed atom or ion. It is followed by the X-ray absorption near edge region (XANES), which means the absorption edge and its close vicinity. The position of the edge depends on the oxidation state, while the shape of the XANES spectrum is in conjunction with the local geometry and the type of the ligands around the absorber. This region can be considered as a fingerprint for a given local structure. The last part is the so called extended X-ray absorption fine structure (EXAFS) region, from which important structural parameters can be extracted, like the coordination number and the interatomic distances around the absorber.

EXAFS always appears above the edge for atoms or ions surrounded by other atoms or ions the solid and liquid phases as well as in molecular gases but nor for noble gases and other atomic gases. This fine structure is due to the wave nature of the electrons. During the absorption of the X-ray photon, a photoelectron is kicked out from an inner electron shell, and its kinetic energy

is equal to the difference between the energy of the X-ray photon (E) and the bonding energy of the electron ($E_0$). These photoelectrons can be considered as spherical waves with $\lambda$ wavelength, $\lambda = \frac{2\pi}{k}$, where $k$ is the wave vector of the photoelectron ($k = \sqrt{\frac{2m(E-E_0)}{\hbar}}$). This photoelectron is scattered by the atoms and/or ions around the absorber and these backscattered waves interfere with the original ones. This interference induces variations in the electron density of the absorber, which depend on the energy of the ejected photoelectron. Constructive interference increases the electron density and therefore, the probability of the photon to be absorbed. A change in the interference form destructive to constructive gives rise to the oscillation above the edge.

The definition of the EXAFS can be derived from the absorption coefficient by normalizing with the atomic absorption coefficient ($\mu_0$). In the simplest case only the single backscattering processes are considered from the surrounding atoms/ions and the EXAFS signal ($\chi$(k)) can be expressed as a sum of sine waves:

$$\chi(k) = \sum_i A_i(k) sin(2kR_i + \delta_i) \tag{4.4}$$

and

$$A_i(k) = \frac{S_0^2 e^{-\frac{2R_i}{\lambda}}}{kR_i^2} \cdot N_i F_i(k) \cdot e^{-2\sigma_i^2 k^2} \tag{4.5}$$

where $A_i$ is the backscattering amplitude, $R_i$ is the distance between the absorber and backscatter, $\delta_i$ is the atom specific phase shift, $S_0^2$ is the amplitude reduction factor, $N_i$ is the coordination number in the $i^{th}$ coordination shell, $F_i(k)$ is the amplitude for the backscatters of the $i^{th}$ coordination shell and $\sigma_i$ is the Debye-Waller coefficient.

Consequently, the EXAFS oscillation includes a lot of important structural information about the local environment of the absorber. The Fourier transform of it gives the so called pseudo radial distribution function, where the peaks appear at $R_i$ distances giving direct structural information. To deduce the exact structural parameters such as the value of the interatomic distances, coordination number and Debye-Waller factor model functions have to be fitted to the experimental spectrum. The interatomic distances can be extracted with high accuracy (within 1 %), while the coordination number with relatively large uncertainty (approximately 10 %). In our work, these parameters were the most interesting ones, together with the Debye-Waller factor.

### $^{119}$Sn Mössbauer spectroscopy measurements

$^{119}$Sn Mössbauer spectroscopy measurements were carried out both for quick-frozen solutions and for solutions at room temperature. The latter method is called capillary Mössbauer spectroscopy (CMS), which is based on the observation that liquids trapped in the capillaries of

certain mesoporous silicate glasses (such as Corning Vycor 'thirsty' glass) display frozen solution like behavior at temperatures much higher than their actual freezing point.[86–89]

'Thirsty' glass samples (Vycor Brand Porous Glass 7930, 12×24×3 mm) were used. Upon standing, the 'thirsty' glass tends to adsorb aerial organics, and accordingly, turns yellowish. The cleaning procedure suggested by the manufacturer[90] included reflux at 100°C in $H_2O_2$ solution (30% w/w) or $HNO_3$ (65% w/w), to which some crystals of $KClO_3$ or $NaClO_3$ is added.

Instead of this, we refluxed the glass samples in a 1:1:1 mixture of $H_2O_2$ (30% w/w), $HNO_3$ (65% w/w) and distilled water. As a result, the yellow color of the glass disappeared within a couple of hours. The full cleaning procedure included a further reflux in HCl (36% w/w) for 2 days, (to remove possible metallic traces from previous measurements), reflux in a 1:1:1 mixture of $H_2O_2$ (30% w/w), $HNO_3$ (65% w/w) and distilled water for 2 days and reflux in distilled water for another 2 days. The cleaned glasses were stored in distilled water prior to use. To check, if tin-containing contaminants remained in the glass, it was dried in a desiccator, and its $^{119}$Sn Mössbauer spectrum was recorded. After 4 days of recording, no traces of tin were detected. Capillary Mössbauer spectra of liquid samples were recorded using a sample holder described previously,[91] which was identical to that used in previously published CMS works. The glass was soaked with the liquid at least 1 day prior to the measurement. The rapid charging of the sample holder made the anaerobic conditions possible (to minimize aerial oxidation of Sn(II) during the measurements).

$^{119}$Sn Mössbauer spectra were recorded with a conventional Mössbauer spectrometer (Wissel) in transmission geometry with constant acceleration mode. The measurements were carried out using a $Ca^{119}_{m}SnO_3$ radiation source of 8 mCi activity. 20 $\mu$m $\alpha$-Fe was used for velocity calibration when a $^{57}$Co/Rh source supplied the $\gamma$ rays, and the isomer shifts are given relative to $CaSnO_3$. The data collection was done at 78 K in a He-cryostat cooled by liquid nitrogen with the sample kept in He atmosphere for the frozen solutions. All sample preparation, including also the rapid freezing, was done in a home-made glove box to minimize the oxidation of the sample. The Mössbauer spectra were analyzed by least-squares fitting of the Lorentzian lines with the help of the MOSSWINN program.[92] The database of the Mössbauer Effect Data Index was used to interpret the results.[93]

Mössbauer spectroscopy was used to investigate the microenvironment around the tin(II) ions. This spectroscopy is based on the phenomena of recoilless $\gamma$ absorption, discovered by Rudolf Mössbauer in 1958.[94] The investigated nucleus has to fulfill several criteria, thus, in practice, only about a dozen of elements can be measured. Among them, the most common is $^{57}$Fe, while the second one is $^{119}$Sn.[95] This is the only Mössbauer active isotope of tin, its natural abundance is ∼8 %, which is enough to get good quality data without enrichment. In $^{119}$Sn Mössbauer spectroscopy the low energy (23.88 keV) transition of the $I = 1/2$ ground state and the $I = 3/2$ excited state is used.

The two parameters of the Mössbauer spectrum, which are the most informative ones for us are the isomer shift ($\delta$) and the quadrupole splitting ($\Delta$).

The isomer shift of the absorption lines is a result of the Coulomb interaction between the the nuclear charge distribution over the finite nuclear volume and the electronic charge density over this volume. This shift is because of the different nuclear volumes in ground and excited states, and the different electron densities at the nuclei in different materials. In case the ground and excited states are unsplit (there are no other hyperfine interactions) but their separation is different in the source and in the absorber by an amount given by the isomer shift. Therefore, the isomer shift is always a relative value to a standard material. Besides the parameters of the nuclei (for example nuclear radii of the ground and excited states) and the temperature, the electronic structure around the nuclei affects the measured isomer shift. The latter depends on the oxidation state and the microenvironment of the observed nuclei (type of the ligand(s), coordination number and geometry).

If I>1/2 for one of the states (e.g. ground and/or excited) the charge distribution is non-spherical around the nuclei and this is described with the nuclear quadrupole moment. Therefore, in an asymmetric electric field, characterized with the electric filed gradient (EFG), an electric quadrupole interaction occurs, which makes the nuclear energy levels split. Because of this, the single line of the spectrum (which is the case in spherical charge distribution) also splits into more lines, separated by the quadrupole splitting. The quadrupole splitting is based on both the nuclear quadrupole moment, which is constant for a given nuclei and on the EFG. The electric field gradient can be obtained from the asymmetric ligand arrangement around the observed atom and/or ion. The value of the quadrupole splitting is a good indicator of the symmetry of the bonding environment and the microstructure of the Mössbauer active atom.

### $^{117}$Sn NMR spectroscopy measurements

The $^{117}$Sn NMR measurements were performed at 178.03 MHz on a 1.75 T Bruker Avance NMR spectrometer (500.13 MHz $^{1}$H frequency), in 5 mm Wilmad NMR tubes. Other experimental conditions: solvent: 10% $D_2O$/90% $H_2O$, the deuterium signal was used to lock the field; relaxation delay: 1 sec; sweep width: 500.5 ppm; pulse width: 1 $\mu$s; temperature: 298.1 K; number of scans: 32.

### Computational methods

Optimizations and frequency analyses were performed using the GAUSSIAN 09 program[96] with density functional theory (DFT) at the B3LYP level, using SDD basis set for tin and lead atoms and 6-31+G** for oxygens and hydrogens. Using more flexible basis sets for the light atoms does not improve the calculated results. The earlier studies of tin complexes proved the suitability of B3LYP method to calculate the nuclear quadrupole splitting (NQS) of $^{119}$Sn.[97–99]

The core electron density directly determines the NQS of the tin atom; thus, the DGDZVP all electron basis set has been applied for the heavy atom to calculate the NQS with high accuracy. We systematically modeled solvent effects by representing $H_2O$ as a polarizable continuum, according to the method implemented in the PCM-SCRF (self-consistent reaction field) procedure in the Gaussian program. In some cases, the hydration shell of these complexes was taken into account explicitly, but the calculated properties did not change significantly compared to the PCM method, therefore, those results are not discussed.

## 4.2 Chromium(III)-containing systems

### 4.2.1 Materials and preparations

#### Preparation of the chromium(III) perchlorate stock solution

The ~1 M chromium perchlorate stock solutions were prepared by the reduction of analytical grade sodium bichromate with hydrogen peroxide in concentrated perchloric acid.

$$Na_2Cr_2O_7 + 3\,H_2O_2 + 8\,HClO_4 \longrightarrow 2\,Cr(ClO_4)_3 + 2\,NaClO_4 + 7\,H_2O + 3\,O_2\uparrow \tag{4.6}$$

The $Na_2Cr_2O_7 \cdot 2\,H_2O$ (Reanal) was dissolved in stoichiometric amount of analytical grade concentrated $HClO_4$ solution (AnalaR Normapur) and 30 % $H_2O_2$ solution (Sigma-Aldrich) was added dropwise under continuous stirring and cooling until the gas evolution stopped. The prepared solution was stirred for two days at 80°C, and it was boiled for two further hours in order to remove the traces of the excess hydrogen peroxide. The precise chromium(III) concentration was determined by the standard iodometric procedure[77] according to the following three reactions.

$$3\,H_2O_2 + 2\,Cr^{3+} + 10\,OH^- \longrightarrow 2\,{CrO_4}^{2-} + 8\,H_2O \tag{4.7}$$

$${Cr_2O_7}^{2-} + 6\,I^- + 14H^+ \longrightarrow 2\,Cr^{3+} + 3\,I_2 + 7\,H_2O \tag{4.8}$$

$$I_2 + 2\,{S_2O_3}^{2-} \longrightarrow 2\,I^- + {S_4O_6}^{2-} \tag{4.9}$$

#### Preparation of the sodium perchlorate solution

The sodium perchlorate stock solutions were prepared by adding concentrated NaOH solution to a concentrated $HClO_4$ solution dropwise under continuous stirring and cooling, while the acid was stoichiometrically neutralized. The precise concentration of the stock solutions was determined by weighting a known volume of the liquid before and after its drying, and measuring the density by a pycnometer.

#### Preparation of the alkaline chromium(III)-containing samples

Each chromium(III)-containing alkaline sample was prepared by weighing the necessary amount of the stock solution (with known concentration and density). The $Cr(ClO_4)_3$ stock solution was added to the previously diluted, cooled and outgassed NaOH solution, and the time of the addition was registered. Each prepared sample was homogenized and outgassed again by ultrasound, and its density was measured. The samples were stored in tightly fitted polypropylene vials with the disclosure of light at room temperature. Each sample was doubled. The first one was opened only for measuring its portions, while the parallel sample was closed until ∼50 % conversion of the reaction. At that time both samples were measured and the average of the concentration difference was less than 3 % with less than 6 % highest deviation. The reactions were followed through 60–360 days.

#### Preparation of the acidic chromium(III)-containing samples

During the preparation of the acidic chromium(III)-containing samples, the proper amount of the $Cr(ClO_4)_3$ stock solution was added by volume, while the NaOH and $NaClO_4$ stock solutions were added by weight in a volumetric flask. The ionic strength was kept constant at 1 M, adjusted by sodium perchlorate. The *p*H and the UV-vis spectra of the solutions with varying total chromium(III) and hydroxide concentrations were followed for up to one year.

### 4.2.2 Instrumentation

#### UV-vis spectroscopy measurements

The UV-vis spectroscopy measurements were carried out with either a Specord 200 (Analytic Jena) or a Shimadzu UV-1650 double beam spectrophotometer in the 200–800 nm range for the alkaline and in the 200–900 nm range for the acidic samples with 1 cm optical path length. The analysis of the spectra and their kinetic information were evaluated with the PSEQUAD,[100] MRA[101] and ZITA[102] program packages.

#### *p*H measurements

The *p*H measurements were carried out with a JENWAY 3540 *p*H & conductivity meter equipped with a JENWAY 924 001 combined electrode filled with a 2 M $NaClO_4$, 1 M NaCl solution saturated with AgCl.

As the *p*H of the solutions had to be followed for an extended period of time, the potentials were measured, not the *p*H values. Two calibration sets were used, each consisted of three solutions with known *p*H values (they were 1.995, 2.995, 3.995 for the first set and 2.518, 2.995, 3.518 for the second one). Potential was measured and the actual $E_0$ and the Nernstian slope of

the electrode was estimated using a slightly modified[1] form of the Nernst equation before each sample measurement. The solutions with known *p*H values were appropriately diluted $HClO_4$ solutions with constant, 1 M ionic strength, adjusted with $NaClO_4$. This way the conditions of the calibration range was as close to the real samples as possible.

### X-ray absorption spectroscopy measurements

The X-ray absorption spectra were collected at the wiggler beamline I811 at MAX-lab, Lund University, Sweden. For the detailed specification of the beamline, see page 19. The measurements were performed in fluorescence mode at the K-edge of chromium. The X-ray absorption energy was calibrated by assigning the first inflection point of the K-edge of metallic chromium to 5989 eV.[81] Higher order harmonics were reduced by detuning the second monochromator to 40 % of its maximum intensity. The samples were placed in Teflon spacers of 0.2 mm thickness with Kapton tape windows. The analysis of the data was performed with the EXAFSPAK[82] and FEFF7[83] program packages.

### Gas chromatographic measurements

The hydogen gas evolved during the reaction was trapped above the reaction solution in a special glass vessel and 250 $\mu$l samples were injected into 60 ml/min $N_2$ flow. Analyses of the gases were performed with gas chromatograph (Agilent 7890A) using HP-PLOT Q column. The gases were detected simultaneously by thermal conductivity and flame ionization detectors.

[1] In preliminary experiments, we experienced some deviations from the Nernst equation, therefore, we introduced an additive term as an empirical parameter (p) to describe the deviation. This way the $E = E_0 + m \cdot \lg(c + p)$ equation was used with three fitted parameters ($E_0$; m; p).

# 5 Results and discussions

## 5.1 Tin(II)

### 5.1.1 Potentiometry

In order to establish the composition of the predominating tin(II) complex in strong alkaline aqueous solutions, the $OH^-$:tin(II) stoichiometric ratio of the predominating complex was determined by potentiometric pH titrations, using a $H_2$/Pt electrode, suitable to work in concentrated aqueous alkaline media.[79,80] The total tin(II) and hydroxide concentrations in the titrated solution were 0.1998 and 1.4992 M, respectively. The ionic strength was adjusted to 4.0 M with NaCl. The titrand was 3.0825 M hydrochloric acid and its ionic strength was also 4 M adjusted with NaCl. The titration curve is shown in Figure 5.1. The system was inhomogeneous from 7.60 to 20.80 ml of the added hydrochloric acid solution (grey area in Figure 5.1). The inhomogeneity is caused by the precipitation of $Sn(OH)_2$ and/or hydrated SnO, since they have very low solubility in the lack of excess hydroxide. The first equivalence point is close to that point of titration in which the $OH^-$:tin(II) ratio is 2.0, while the second one corresponds to the complete neutralization of the initially added hydroxide. Because of the inhomogeneity, only the initial part of the titration curve (corresponding to titrant consumption $< 7.60$ ml) can be evaluated. In this range, only the excess NaOH, unreacted with tin(II), is neutralized by the added hydrochloric acid. Consequently, the change of the observed cell potential ($E$) depends on the concentration of the free hydroxide, which is determined by the composition of the $[Sn(OH)x]^{2-x}$ complex.

The potential differences between the neighboring titration points, $\Delta E$, were used for the evaluation, because the use $E_0$ (and therefore the experimental uncertainty caused by its inclusion in the evaluation) can be eliminated this way. The theoretical $\Delta E$ values were calculated from the Nernst equation assuming $x$=3 and 4, exclusively. As it is clearly seen in Figure 5.1, the calculated $\Delta E$ values describe the observed ones almost perfectly for $x = 3$, indicating that the $OH^-$:tin(II) stoichiometric ratio is strictly, or at least predominantly, 3:1 even at such high hydroxide concentrations. This means that neither $[Sn(OH)_4]^{2-}$ nor its dehydrated forms ($[SnO_2]^{2-}$ and $[SnO(OH)_2]^{2-}$) can be present in significant concentrations. On the other hand,

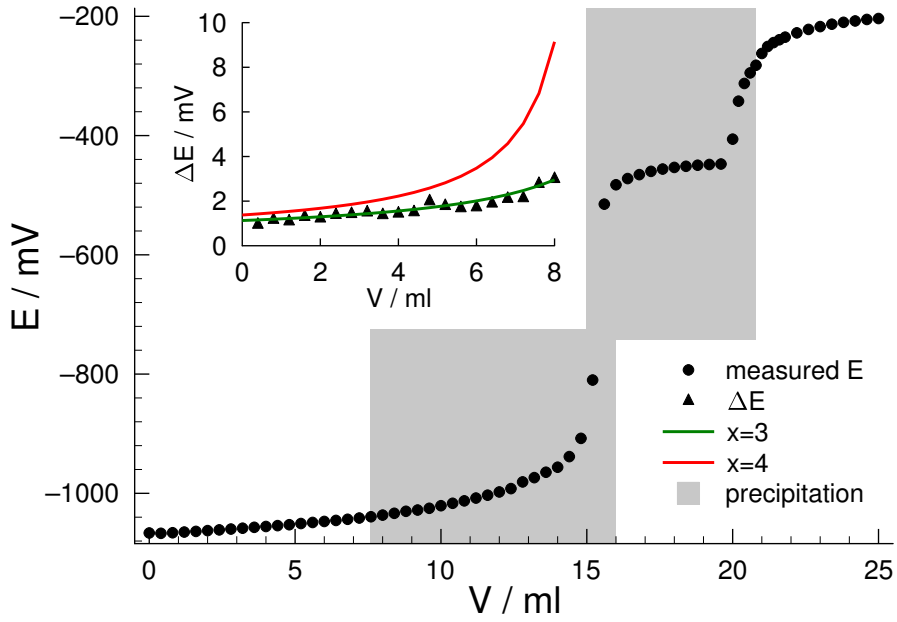


**Figure 5.1.** The potentiometric titration curve of 40 ml solution containing 0.1998 M Sn(II) and 1.4992 M NaOH; titrant: 3.0825 M HCl. The gray area shows the inhomogeneous region of the titration. Insert: the observed and calculated potential differences for $x = 3$ and 4, where $x$ stands for $[\mathrm{Sn(OH)}x]^{2-x}$.

the formation of either $[\mathrm{Sn(OH)_3}]^-$ or its dehydrated form ($[\mathrm{SnO(OH)}]^-$) cannot be distinguished from each other by potentiometry.

### 5.1.2 Raman spectroscopy

Background subtracted FT-Raman spectra of solutions with $c_{\mathrm{NaOH}} = 4.0$ M and varying tin(II) concentration are shown in Figure 5.2. With increasing tin(II) concentration, two peaks emerge at ~430 and ~490 $\mathrm{cm^{-1}}$. Both are due to Sn–O vibrations, as, according to the literature, a broad and weak spectral feature is seen in the Raman spectra of SnO, $\mathrm{Sn(OH)_2}$ and $\mathrm{SnO_2}$ in the solid state at ~470 $\mathrm{cm^{-1}}$.[103–105]

The peak at ~580 $\mathrm{cm^{-1}}$ is due to formation of tin(IV) species,[105,106] since its intensity increased at the expense of the other two peaks upon bubbling air through the solution. This band is very strong; therefore, it causes significant variations in the Raman spectra even if only a few percent of tin(II) is oxidized to tin(IV). This is unfortunately inevitable during manipulating the solutions and collecting the spectra.

Raman spectra of a more extended series of solutions with varying compositions were also recorded. The obtained spectral parameters are given in Table 5.1. The peak positions ($\tilde{\nu}$) and widths ($\sigma$) show only minor changes with varying solution composition. The slight increase in ($\tilde{\nu}$) with increasing concentration of sodium hydroxide is at the edge of significance although

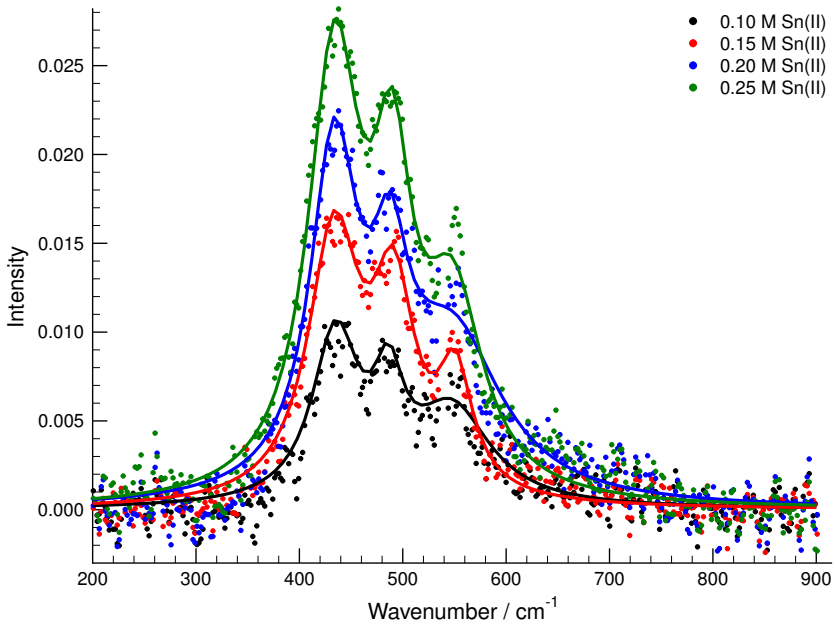


**Figure 5.2.** The experimental (symbols) and the fitted (lines) Raman spectra of the alkaline solutions with varying $c_{\mathrm{Sn}}$ at $c_{\mathrm{NaOH}} = 4\,\mathrm{M}$.

**Table 5.1.** Raman spectroscopic parameters of alkaline solutions containing Sn(II). The spectrum of the hydroxide solution with the appropriate concentration as background has been subtracted.

| | | Band at ~430 $\mathrm{cm}^{-1}$ | | | Band at ~490 $\mathrm{cm}^{-1}$ | | |
|---|---|---|---|---|---|---|---|
| $c_{\mathrm{Sn(II)}}$ | $c_{\mathrm{NaOH}}$ | $\tilde{\nu}$ | $\sigma$ | I | $\tilde{\nu}$ | $\sigma$ | I |
| (M) | (M) | ($\mathrm{cm}^{-1}$) | ($\mathrm{cm}^{-1}$) | (a.u.) | ($\mathrm{cm}^{-1}$) | ($\mathrm{cm}^{-1}$) | (a.u.) |
| 0.10 | 4.0 | 434.9 | 55 | 0.81 | 486.2 | 35 | 0.30 |
| 0.15 | 4.0 | 433.4 | 61 | 1.44 | 491.1 | 50 | 0.83 |
| 0.20 | 4.0 | 433.4 | 56 | 1.67 | 487.7 | 43 | 0.64 |
| 0.25 | 4.0 | 433.7 | 62 | 2.40 | 489.8 | 45 | 1.08 |
| 0.10 | 8.0 | 438.7 | 69 | 0.80 | 496.7 | 53 | 0.68 |
| 0.15 | 8.0 | 440.5 | 69 | 1.72 | 495.3 | 35 | 0.42 |
| 0.25 | 8.0 | 437.6 | 54 | 1.99 | 492.6 | 58 | 1.36 |
| 0.10 | 4.0[a] | 430.6 | 70 | 1.00 | 490.2 | 52 | 0.63 |
| 0.20 | 4.0[a] | 432.9 | 68 | 1.81 | 489.9 | 53 | 1.02 |
| 0.10 | ~14[a] | 448.0 | 66 | 1.17 | 505 | 48 | 0.65 |

[a] KOH instead of NaOH

the last three rows (measurements in KOH) also suggest this shift.[1] The Raman parameters obtained in media containing potassium hydroxide instead of sodium hydroxide are practically identical. The peak intensity (I, given in arbitrary unit in the table) is roughly linearly proportional to the total concentration of tin(II) (Figure 5.3). These observations suggest that there

[1] The optical resolution of the instrument used was $4\,\mathrm{cm}^{-1}$, and the calculation standard errors were 1–2 cm−1 for the peak positions and 4-7 cm−1 for the peak widths.

is only one tin(II)-containing species in these solutions, the composition and structure of which is independent of the concentrations of the solutes.

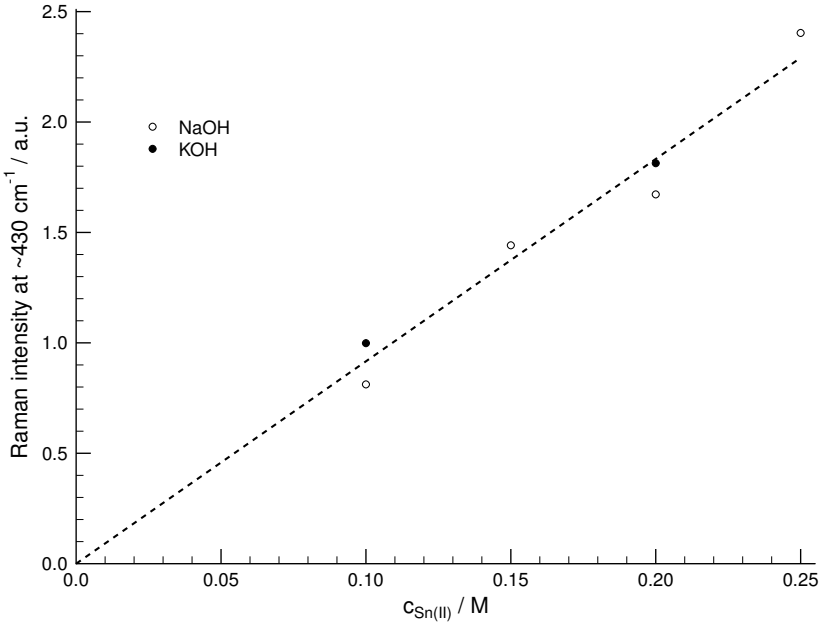


**Figure 5.3.** Integrated Raman band intensities for the mode at 430 cm$^{-1}$, after background subtraction and deconvolution, as a function of the $c_{\mathrm{Sn}}$.

### 5.1.3 Mössbauer spectroscopy

The structure of a complex determined in frozen solution is not necessarily exactly the same as the one in the liquid state. Because of this, we wanted to perform Mössbauer spectroscopy measurements not only in frozen solutions, but also in liquid state with the help of the capillary Mössbauer spectroscopy (CMS). As there were no available literature CMS data for tin(II)-containing aqueous solutions, some acidic samples were investigated first, as they are considered to be less oxygen sensitive.

The first sample was prepared by the cementation reaction between metallic tin and copper(II) perchlorate, and contained ~0.08 M tin(II) in ~0.2 M $HClO_4$ solution. The sample was $^{119}$Sn enriched, in order to increase the concentration of the Mössbauer active nuclei. As it is seen in Figure 5.4 (A), a line appeared at around 0 mm/s velocity, which is characteristic to tin(IV). For tin(II), the lines (in this particular case a doublet) are expected to show up in the velocity region of 2–5 mm/s, where the spectrum lines cannot be separated well from the noise. In order to check whether there is any tin(II) in the solution at all, the conventional transmission Mössbauer spectrum of the frozen solution was also recorded at 80 K, right after the CMS measurement. The spectrum is shown in Figure 5.4 (B). It was expected that the tin was present in this sample mostly as tin(II). However, it is clear from the spectrum of

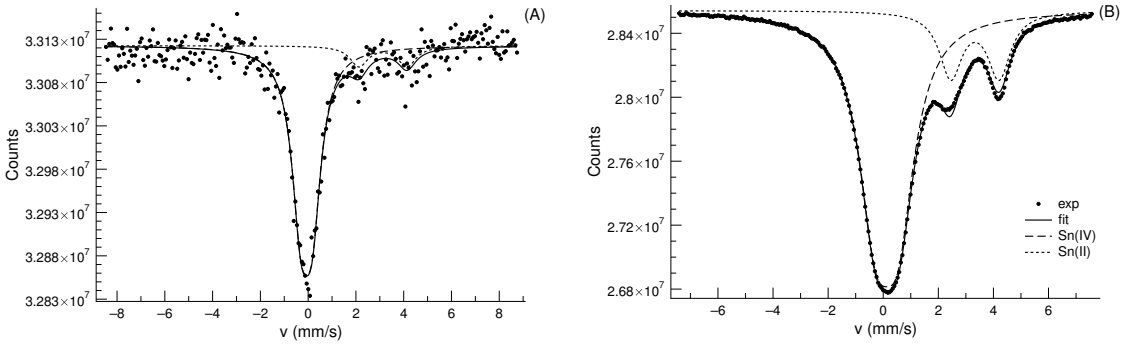


**Figure 5.4.** $^{119}$Sn CMS spectrum of a solution containing (nominally) $^{119}Sn(ClO_4)_2$ (∼0.08 M) in $HClO_4$ (∼0.20 M) at room-temperature (A), and $^{119}$Sn Mössbauer spectrum of the frozen solution of the same sample at 80 K (B). The points and lines denote the measured and calculated spectra, respectively.

the frozen solution that a significant amount of tin is present in the sample as tin(IV). There might be numerous explanations for this experimental finding, but the most plausible one is that the exclusion of aerial oxygen was not successful during the preparation procedure. Redox reaction within the glass pores might also be possible, however; based on previous experience with 'thirsty glasses', it is unlikely. It is not expected either that tin(II) would be unable to migrate into the mesopores of the glass due to some sterical reasons. The exact determination of the relative occurrence of tin(II) and tin(IV) in this sample from the relative areas of the Mössbauer spectral components is not possible, because the line areas strongly depend on the unknown Lamb-Mössbauer factors belonging to the species having different valence states.[95] We can conclude from the spectrum (Figure 5.4 (B)) that more than 25 % tin(II), at least, is present in the solution at 80 K, taking into consideration the common case of larger f-factor for tin(IV) than for tin(II).[93] However, this tin(II) quantity is hardly or not at all detectable (Figure 5.4 (A)) by the capillary Mössbauer measurement at room temperature.

CMS experiments were also performed with alkaline (∼4 M NaOH) solutions containing 0.06 M $Sn(ClO_4)_2$ (Figure 5.5 (A)). The 80 K spectrum of the frozen solution is shown in Figure 5.5 (B). Similarly to that obtained for the acidic sample, only the tin(IV) signal might be detectable in the solution. Moreover, during the collection of the spectrum (several days), the 'thirsty' glass visibly deteriorated, first (after a couple of days) it started to break to pieces; then, fully disintegrated and finally dissolved. With this sample, due to the chemical reaction, the freezing was not possible. The strongly alkaline solutions necessary for our studies seemed to pose an irreversible effect on the mesoporous glass carrier; therefore, from this point, CMS measurements were restricted to acidic solutions.

For relatively dilute tin(II) solutions, we failed to collect CMS pattern. From the possible explanations listed above, the most likely one seemed to be the oxygen sensitivity of tin(II), and its oxidation to tin(IV) during the sample preparation or the (rather lengthy) spectrum

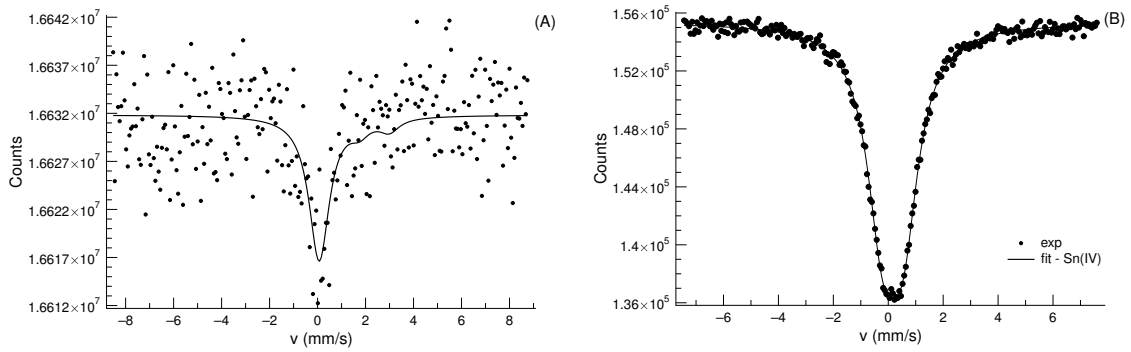


**Figure 5.5.** $^{119}$Sn CMS spectrum of a solution containing (nominally) $^{119}Sn(ClO_4)_2$ (∼0.06 M) in NaOH (∼4 M) at room-temperature (A) and $^{119}$Sn Mössbauer spectrum of a frozen solution with the same concentrations at 80 K (B). The points and lines denote the measured and calculated spectra, respectively.

collection. Therefore, we decided to use a more robust preparation route, yielding solutions with much larger tin(II) concentrations. Via dissolving metallic tin in HCl under aerobic conditions, solutions with ∼0.6 M $SnCl_2$ and ∼1.5 M HCl could be prepared. Under these conditions, tin(II) is present exclusively in the form of chlorido complex, $[SnCl_3]^-$;[107] thus, there is an enhanced solubility of tin(II) in HCl relative to $HClO_4$.

The CMS pattern of an acidic solution is shown in Figure 5.6 (A). As it is shown in the figure, the spectrum is without lines, neither tin(IV) nor tin(II) pattern can be observed. The spectra of this sample were also recorded as frozen solution at various temperatures between 20 and 200 K. At the lowest temperature (20 K), a well detectable pattern is seen (Figure 5.6 (B)), which can be assigned mainly to tin(II). Very small tin(IV) contribution is seen even at the lowest temperature, which indicates that oxidation of tin(II) to tin(IV) via this preparation route (despite the aerobic conditions) is negligible. This Mössbauer effect, however, decreases with raising temperature, and the signal intensity becomes zero at around 200 K. Thus, it seems likely that the "undetectable" tin(II) CMS signal described above (beside the partial oxidation of tin(II) and formation of tin(IV) in the more dilute solutions), can be due to the very strong temperature dependence of the Lamb-Mössbauer factor of tin(II) species.

In order to further strengthen this argument, the temperature dependence of Mössbauer spectra of a quenched aqueous solution containing 0.2 M $SnCl_2$ in ∼4.0 M NaOH was also recorded. The series of the fitted spectra normalized to the baseline is shown in Figure 5.7. The temperature dependence of the normalized area of $^{119}$Sn Mössbauer spectrum of this sample is also enormous. The line intensity becomes practically zero well below the melting of the frozen solution (Figure 5.8).

The $^{119}$Sn Mössbauer spectrum consists of a slightly asymmetric doublet (Figure 5.9). The typical isomer shift and quadrupole splitting are $\delta = 2.58$ mm/s and $\Delta = 2.06$ mm/s, respectively. These Mössbauer parameters are in the range of those found for $Sn(OH)_2$ ($\delta = 2.3$–$2.95$ mm/s

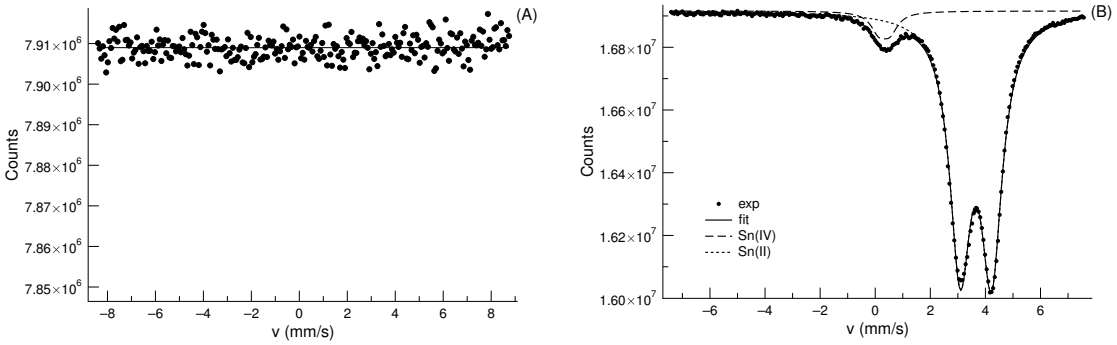


**Figure 5.6.** $^{119}$Sn CMS spectrum of a solution containing (nominally) ∼0.6 M $SnCl_2$ and ∼1.5 M HCl at room temperature (A) and $^{119}$Sn Mössbauer spectrum of the frozen solution of the same sample at 20 K (B). The points and lines denote the measured and calculated spectra, respectively.

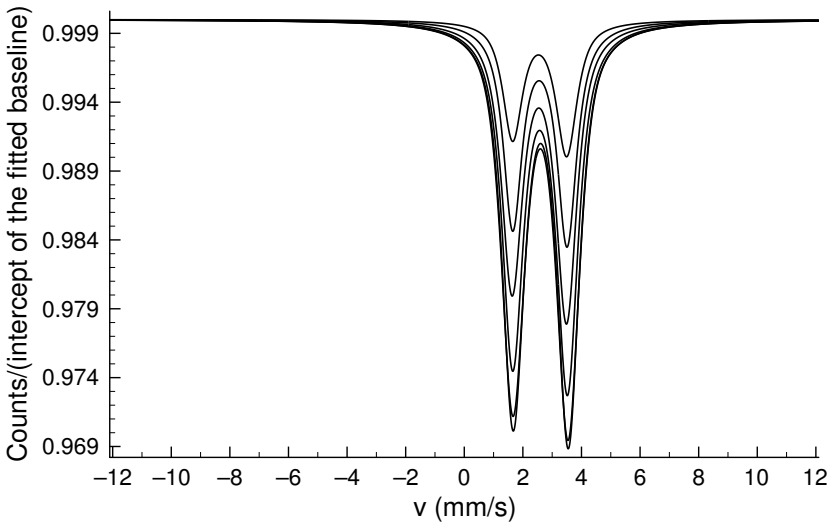


**Figure 5.7.** The dependence of the fitted $^{119}$Sn Mössbauer spectra of a frozen solution containing $SnCl_2$ (∼0.2 M) and NaOH (∼4.0 M) on the temperature. An upper curve belongs to a higher temperature value.

and $\Delta = 2.13$–$3.05$ mm/s)[108,109] as well as for SnO ($\delta = 2.6$–$3.4$ mm/s and $\Delta = 1.3$–$2.28$ mm/s), as reported in the literature.[110–113] The Mössbauer spectra reflect that tin is present in a single microenvironment solely as tin(II) in strong alkaline solution. This micro environment can be associated with the $[Sn(OH)_3]^-$ complex having trigonal pyramidal geometry. No significant change was found in the Mössbauer parameters of this doublet when the concentration of tin(II) or NaOH was changed (Table 5.2).

Since the hyperfine interactions detected by the Mössbauer spectroscopy are mostly affected by the first coordination sphere of tin, mainly the effect of oxygen nearest neighbor environment of tin(II) can be detected in the alkaline solutions, which remains unchanged with changing solution composition. The $\Delta$ values were calculated according to literature procedures[97] for $[Sn(OH)_3]^-$ and $[SnO(OH)]^-$. It was found that the calculated $\Delta$ value for the $[SnO(OH)]^-$

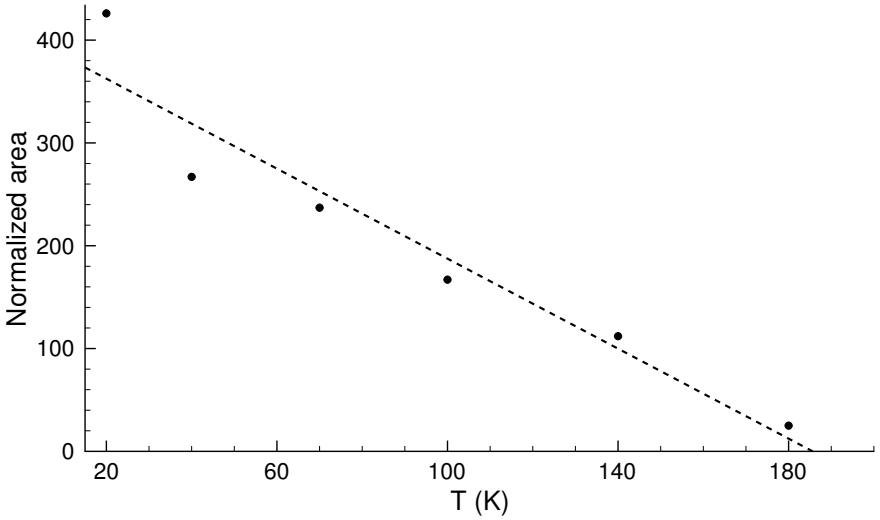


**Figure 5.8.** The dependence of the relative spectral area in $^{119}$Sn Mössbauer spectra of a frozen solution containing $SnCl_2$ (∼0.2 M) and NaOH (∼4.0 M) on the temperature.

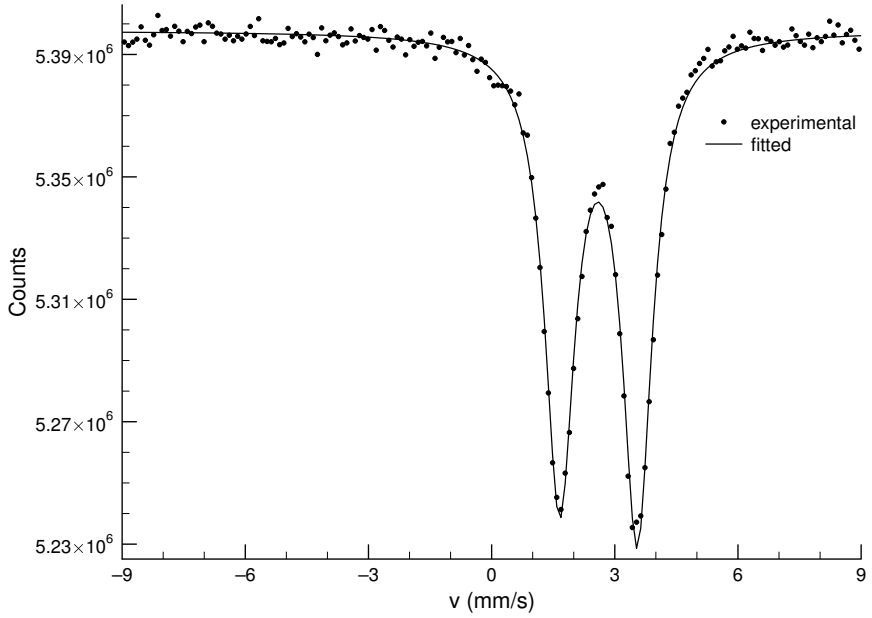


**Figure 5.9.** $^{119}$Sn Mössbauer spectrum of the frozen solution with $c_{Sn(II)} = 0.2$ M and $c_{NaOH} = 4$ M, (T = 20 K).

complex was much larger (3.11 mm/s) than the experimentally observed one. The calculated Δ value for $[Sn(OH)_3]^-$ was 2.62 mm/s. The $\delta$ (2.72 mm/s) and Δ (2.26 mm/s) values[114] obtained for the solid $NaSn(OH)_3$ are also close to those found in this study; however, the local structure of tin(II) in this compound is not established. Based on the analogy between $F^-$ and $OH^-$, it is remarkable that the Δ values for the $MSnF_3$ compounds (M = Na, K, Rb and Cs)[115] are in the range of 1.84–2.0 mm/s, while Δ = 2.15 mm/s for $SnF_2$;[116] tin(II) has trigonal pyramidal

**Table 5.2.** Mössbauer parameters obtained for rapidly frozen aqueous alkaline solutions containing Sn(II). Measurements were performed at 80 K.

| $c_{Sn(II)}$ (M) | 0.01 | 0.1 | 0.1 | 0.2 | 0.2 | 0.2 | 0.5 |
|---|---|---|---|---|---|---|---|
| $c_{NaOH}$ (M) | 0.1 | 1.0 | 4.0 | 4.0 | 4.0 | 12.0 | 8.0 |
| $\delta$ (mm/s) | 2.60 | 2.59 | 2.58 | 2.59 | 2.47 | 2.55 | 2.61 |
| $\Delta$ (mm/s) | 2.08 | 2.03 | 2.01 | 2.00 | 1.87 | 2.02 | 1.83 |

$\delta$ and $\Delta$ denote the isomer shift and quadrupole splitting, respectively. The standard deviations are $\pm 0.03$ mm/s and $\pm 0.06$ mm/s for $\delta$ and $\Delta$, respectively.

configuration in solid $SnF_2$.[117] All of these considerations makes the existence of $[Sn(OH)_3]^-$ more possible.

### 5.1.4 $^{117}$Sn NMR spectroscopy

The $^{117}$Sn NMR spectrum of a solution containing 0.1 M $SnCl_2$ and 4 M NaOH consists of a sharp singlet peak at 727 ppm relative to the also singlet peak of a solution of 0.5 M $Sn(ClO_4)_2$ in 1 M $HClO_4$ (Figure 5.10). This can be related to a single species, which is in complete agreement with the previous observations. The exchange of the water molecules around the tin(II) ion for hydroxide ions results in a large upfield shift. The chemical shift did not change within the experimental error when the tin(II) or the hydroxide concentration was varied.

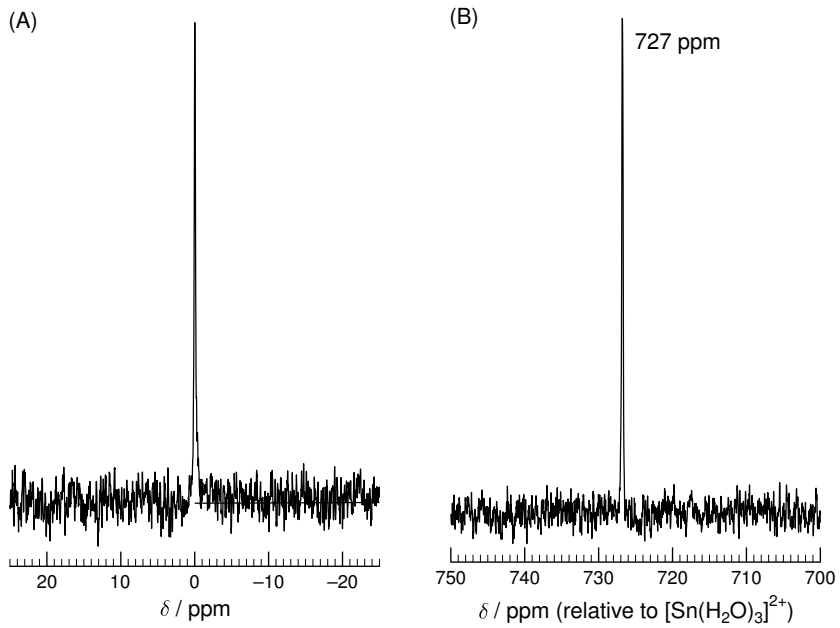


**Figure 5.10.** The $^{117}$Sn NMR spectrum of a solution containing 0.5 M $Sn(ClO_4)_2$ and 1 M $HClO_4$ 0.1 M $SnCl_2$ (in which the tin(II) is present as $[Sn(H_2O)_3]^{2+}$) (A) and 0.1 M $SnCl_2$ in 4 M NaOH, chemical shift is relative to the acidic sample (B).

### 5.1.5 Quantum chemical calculations

For *ab initio* calculations, a three-legged stool like (trigonal pyramid) structure was assumed for the $[Sn(OH)_3]^-$ complex and a V-shaped arrangement for the $[SnO(OH)]^-$ complex, the O–Sn–O angle being close to 90 ° in both cases (see Figure 5.11).

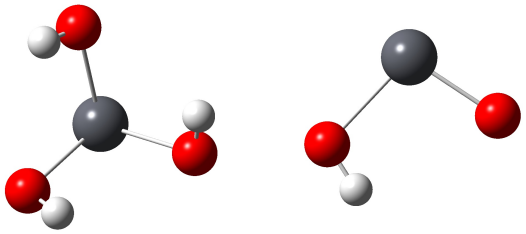

**Figure 5.11.** Ball and stick models for the $[Sn(OH)_3]^-$ and for the $[SnO(OH)]^-$ complexes.

The primary Sn–O bond lengths were found to be 2.10 Å, and 1.98/2.13 Åfor the three- and two coordinated complexes. The Raman spectra of these species have been calculated (Figure 5.12). In the calculated spectra of both species, peaks are seen at around 430 and 490 $cm^{-1}$, with larger intensity corresponding to the band at the smaller wavenumber, which is in excellent agreement with the experimental spectrum (Figure 5.2 on page 29). The striking difference is that the most intense calculated peak corresponding to $[SnO(OH)]^-$ is found at 700 $cm^{-1}$, which is completely missing in the experimental spectrum (Figure 5.2), strongly suggesting that the observed spectrum corresponds to the three-coordinated complex $[Sn(OH)_3]^-$.

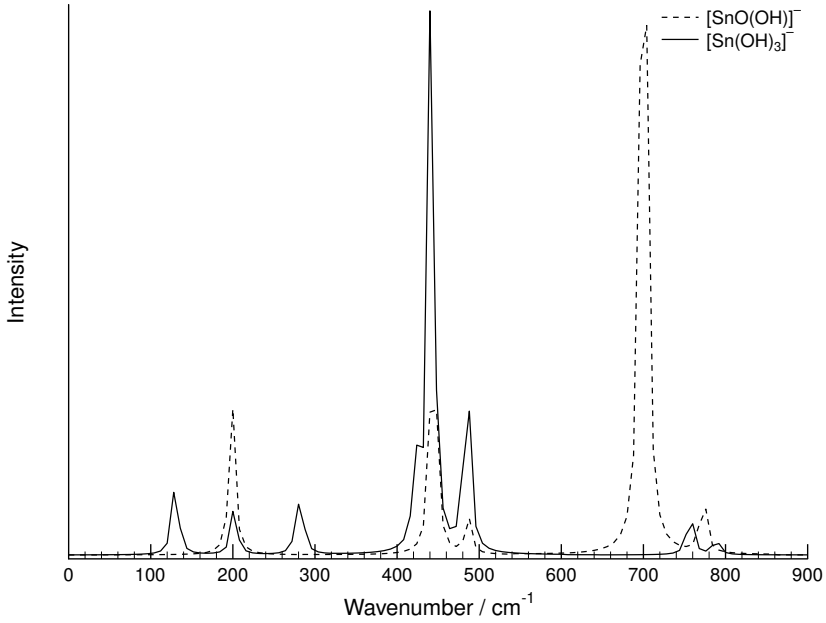


**Figure 5.12.** Calculated Raman spectra of $[Sn(OH)_3]^-$ and $[SnO(OH)]^-$.

### 5.1.6 X-ray absorption spectroscopy

The selection of an appropriate, non-interfering counter anion was the first step during the investigation. It is convenient to prepare tin(II) stock solutions using hydrochloric acid, since the dissolution is rapid, and the solubility of $SnCl_2$ is high in hydrochloric acid, due to the formation of chlorido complexes. The solubility of $Sn(ClO_4)_2$ is significantly lower than that of $SnCl_2$, and the dissolution of SnO or metallic tin is much slower in perchloric than in hydrochloric acid. It is therefore important to secure that tin(II)-chlorido complexes are not out-competing the tin(II)-hydroxido complexes in strong alkaline solution. As no literature data are available for the tin(II)-chloride system at pH>13, X-ray absorption spectroscopy was applied to study whether tin(II)-chlorido or chlorido-hydroxido mixed complexes were formed under such conditions or not. XAS spectra of 0.1 M $SnCl_2$ in 1 M hydrochloric acid, in 4 M NaOH, and in 4 M NaOH + 1 M NaCl, were compared to the spectra of 0.1 M $Sn(ClO_4)_2$ in 1 M perchloric acid and in 4 M NaOH.

The X-ray absorption near edge structure (XANES) regions and the Fourier transform of the $k^3$-weighted extended X-ray absorption fine structure (EXAFS) data of the measured samples are presented in Figure 5.13. As the figure shows, the spectra of the two acidic samples are clearly distinguishable by both the near-edge region and the Fourier transform of the EXAFS region.

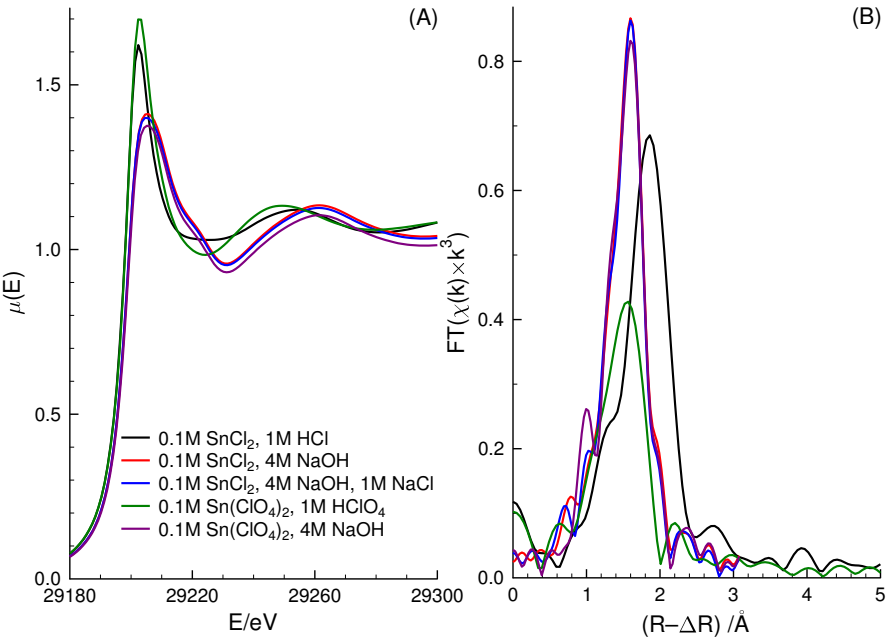


**Figure 5.13.** The near-edge region of the Sn K edge X-ray absorption spectra of 0.1 M $SnCl_2$ in 1 M hydrochloric acid, in 4 M NaOH, and in 4 M NaOH + 1 M NaCl, compared to the spectra of 0.1 M $Sn(ClO_4)_2$ in 1 M perchloric acid and in 4 M NaOH (A), as well as, the Fourier transform of the $k^3$-weighted EXAFS data of them (B).

In 1 M hydrochloric acid, tin(II) is almost exclusively present as $[SnCl_3]^-$ complex,[107] and the fitting of the spectrum gave a mean Sn–Cl bond distance of 2.475 Å, a Debye-Waller factor ($\sigma^2$) of 0.0099 Å$^2$, and a coordination number ($N$) of 3, with an assumed trigonal pyramidal geometry. The EXAFS and Fourier transform fits are shown in Figure 5.14. The above calculated parameters are in good agreement with the relevant solid crystal structures.

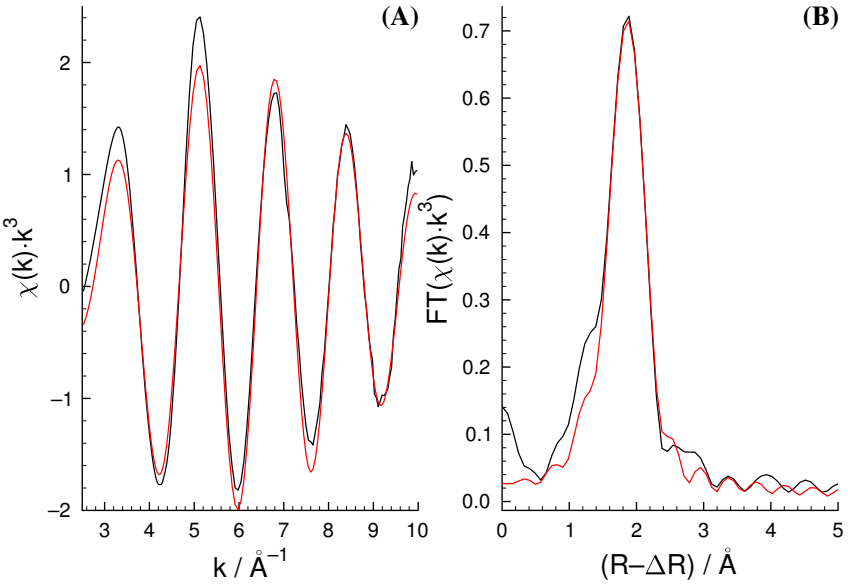


**Figure 5.14.** The experimental EXAFS spectrum of the Sn K edge X-ray absorption spectra of 0.1 M $SnCl_2$ in 1 M hydrochloric acid (black) and the fitted spectrum (red) (A), together with the Fourier-transform of the $k^3$-weighted EXAFS data of it (B).

In 1 M perchloric acid, tin(II) is present as $[Sn(H_2O)_3]^{2+}$ ions,[38] where $N = 3$, $r = 2.178$ Å, $\sigma^2 = 0.0153$ Å$^2$. The differences between the black and green curves in Figure 5.13 explain the significantly different calculated parameters. On the contrary, the spectra of the three alkaline samples are identical, even if a large excess of chloride ions (1 M) is present. From this, it is clear that the presence of chloride ions, also in high concentrations, has no effect on the tin(II) speciation as long as the free hydroxide concentration exceeds 0.1 M. Therefore, chloride can be considered as truly non-interfering counter ion in the experiments performed on tin(II) in strong alkaline aqueous solutions.

The edge positions show that these samples contained exclusively tin(II), as the experimentally observed reference edge energy for tin(II) in solid SnO and for tin(IV) in solid $SnO_2$ was 29207.45 and 29211.45 eV, respectively, and the edge energy of the samples was found to be 29207.13 eV. Thus, the experimental protocol employed during the experiments was suitable to protect the samples from aerial oxidation.

By combining the information obtained from the potentiometric titrations, Raman, Mössbauer, $^{117}$Sn NMR and K edge Sn XANES spectroscopy studies, and the quantum chemical

calculation of the Raman spectra assuming either $[Sn(OH)_3]^-$ or $[SnOOH]^-$ complex, it can be stated beyond any doubt that there is only one single tin(II) species completely predominating in strong alkaline solution, $[Sn(OH)_3]^-$, independent of tin(II) concentration and free hydroxide concentration above 0.1 M.

This is further evidenced by that all spectra of tin(II) in Figure 5.15 are superimposable, and that the local structure of tin(II) in these alkaline solutions is identical and independent of the total concentration of both NaOH and tin(II) within the concentration range covered.

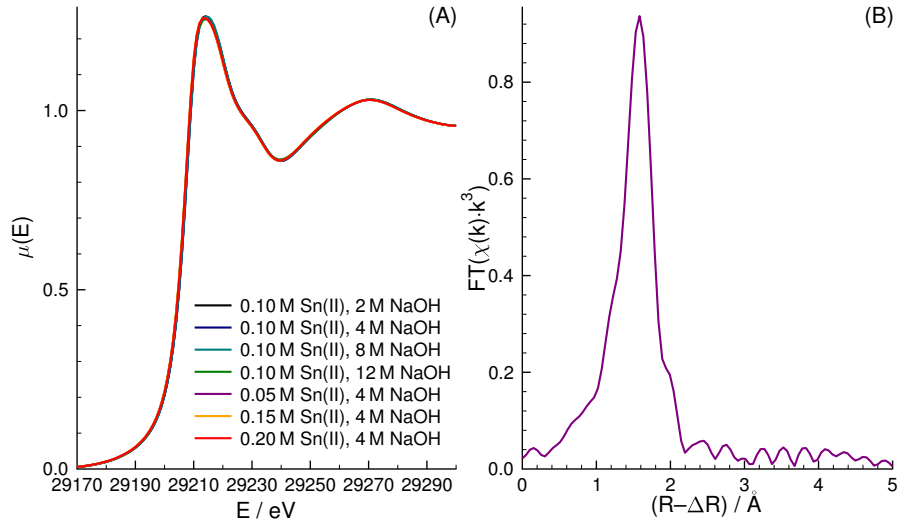


**Figure 5.15.** The near-edge region of the alkaline Sn K edge X-ray absorption spectra of all the alkaline solutions investigated (see Table 5.3 in detail) (A) and the Fourier-transform of the $k^3$-weighted EXAFS data for one specific sample (B).

The structure of the trihydroxidostannate(II), $[Sn(OH)_3]^-$, complex has been determined in the tin(II) and hydroxide concentration ranges of 0.05–0.20 and 2–12 M, respectively, the compositions of the alkaline tin(II) solutions prepared for the detailed study are given in Table 5.3. In the following, details will only be given for solution containing 0.05 M tin(II) in 4 M NaOH (signed as Sn5_4 in the table), while data for the remaining solutions are also given in Table 5.3.

The Fourier transform of the $k^3$-weighted EXAFS spectrum is given in Figure 5.15 (B). This Fourier transform only has a single peak related to the primary Sn–O bond distance at ∼2.1 Å(∼1.6 Å, not phase corrected). According to this single peak, tin(II) is expected to have a simple local environment, and no multiple scattering from the atoms in the first coordination sphere was detected. It indicates low symmetry around tin(II), as expected from the trigonal pyramidal configuration of three-coordinated tin(II) complexes. Polynuclear tin(II) complexes have not been detected under these conditions, since no Sn···Sn pair-interactions are seen on Fourier-transform of the $k^3$-weighted EXAFS data. Bond lengths are more accurately determined by EXAFS than the corresponding coordination numbers,[118] but as the other

**Table 5.3.** Composition of alkaline aqueous tin(II) samples studied, and the structural parameters in the refinements of the EXAFS data collected at ambient temperature using the EXAFSPAK program package, including the number of Sn–O bond distances ($N$), the mean Sn–O bond distance ($r$), the Debye-Waller factor coefficient ($\sigma^2$), the threshold energy ($E_0$), the amplitude reduction factor ($S_0^2$) and the goodness of fit (F), as expressed in the EXAFSPAK program package, Ref. 82.

| $N=3$ | $c_{\mathrm{NaOH}}$/M | $c_{\mathrm{Sn(II)}}$/M | $r$/Å | $\sigma^2$/Å$^2$ | $E_0$/eV | $S_0^2$ | $F$/% |
|---|---|---|---|---|---|---|---|
| Sn10_2 | 2 | 0.1 | 2.080 | 0.0040 | 29225.9 | 1.21 | 15.6 |
| Sn10_4 | 4 | 0.1 | 2.080 | 0.0037 | 29225.3 | 1.21 | 13.4 |
| Sn10_4 | 8 | 0.1 | 2.075 | 0.0038 | 29255.6 | 1.18 | 18.0 |
| Sn10_12 | 12 | 0.1 | 2.077 | 0.0039 | 29226.3 | 1.16 | 18.0 |
| Sn5_4 | 4 | 0.05 | 2.076 | 0.0038 | 29225.7 | 1.18 | 14.2 |
| Sn15_4 | 4 | 0.15 | 2.078 | 0.0038 | 29225.7 | 1.16 | 14.6 |
| Sn20_4 | 4 | 0.20 | 2.076 | 0.0040 | 29255.1 | 1.20 | 19.9 |

spectroscopic methods applied in this study clearly show the presence of only the trihydroxidostannate(II) complex, the coordination number has been locked to three in all refinements.

As a consequence, the relationship between the bond distance and the coordination number can be used to estimate the coordination number from the observed bond distance in most cases.[119,120] The $r$(Sn–O) and $N$ values of solid O-coordinated tin(II) compounds were collected from the Inorganic Crystal Structure Database[121] and the Cambridge Crystal Structure Database,[122] as previously done for lead(II) by others.[123] The data collected are shown in Figure 5.16.

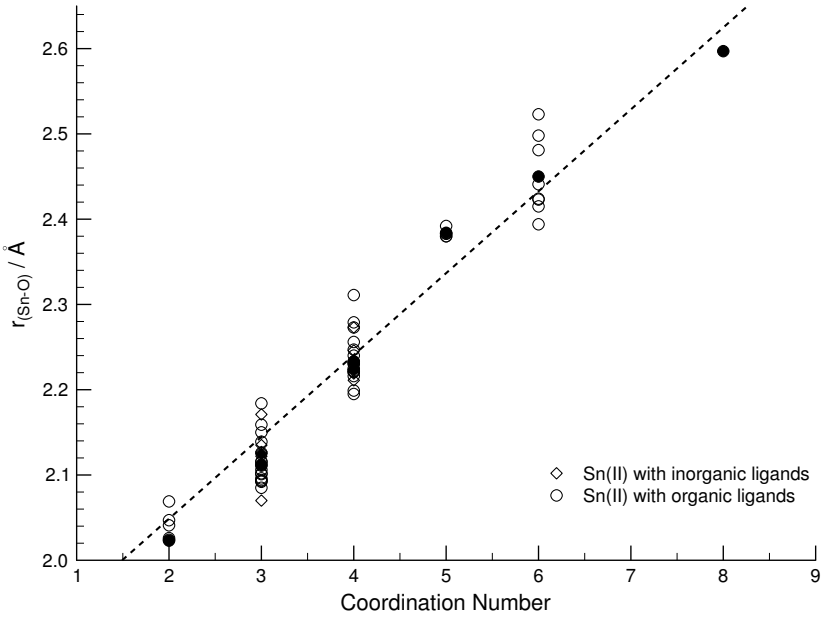


**Figure 5.16.** The relationship between the mean Sn–O bond lengths and the coordination number in various O-coordinated tin(II) compounds. The filled symbols stand for the average values. The dashed line represents the linear trend-line of the mean M-O bond distances as function of coordination number.

It is clearly seen that the spread in the Sn–O bond distances for complexes with the same coordination number and geometry is rather large, the Sn–O bond lengths are in the range 2.066–2.185 Å for $N = 3$.[2] During the fitting of the EXAFS data of sample Sn5_4, $N$ was held constant ($N = 3$), and a bond length, $r(\text{Sn–O}) = 2.076$ Å with a small Debye-Waller factor, $\sigma^2 = 0.0038$ Å$^2$, were obtained. Although, the calculated length is short, it is still in the range acceptable by the literature data. It should also be mentioned that a mean Sn–O bond distance of 2.080 Å has been reported earlier for the $[Sn(OH)_3]^-$ unit in solid state.[15] It is also clear from Table 5.3 that the evaluation of any sample leads to the same conclusion.

## 5.2 Lead(II)

### 5.2.1 Raman spectroscopy and quantum chemical calculations

The Raman spectrum of a lead(II)-containing aqueous alkaline solution ($c_{Pb(NO_3)_2}$=0.1 M with $c_{NaOH}$=4.0 M) has been recorded. A strong peak at ~424 cm$^{-1}$ and a shoulder at ~355 cm$^{-1}$ were observed on the spectrum, corresponding to Pb–O asymmetrical and symmetrical stretching vibrations, respectively. A strong signal was also observed at 1048 cm$^{-1}$, due to the symmetric stretching mode of $NO_3^-$ ion. The Raman spectrum of a solution with similar composition has been reported in Ref. 43, with a peak at 419 cm$^{-1}$ and a shoulder at 377 cm$^{-1}$. These values are in good agreement with those in this study. In Ref. 43, the sample has been prepared from $PbO_{(s)}$ and a signal at 1064 cm$^{-1}$ was assigned to the species $[PbO_2]^{2-}$. It is important to note that there are obvious similarities between the Raman spectra of strong alkaline solutions containing tin(II) and lead(II). In the former, a strong peak was found at 430 cm$^{-1}$ and a weak at 490 cm$^{-1}$, and were assigned to the $[Sn(OH)_3]^-$ complex species. The lower wavenumbers for the lead(II) complex are expected resulting from its weaker electrostatic contribution to the Pb–O due to larger ionic radius.

Quantum mechanical calculations were performed to obtain proposed bond lengths and Raman band positions for the complexes with the possible structures. The results of these calculations are summarized in Table 5.4, the structure of the considered species can be seen in Figure 5.17.

As expected, the calculated bond lengths for Pb–O single bonds are significantly longer (2.23–2.43 Å), than those of Pb=O double bonds (1.99–2.10 Å). The calculated bond length for single bonds is very close to that obtained experimentally. On this ground, the formation of the fully dehydrated species $[PbO_2]^{2-}$ can be ruled out. If there were a mixed oxido-hydroxido complex, the two different bond lengths would be present in a single species. Since the exchange of the $H^+$ between the two oxygen atoms is slow in comparison with the EXAFS timescale, two

[2]This is most likely due to the stereochemical impact of the occupied anti-bonding orbitals of tin(II), and the energy difference between the occupied bonding and anti-bonding orbitals for different ligands.

**Table 5.4.** Comparison of the experimentally found and calculated bond lengths, as well as, Raman band positions for various hypothetic oxido-hydroxido complexes of Pb(II).

| | $N$ | $r$(Pb−O) (Å) | $r$(Pb=O) (Å) | Raman peaks ($cm^{-1}$) |
|---|---|---|---|---|
| | | Experimental | | |
| sample | – | 2.216 | | 355w, 424s[a] (377w, 419s)[b] |
| | | *ab initio* | | |
| $[Pb(OH)_3]^-$ | 3 | 2.232 | – | 370s, 413s |
| $[PbO(OH)_2]^{2-}$ | 3 | 2.430 | 2.050 | 222w, 256w, 523s |
| $[PbO(OH)]^-$ | 2 | 2.256 | 1.990 | 363w, 603s |
| $[PbO_2]^{2-}$ | 2 | – | 2.103 | 203w, 452s, 496s |
| $Pb(OH)_2$ | 2 | 2.123 | – | 458w, 488s |
| $[Pb(H_2O)_3]^{2+}$ | 3 | 2.440 | – | 261w, 291w |

w: weak, s: strong
[a] this work
[b] data from Ref. 43

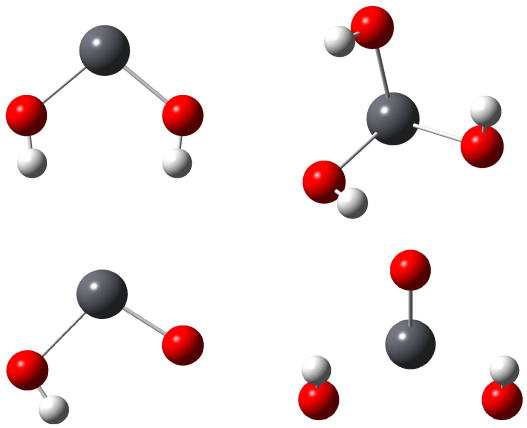

**Figure 5.17.** Ball and stick models for the oxido-hidroxido complexes of Pb(II) studied.

distinct peaks should be seen for $[PbO(OH)]^-$, which is obviously not the case (see Table 5.4 and Fig. 5.18 (A) later). On that ground, $[PbO(OH)_2]^{2-}$ and $[PbO(OH)]^-$ can be ruled out and the $[Pb(OH)_3]^-$ complex is the only reasonable lead(II) complex present in strong alkaline aqueous solution. The comparison of the observed and calculated Raman data in Table 5.4 also support the exclusive formation of $[Pb(OH)_3]^-$. The calculated Raman peak positions for this species almost perfectly match with those obtained here and in previous studies. On the other hand, the band positions for the other species show no resemblance to the observed one, and can therefore be excluded.

### 5.2.2 X-ray absorption spectroscopy

EXAFS measurements were carried out on aqueous samples containing 0.2 M lead(II) in 4.0, 8.0 and 16.0 M NaOH. The essence of the results are given in Table 5.5. No change in the local structure around lead(II) was observed with changing hydroxide concentration, and there was only one kind of species detected (Figure 5.18).

**Table 5.5.** Composition of alkaline aqueous lead(II) samples studied, and the structural parameters in the refinements of the EXAFS data collected at ambient temperature using the EXAFSPAK program package, including the number of Pb–O bond distances ($N$), the mean Pb–O bond distance ($r$), the Debye-Waller factor coefficient ($\sigma^2$), the threshold energy ($E_0$), the amplitude reduction factor ($S_0^2$) and the goodness of fit (F), as expressed in the EXAFSPAK program package, Ref. 82.

| $N = 3$ | $c_{\mathrm{NaOH}}$/M | $c_{\mathrm{Sn(II)}}$/M | $r$/Å | $\sigma^2$/Å$^2$ | $E_0$/eV | $S_0^2$ | $F$/% |
|---|---|---|---|---|---|---|---|
| Pb20_4 | 4 | 0.2 | 2.216 | 0.033 | 13064.0 | 1.01 | 18.5 |
| Pb20_8 | 8 | 0.2 | 2.222 | 0.033 | 13064.7 | 0.71 | 25.7 |
| Pb20_16 | 16 | 0.2 | 2.216 | 0.021 | 13065.0 | 0.51 | 22.0 |

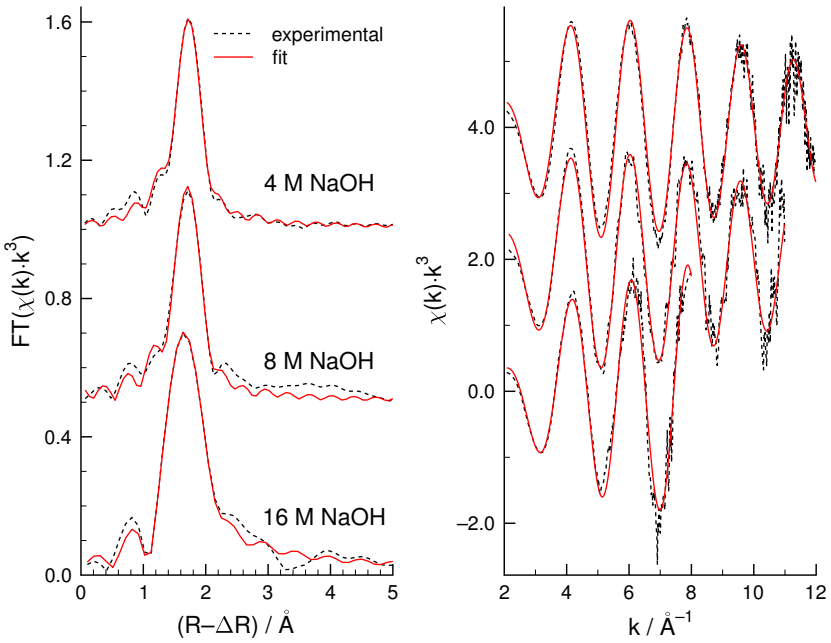


**Figure 5.18.** The experimental and the fitted Fourier-transform of the k$^3$-weighted EXAFS data of the alkaline lead(II) samples: Pb20_4, Pb20_8 and Pb20_16 (A); the experimental and the fitted k$^3$-weighted EXAFS data, respectively (B).

In this species, the Pb–O bond distance was determined to be 2.216 Å. It is indeed shorter than the average Pb–O bond distance for the three-coordinated lead(II) complexes with O-donor ligands, (2.318 Å, calculated as the average of ten known structures taken from databases).[121,122] However, it is still within the interval of the observed bond distances. For lead(II), to the best of

our knowledge, the structure of only one O-coordinated complex with $N = 2$ has been reported so far (with $r(\text{Pb–O}) = 2.189$ Å).[122] The fitting of out experimental EXAFS data was carried out with holding the coordination number fixed at 3 first. However, similarly to that observed for analogous systems containing Sn(II), good agreement was also achieved between the observed and calculated data by assuming $N = 2$. On the other hand, the case for $N = 4$ was discounted on the ground that the experimentally obtained $r(\text{Pb–O}) = 2.216$ Å is far out of the bond length interval obtained for solid complexes with $N =$ (2.30–2.46 Å). Therefore, the formation of any kind of 4-coordinate lead(II)-hydroxido complex, e.g., $[\text{Pb(OH)}_4]^{2-}$, in strong alkaline aqueous solution can be ruled out.

From extended X-ray absorption fine structure spectroscopy (EXAFS), bond lengths ($r$(Pb–O)) can be more accurately determined than the corresponding coordination numbers ($N$).[118] The relationship between the bond distance and the coordination number may be extracted from single crystal X-ray data. In many cases (i.e., for the transition metal complexes), this relationship can be used to estimate the coordination number from the observed bond distance.[118,120,123] The $r$(Pb–O) and $N$ values of crystalline solid O-coordinated lead(II) compounds were collected from the Inorganic Crystal Structure Database[121] and the Cambridge Crystal Structure Database,[122] and were published in a paper.[123]

The $r$(Pb–O) vs. $N$ data collected are shown in Figure 5.19. The bond lengths for O-coordinated lead(II) complexes are spread over a wide interval (e.g., 2.216–2.464 Å for $N = 3$). This is most likely due to the stereochemical impact of the occupied antibonding orbitals of lead(II).[124–127]

Based on the above detailed experiments and calculations, it can be said that the analogy between the tin(II)- and lead(II)-containing alkaline aqueous solutions is strict, the existence of only one dominating species can be proven experimentally, and the structure of these species are very similar in both chemical systems.

## 5.3 Chromium(III) in concentrated alkaline media

### 5.3.1 Preliminary experiments

Since spontaneous chromium(VI) formation from chromium(III) in alkaline media was not a generally accepted observation, it should be confirmed or refused, first. Its counterion dependence had to be investigated as well to complete these tasks. UV-vis spectra of three different solutions (including 8 M NaOH) were registered in time. The first solution contained $\text{Cr(ClO}_4)_3$ additionally, while the two others contained dissolved $\text{Cr(OH)}_3$—precipitated and washed from chromium nitrate and chromium sulphate solutions, respectively—in the same concentration. Each sample behaved the same way, proving that the quality of the counterion does not have

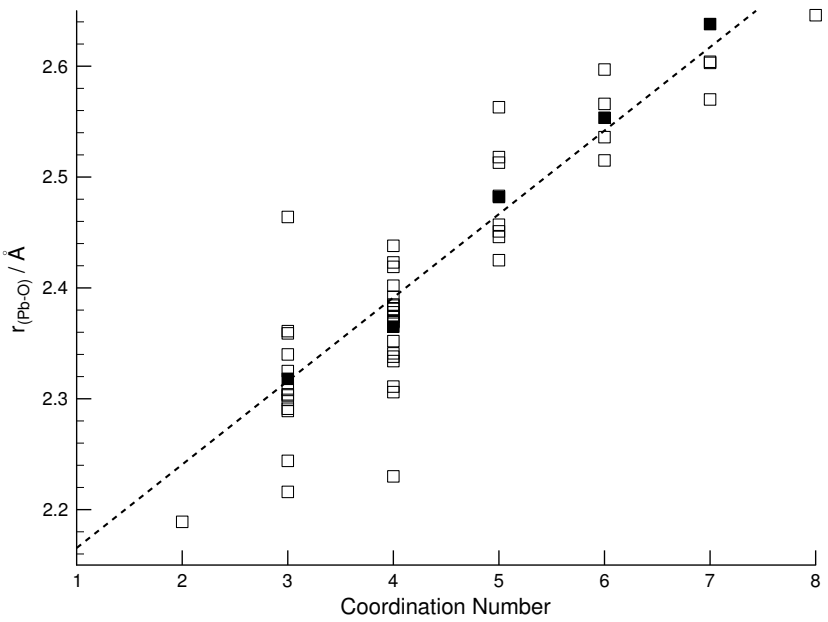


**Figure 5.19.** The relationship between the mean Pb–O bond lengths and the coordination number. The filled symbols stand for the average values. The dashed line represents the linear trend-line of the mean Pb-O bond distances as function of coordination number.

any effect on the reaction. A representative series of spectra is presented in Figure 5.20. The initial spectrum can be described with two absorbance maxima at 426 and 590 nm, while a new absorbance peak with the maximum at 374 nm begins to appear even after a few hours, and it increases with time. This peak is typical for $CrO_4^{2-}$ in alkaline media, as it can be seen in the figure. The molar absorbance of $CrO_4^{2-}$ at 374 nm is $\varepsilon$=4749.51 $dm^3mol^{-1}cm^{-1}$, while this value is more than three orders of magnitude lower for $[Cr(OH)_4]^-$ at 590 nm, thus the large increase in the absorbance at 374 nm belongs to a very small conversion of chromium(III) to chromium(VI).

### 5.3.2 Initial speciation in alkaline solutions

UV-vis spectra of $Cr(ClO_4)_3$ solutions in 8 M NaOH were registered right after homogenizing the stock solutions. The time spent between the measurement and the solution preparation was not longer than ten minutes to avoid noticeable redox reaction. The logarithm of chromium(III) concentration was varied evenly in more than two orders of magnitude, the concentrations were 0.0022; 0.0038; 0.0052; 0.0075; 0.0112; 0.0149; 0.0225; 0.0299; 0.0374; 0.0523; 0.0748; 0.0022; 0.1496; 0.2258; 0.2996 and 0.3747 M.

Two subsets of the measured absorbances were chosen for further evaluation. The maximum absorbance had to be 1.25 AU (absorbance unit) for both. All the 12 measured curves fulfilled this requirement in the 720–850 nm wavelength range, while the first nine curves completely

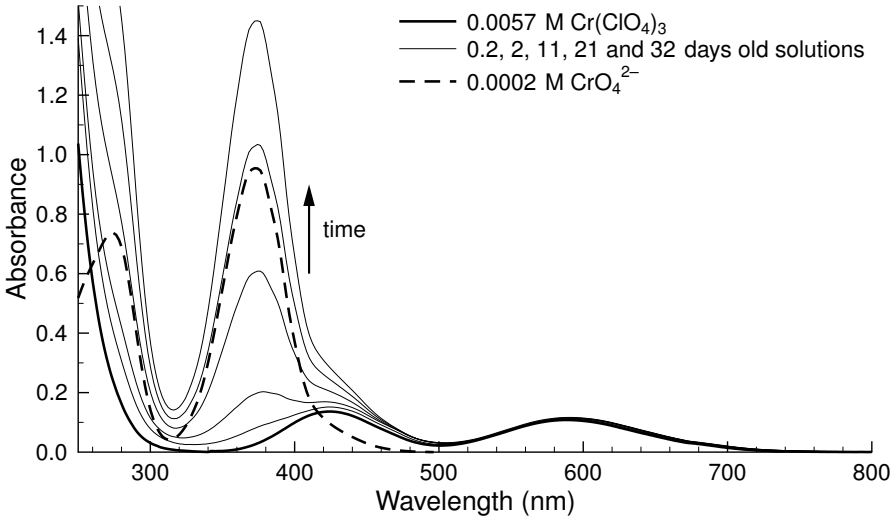


**Figure 5.20.** UV-vis spectra of Cr(III)/Cr(VI) ions in 8 M NaOH. The lowest solid curve is the initial spectrum of 0.0057 M $Cr(ClO_4)_3$, the upper five ones were recorded at given times after dissolving appropriate amount of $Cr(OH)_3$ (precipitated from $Cr(NO_3)_3$) and the dashed curve corresponds to the pure alkaline $CrO_4^{2-}$ solution.

below this upper limit. However, to exclude any absorption of $CrO_4^{2-}$, 600–850 nm was chosen as a second subset. The calculations detailed below were carried out for both subsets and gave the same results.

The number of independent absorbing species was determined by matrix rank analysis (MRA) using the MRA program package.[101] The calculations showed that the rank is strictly one with 0.0008 and 0.0006 AU uncertainty for the first and second subsets, respectively. Since the oligomerization assumed in the previous literature would not lead to provide constant concentration ratio of the oligo- and mononuclear species, the rank one means the absence of any significant oligomerization process.

Non-linear parameter estimation was also used to find other species than $[Cr(OH)_4]^-$. The PSEQUAD package[100] was used to ascertain about the existence of bi-, tri-, tetra- and other oligonuclear species. These calculations have also confirmed that only $[Cr(OH)_4]^-$ exists in significant concentration. It can describe both subsets within the uncertainty of 0.002 AU, which is about the experimental error. Regarding additional species can have changed this value to 0.001 AU. This decrease of the average deviation is insignificant, moreover, the distribution of the deviations remains the same. Consequently, only $[Cr(OH)_4]^-$ exists in 8 M sodium hydroxide right after preparing the solutions. Our statement is in contradiction only with the conclusion of Ref. 47 (where the dimerization was assumed to be completed within 100 s).

Figure 5.21 illustrates our results. All spectra are normalized to the one belonging 0.0299 M chromium(III)-containing solution by multiplying the measured absorbances with the ratio of

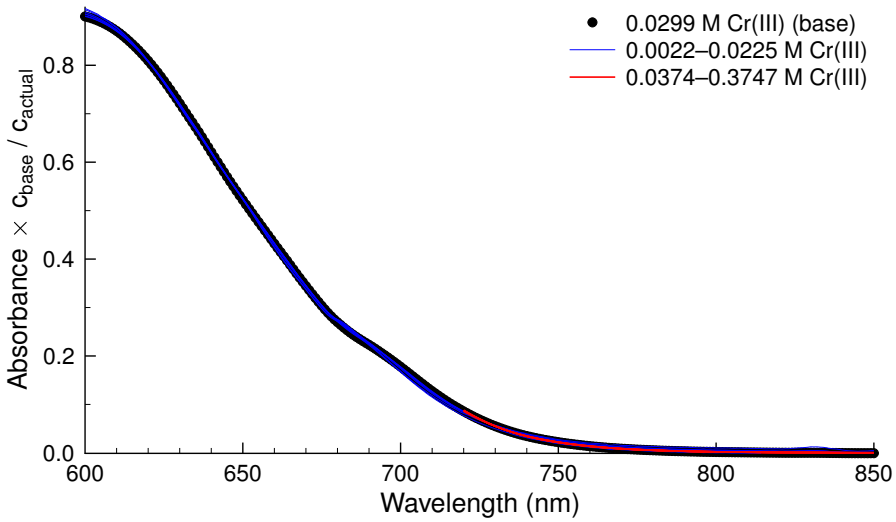


**Figure 5.21.** The normalized UV-vis spectra of $Cr(ClO_4)_3$ solutions in 8 M NaOH registered right after the mixing.

**Table 5.6.** The initial concentrations of the chromium(III)-containing alkaline samples prepared for kinetic experiments.

| No. | $c_{NaOH}$ (M) | $c_{Cr(III)}$ (mM) | No. | $c_{NaOH}$ (M) | $c_{Cr(III)}$ (mM) | No. | $c_{NaOH}$ (M) | $c_{Cr(III)}$ (mM) |
|---|---|---|---|---|---|---|---|---|
| 1 | 7.97 | 42.50 | 9 | 7.98 | 4.31 | 17 | 4.95 | 0.333 |
| 2 | 7.99 | 33.98 | 10 | 7.98 | 3.36 | 18 | 6.49 | 0.363 |
| 3 | 8.00 | 25.41 | 11 | 7.99 | 2.55 | 19 | 6.98 | 0.332 |
| 4 | 8.00 | 16.86 | 12 | 7.98 | 1.69 | 20 | 8.95 | 0.334 |
| 5 | 8.00 | 12.66 | 13 | 7.98 | 0.998 | 21 | 9.99 | 0.336 |
| 6 | 7.99 | 8.41 | 14 | 7.96 | 0.416 | 22 | 11.95 | 0.335 |
| 7 | 7.97 | 6.89 | 15 | 7.99 | 0.372 | 23[a] | 3.03 | 0.339 |
| 8 | 8.00 | 5.25 | 16 | 7.97 | 0.256 | 24[b] | 8.00 | 0.343 |

[a] 4 M $NaClO_4$ was also added to this sample.
[b] Oxygen gas has been bubbled through the reactive solution for one hour every second day.

0.0299 M and the actual concentration. The figure unequivocally shows that there is no change in the shape of the spectra, which would indicate any other species than $[Cr(OH)_4]^-$, initially.

### 5.3.3 The redox reaction in strongly alkaline media

The oxidation of chromium(III) to chromium(VI) was studied in the functions of the initial $Cr(ClO_4)_3$ and NaOH concentrations. The effect of added oxygen was also investigated on the kinetic curves. The composition of the samples are given in Table 5.6.

Samples 1–16 form a series, in which the initial chromium(III) concentration decreases at constant ∼8 M NaOH concentration. After preparing the reactive solutions, the UV-vis spectra

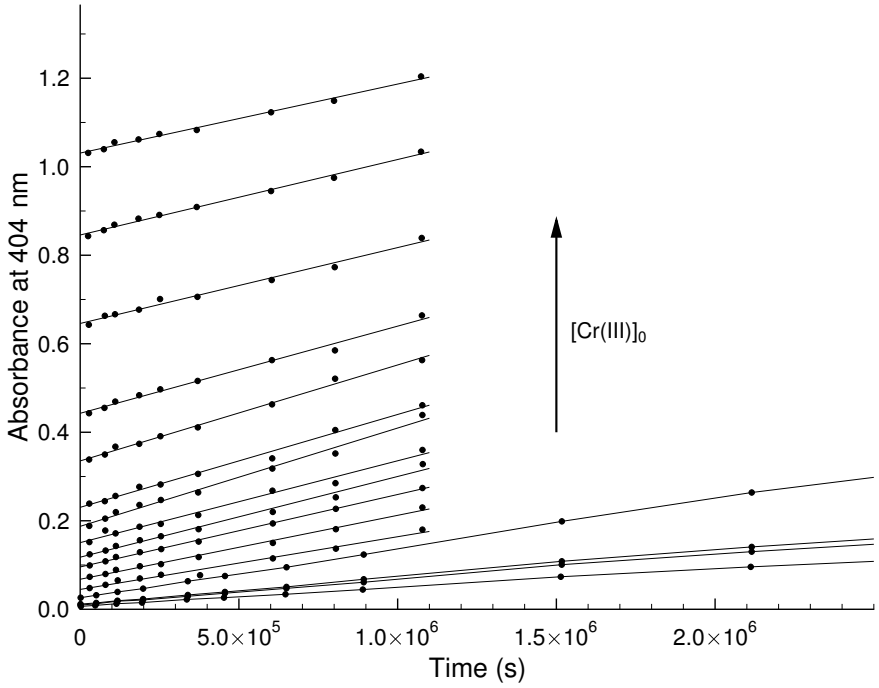


**Figure 5.22.** Absorbance vs. time curves at 404 nm, while the initial chromium(III) concentration increases from ∼0.00025 M to ∼0.04 M in 8 M NaOH solution. The concentrations are given in Table 5.6 as samples 1–16.

of the samples were recorded along the time passed. Figure 5.22 illustrates the absorbance changes during the first few weeks. During this period, the absorbance change caused by the decrease of chromium(III) cannot be larger than 0.003 AU, consequently, only the increasing chromium(VI) causes the measured absorbance change. It can be seen from Figure 5.22 and Table 5.6 that the initial rate of chromium(VI) production is proportional to the initial chromium(III) concentration, when its value is lower than ∼0.001 M. Higher initial concentrations do not produce higher initial rate, showing a pseudo-zeroth-order behavior on the initial chromium(III) concentration. To illustrate this, 404 nm seemed to be the best. Lower wavelength would be out of the valid range of Beer-Lambert law due to the high molar absorbance of chromium(VI), while the contribution of chromium(III) to the measured absorbance becomes more and more significant at higher wavelength.

Due to the slow reaction, no more than 10% of chromium(III) is oxidized during the first few weeks. Samples 1–8 could not be investigated further, since they started to be opalescent, which turned to precipitation after a few months. Solutions 9–12 remained clear, but their absorbances had run out of the detectable absorbance range, when the reaction was still going on. Only samples 13–16 could have been followed until the reaction has practically been finished. Figure 5.23 shows representative absorbance vs. time curves for the reaction (sample 15 is not shown, since it is practically identical to sample 14).

The curves characterizing the chromium(VI) formation (at 294, 314 and 404 nm) show the same structure. They can be divided into three ranges. If the reaction time is less than $2 \cdot 10^6$ s, the absorbance increases almost linearly. The second stage ends at $\sim 10^7$ s, and, at a first glance, it also seems to be linear but with smaller slope. A more careful examination in this stage, however, can reveal a small acceleration in absorbance increase. This shape suggest that either formally zeroth-order reaction steps and/or feedback reactions are necessary to describe the kinetics in this time range. The final stage starts at $\sim 10^7$ s, and simple exponential curves describe it satisfactorily. The lowest part of the figure suggests that the chromium(III) concentration decreases exponentially, but the absorbance change is close to the experimental uncertainty.

Figure 5.23 also contains the kinetic curves recorded, when the solution was saturated with $O_2$. Their structure is identical to that of the above detailed ones, only the reaction is faster about 3–4 times.

The curves in Figure 5.23 prove that the oxidation of chromium(III) to chromium(VI) proceeded stoichiometrically, since the last measured absorbances practically equal to the previously calculated ones if only chromium(VI) is in the solutions exclusively, when the reaction is over. All absorbance vs. time curves have the same structure in samples 13–24.

The hydrogen developed was also monitored by gas chromatography in several experiments, and 55?70 % of the stoichiometrically expected amount were measured.

### The effect of hydroxide concentration on the reaction rate

The NaOH concentration was varied between 3 and 12 M (samples 15 and 17–23 in Table 5.6) at nearly constant initial chromium(III) concentration. Constant ionic strength could not be set in these solutions due to the limited solubility of $NaClO_4$, thus, the ionic strength of these samples was basically equal to their alkaline concentrations. The viscosity in the samples also increased along increasing NaOH concentration.

The main observation was that both the absorbances at all stages and the initial rate of the absorbance change go through a maximum with changing NaOH concentration (at around 6–8 M). Figure 5.24 illustrates this trend at 336 nm, where the absorbance of chromium(III) can be neglected. Since sample 23 also fits into this trend, the effect is not the result of the varying ionic strength only; the initial hydroxide concentration must play a role in the mechanism.

The hydroxide concentration dependence of the reaction cannot be used in non-linear parameter estimation due to the large differences in the ionic strength. Nevertheless, the experiments can be interpreted, at least qualitatively. Presuming that the rate determining reaction step is a second-order one regarding to the hydroxide and the $[Cr(OH)_4]^-$, the change of the apparent rate coefficient can be calculated. Taking the extended Debye-Hückel theory (including the Davies correction) into account for interpreting the influence of ionic strength, as well as apply-

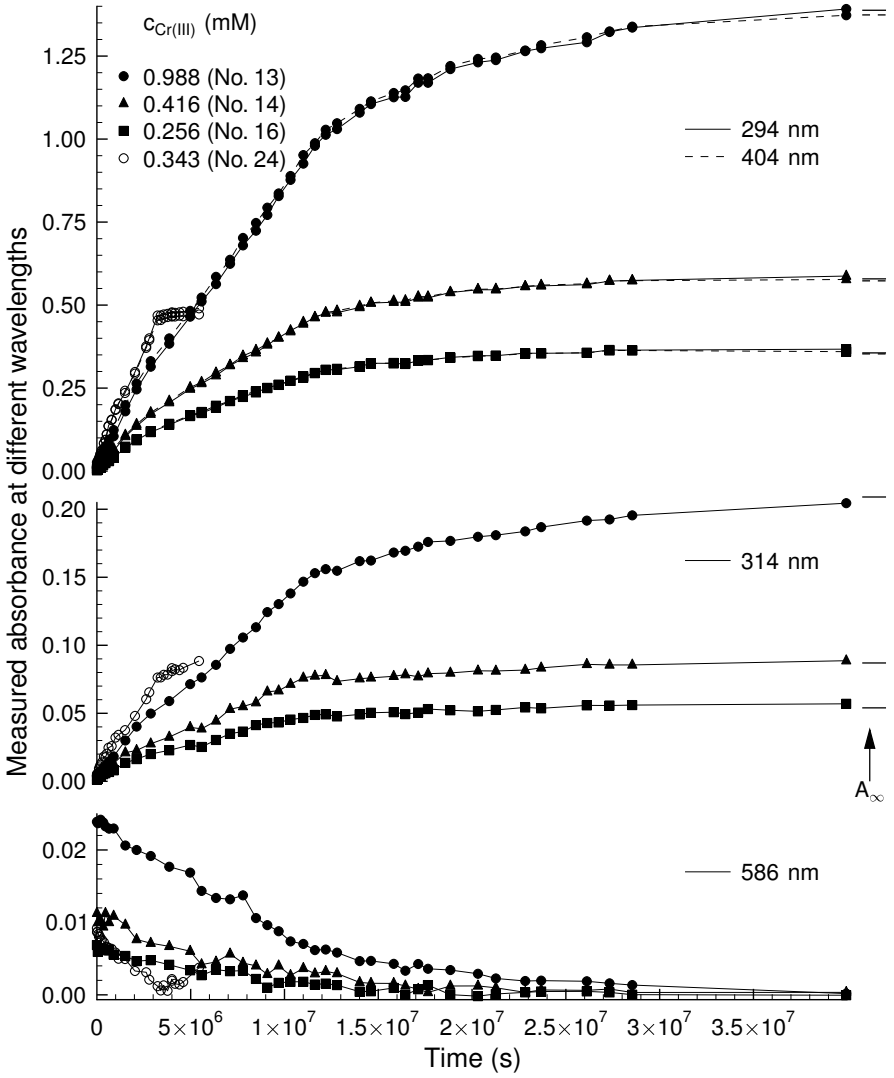


**Figure 5.23.** Absorbance vs. time curves for sample 13, 14, 16 and 24 at four different wavelengths. The molar absorbance values of Cr(VI) are almost identical at 294 and 404 nm, and they show minimum at 314 nm. The absorbances at 586 nm belong to the Cr(III), exclusively. The empty circle denotes the reaction, which was followed in a solution saturated with $O_2$. The rightmost horizontal lines indicate the calculated final absorbances if only Cr(VI) is present.

ing the Stokes-Einstein equation to consider the change of the viscosity, the following relation can be derived:

$$k(c_b) \sim \frac{10^{\left(\frac{1.02\sqrt{c_b}}{1+Br\sqrt{c_b}} + C_D c_b\right)} \cdot k_B T}{\pi \beta r \eta(c_b)}$$

where $c_B$ is the NaOH concentration, $k(c_B)$ is the concentration dependent second order rate coefficient, $B$ is the constant of the extended Debye-Hückel equation, $k_B$ is the Boltzmann constant, $T$ is the absolute temperature, $\beta$ can either be 4 or 6 (dependig on the assumptions

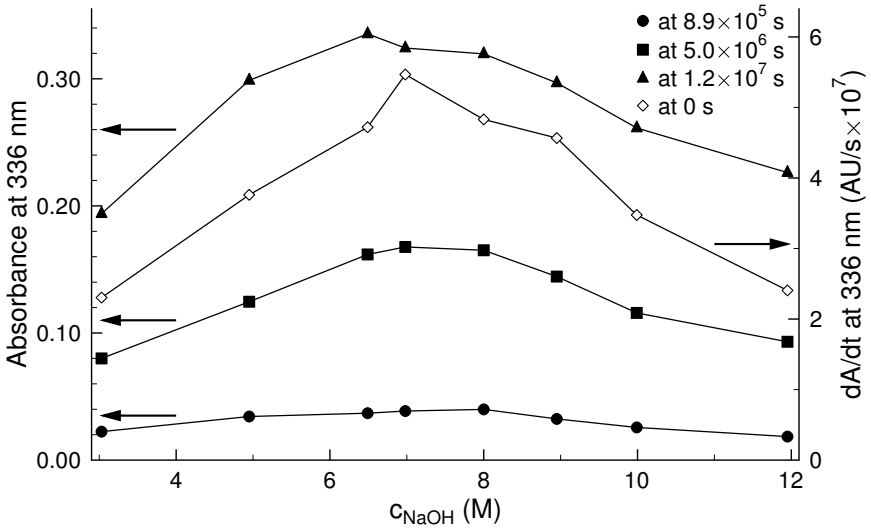


**Figure 5.24.** The measured absorbances at 336 nm (filled symbols) and the initial rate of the absorbance change (empty symbols) as a function of the NaOH concentration. To omit the effect of slightly changing initial chromium(III) concentration, every measured data were normalized to the planned 0.333 mM. The different times are representative for each stage of the reaction.

for the Stokes-Einstein equation), $C_D$ is the Davis constant, $r$ is the effective ion radii and $\eta(c_B)$ is the viscosity. The viscosity dependence of the highly concentrated NaOH solutions can be approximated by a five order polynomial.[76]

Depending on the values assumed for $r$ (2–9 Å) and for $C_D$ (–0.2 – +0.07), this expression shows a maximum in the 2–6 M range of hydroxide concentration. It means that it corresponds to our experiments assuming one for the partial orders of both the hydroxide and the chromium(III).

### Proposing the mechanism

Nonlinear parameter estimation was used to find the steps of the reaction.[102] The program package used is able to fit the parameters of any kinetic model using arbitrary number of kinetic curves simultaneously. Samples 13, 14 and 16 (in Table 5.6) were used in the calculations, since their kinetic curves remained in the valid range of Beer-Lamber law during the whole reaction time (∼1 year, see Figure 5.23). To reduce the calculation time, absorbances measured at four different wavelengths were chosen. At 294 and 404 nm, the molar absorbances of $CrO_4^{2-}$ are the same, but these values are different for $[Cr(OH)_4]^-$. At 314 nm, the molar absorbance of $CrO_4^{2-}$ shows a minimum, thus, the effect of the possible intermediates may be indicated here. Finally, the $[Cr(OH)_4]^-$ consumption can be followed at 586 nm. Four colored species were assumed in any kinetic model: $[Cr(OH)_4]^-$, $CrO_4^{2-}$, one chromium(IV) and one chromium(V) species. The precise composition of the two latter ones is not known, therefore they will be designated as $Cr^{IV}$ and $Cr^{V}$, respectively. During the calculations, the molar absorbances of the first two ones

**Table 5.7.** The rate coefficients of the finally proposed mechanism. The AR stands for the calculated average residuals by removing the corresponding steps from the mechanism.

| | Value | AR (AU) | Note |
|---|---|---|---|
| $k_1$ | $(3.0 \pm 0.2) \times 10^{-8}\,\mathrm{M^{-1}s^{-1}}$ | – | $a$ |
| $k_2/k_4$ | $(0.30 \pm 0.09)$ | 0.0087 | $b$ |
| $\frac{k_2}{k_4\sqrt{k_7}}$ | $(2.1 \pm 0.5) \times 10^{6}\,\mathrm{M^{-1/2}s^{1/2}}$ | 0.027 | $a$ |
| $k_4$ | $>5 \times 10^{-5}\,\mathrm{M^{-1}s^{-1}}$ | – | $a, c$ |
| $k_5$ | $(1.4 \pm 0.5) \times 10^{-4}\,\mathrm{M^{-2}s^{-1}}$ | 0.0084 | $b$ |
| $k_6/k_4$ | $(4.1 \pm 1.4) \times 10^{3}\,\mathrm{M^{-1}}$ | 0.026 | $a$ |
| $k_7$ | $7.7 \times 10^{9}\,\mathrm{M^{-1}s^{-1}}$ | – | $a, d$ |
| $k_8/\sqrt{k_7}$ | $(0.67 \pm 0.19)\,\mathrm{M^{-1/2}s^{-1/2}}$ | 0.021 | $a$ |

[a] These values are essential.
[b] Omitting these values increases the residuals slightly without changing the curvatures.
[c] The figures in this article were calculated with $k_4$=0.001 $\mathrm{M^{-1}s^{-1}}$.
[d] This value is taken from Ref. 128.

were fixed, while these parameters for the other two species were fitted together with the rate coefficients.

Several dozens of different kinetic models were tested to fit onto the experimental kinetic curves. The steps of the mechanism proposed finally are the followings:

$$\cdot\mathrm{Cr(OH)_4^-} + \mathrm{OH^-}\,(+\mathrm{H_2O}) \xrightarrow{k_1} \mathrm{Cr^{IV}} + \cdot\mathrm{H}\,(+6\,\mathrm{OH^-}) \tag{R5.1}$$

$$\mathrm{Cr^{IV}}\,(+\mathrm{H_2O}) \xrightarrow{k_2} \cdot\mathrm{Cr^{V}} + \cdot\mathrm{H}\,(+\mathrm{OH^-}) \tag{R5.2}$$

$$\cdot\mathrm{Cr^{V}} + \cdot\mathrm{H}\,(+\mathrm{OH^-}) \xrightarrow{k_3} \mathrm{Cr^{IV}}\,(+\mathrm{H_2O}) \tag{R5.3}$$

$$\cdot\mathrm{Cr^{V}}\,(+7\,\mathrm{OH^-}) \xrightarrow{k_4} \mathrm{CrO_4^{2-}} + \cdot\mathrm{H}\,(+3\,\mathrm{H_2O}) \tag{R5.4}$$

$$\cdot\mathrm{Cr(OH)_4^-} + \cdot\mathrm{Cr^{V}} + \mathrm{OH^-} \xrightarrow{k_5} 2\,\mathrm{Cr^{IV}}\,(+5\,\mathrm{OH^-}) \tag{R5.5}$$

$$\mathrm{Cr^{IV}} + \mathrm{CrO_4^{2-}}\,(+4\,\mathrm{H_2O}) \xrightarrow{k_6} 2\,\cdot\mathrm{Cr^{V}}\,(+8\,\mathrm{OH^-}) \tag{R5.6}$$

$$2\,\cdot\mathrm{H} \xrightarrow{k_7} \mathrm{H_2} \tag{R5.7}$$

$$\mathrm{Cr^{IV}} + \cdot\mathrm{H}\,(+\mathrm{H_2O}) \xrightarrow{k_8} \cdot\mathrm{Cr^{V}} + \mathrm{H_2}\,(+\mathrm{OH^-}) \tag{R5.8}$$

Because of the unknown composition of the intermediates, each reaction equation is given in two rows. The first one shows the essence of the step and its left side also defines the corresponding rate equation. The second row contains the compounds in parentheses needed to form stoichiometrically correct equations. The final parameter values are given in Tables 5.7 and 5.8.

**Table 5.8.** The molar absorbance values ($\varepsilon$, given in $dm^3mol^{-1}cm^{-1}$) used/fitted together with the rate coefficients during the nonlinear parameter estimation. The values indicated without errors was determined independently.

| wavelength (nm) | 294 | 314 | 404 | 586 |
|---|---|---|---|---|
| $\varepsilon([Cr(OH)_4]^-)$ | 8.34 | 4.20 | 25.90 | 24.80 |
| $\varepsilon(Cr^{IV})$ | $453 \pm 30$ | $79 \pm 13$ | $443 \pm 26$ | $39 \pm 5$ |
| $\varepsilon(Cr^{V})$ | – | – | $90 \pm 70$ | – |
| $\varepsilon(CrO_4^{2-})$ | 1391 | 209.7 | 1377 | 0.0 |

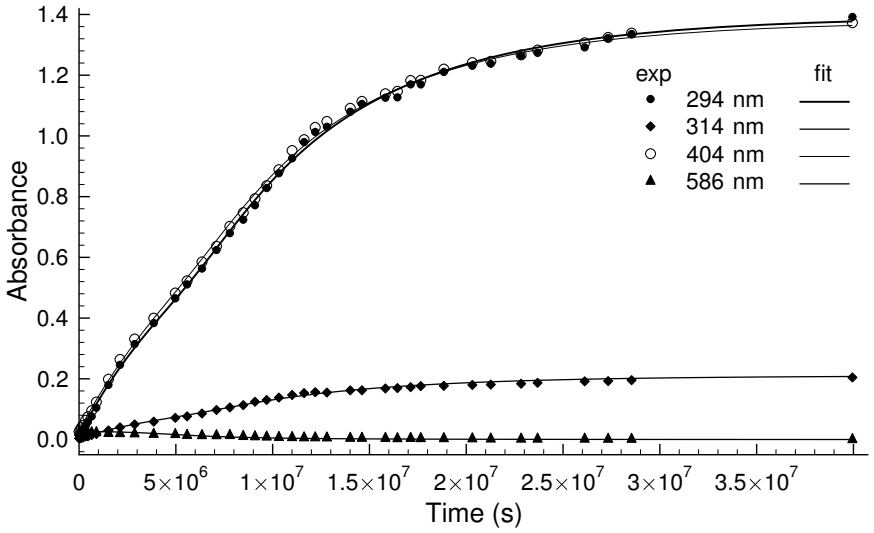


**Figure 5.25.** The measured absorbances (symbols) and the corresponding calculated curves (lines) using the finally proposed mechanism in case of sample 13.

The proposed steps are essentially the stepwise oxidation of chromium(III) to chromium(VI) through chromium(IV) and chromium(V). It requires a temporary formation of a radical, which is the hydrogen radical actually (other possibilities are also detailed below). Its recombination in water is a well-studied reaction, and the rate constant reported in Ref. 128 was used in our calculations as step R5.7.

The evaluation of the hydroxide dependent experiments has suggested that the starting R5.1 is a simple second order reaction. Among several possible steps, R5.8 and R5.4 were proven to be the most suitable ones to describe the consecutive oxidation steps until the chromate is formed. The completion of the reaction, however, is not so straightforward.

Using only these steps would produce simple exponential curves without any sign of the three stages. Two more steps are necessary to simulate the shapes of the experimental curves. Step R5.3 gives the temporary reduction of chromium(V) by the hydrogen radical, while step R5.6 describes a synproportionation reaction between chromium(IV) and chromium(VI). They can be considered as feedback reactions to explain the deviations from the exponential shape.

The above six steps are able to describe the experiments well, but two additional reactions improve the fit significantly. Step R5.2 is a parallel way to oxidize chromium(IV) to chromium(V), and step R5.5 is another synproportionation to produce chromium(IV) from chromium(III) and and chromium(V). The eight reaction steps together result in an average deviation (AR) of 0.0073 AU between the experiment and the calculated data. The third column in Table 5.7 gives the AR values calculated after mutual omission of the reaction steps if they were possible.

Table 5.8 gives the molar absorbance values used/fitted during the calculations. As it is clearly seen, these values could have been determined for chromium(IV) only and could not for chromium(V). It does not mean, however, that chromium(V) is capable for only weak light absorption. Due to the calculated concentration vs. time curves, the chromium(V) concentration is so small during the whole reaction time that its contribution to the absorbance is close to the experimental uncertainty. This explanation also agrees well with the result of matrix rank analysis carried out for the entire reaction time. The latter calculations showed that at least three independent colored species exist and the fourth species might exist, too.

The effect of the presence of oxygen (i.e., the 3–4 times faster reaction) is also to be explained. The key step cannot be the reaction of $[Cr(OH)_4]^-$ with $O_2$ since $[Cr(OH)_4]^-$ is almost the exclusive form of chromium(III) at $p$H$\geq$13, and the chromate formation cannot be noticed experimentally at $p$H$\sim$13. More probably, either the

$$Cr^{IV} + O_2 \longrightarrow Cr^{V} + \cdot O_2^- \qquad \text{(R5.9)}$$

or

$$Cr^{V} + O_2 \longrightarrow Cr^{VI} + \cdot O_2^- \qquad \text{(R5.10)}$$

reaction occurs, and the superoxide radical is reduced in more rapid subsequent reactions, corresponding to the

$$Cr(OH)_4^- + \cdot O_2^- \longrightarrow CrO_4^{2-} + 2\,H_2O$$

overall stoichiometry. These reactions do not influence the rate of the starting step R5.1, but they make a fast, subsequent transfer of four electrons, i. e., they open a new path for the chromate formation *only* if the first step of the original pathway took place. This way, the upper limit of the acceleration of $CrO_4^{2-}$ production is fourfold, interpreting the experimentally observed three-fourfold ratio quite well. Unfortunately, neither step R5.9 nor R5.10 is enough to describe the experimental effect alone. This combination resulted very high correlation with each other and the rate constants of the proposed mechanism, thus, trusted rate constants cannot be given for steps R5.9 and R5.10.

There is another experimental proof for the rightness of the proposed model. Although samples 9–12 could not be followed quantitatively in the entire time range (due to the high absorption of chromate), their spectra were recorded at $\sim 4 \cdot 10^7$ s (about 460 days). Surprisingly, there was not any sign for the presence of chromium(III). The proposed mechanism without the feedback steps; however, would suggest that 6.6 % of the original chromium(III) concentration have remained for each curve and this amount is easily detectable by UV-vis spectrometry. The chromium(III) concentration vs. time curves simulated by the full proposed mechanism for samples 9–12 clearly show an accelerated consumption of chromium(III), in accord with the observation. It also means that the chromium(III) to chromium(VI) transition can be even faster at higher initial concentration of chromium(III), although the chromate formation could not be followed so easily, due to the higher absorbances and the precipitation.

Finally, it has to be noted that not only our proposed steps are able to describe the experiments so well as it is shown in Figure 5.25. Step R5.7 is not the only reaction the hydrogen radical takes part in. This species is capable to react with either water or hydroxide very fast, to form other radicals, as it is summarized well in Refs. 128,129. To take the appropriate reactions from these references, the role of the hydrogen radical can be substituted by another radical (e.g., ·OH), and after adjusting the stoichiometries of steps R5.1–R5.8, the modified mechanism is able to serve as an identical replacement of our proposed one.

### 5.3.4 X-ray absorption spectroscopy

The previously reported[49] oligomerization is in contradiction with our results. To resolve it, time dependent EXAFS experiments were carried out. The spectra of a series of 0.5 M chromium(III) and 8 M NaOH were collected in order to verify the previous results. The solutions were aged for various times up to one month. Since the oxidation of chromium(III) is very slow under these conditions (at least initially), the forming chromium(VI) within this time range did not disturb the EXAFS measurements. The freshly prepared and the one week aged solutions were clear green and had quite low viscosity, while the more aged ones were more viscous and some precipitate appeared in them. These kinds of changes were explained by the oligomerization of $[Cr(OH)_4]^-$ previously.[49] On the contrary, all the EXAFS spectra and their Fourier transforms were the same, regardless of the age of the solutions (see Figure 5.26)

This fact can indicate two possibilities: the oligomerization takes place within minutes, or there is no oligomerization, and the above mentioned changes of the solution in time have to be explained differently. By the result of the UV-vis measurements, the second option is much more likely. The results of the EXAFS measurements are presented through the example of the one week aged sample, seen in Figure 5.27.

The model is described with three different Cr–O interatomic distances. The first coordination sphere consists of six Cr–O interatomic distances (belonging to the coordinating four

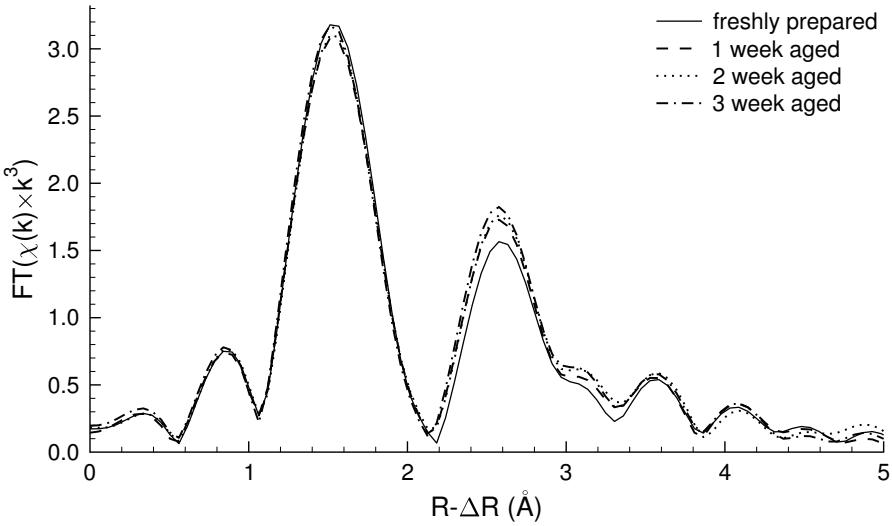


**Figure 5.26.** The Fourier transform of the EXAFS spectrum of solution containing 0.5 M Cr(III) and 8 M NaOH, aged for varying time.

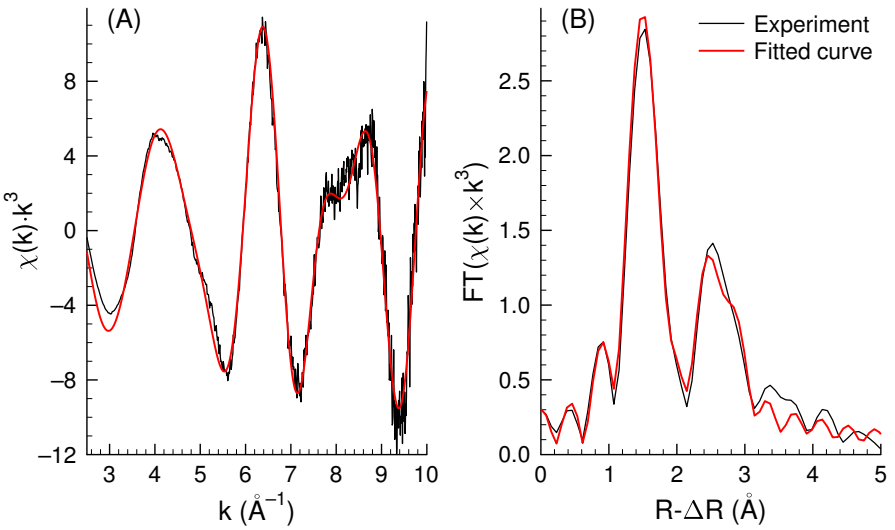


**Figure 5.27.** The experimental and fitted EXAFS spectra (A) for the 1 week aged sample and its Fourier transform (B).

$OH^-$ ions and two $H_2O$ molecules) at 1.99 Å with $\sigma^2$=0.00154 Å$^2$. The second, wide peak of the pseudo-radial distribution function can be described with two distances at 2.93 Å and 3.29 Å, both with coordination number of 8 and with Debye-Waller factors of 0.00189 and 0.01208 Å$^2$, respectively (F=17.85 %). This can be considered as the second hydration sphere of the $[Cr(OH)_4]^-$ complex. Any attempt to describe the second peak by Cr–Cr interatomic distances (i.e., by oligomers) failed to provide better agreement between the experimental and calculated curves, in accordance with UV-vis measurements. It has to be noted; however, that an assumed interatomic Cr–Cr distance is able to simulate the experiments with almost identi-

cal calculated curves, i.e., EXAFS is probably not a well-suited method to distinguish between the different models.

## 5.4 Chromium(III) in slightly acidic media

To study the hydrolysis of chromium(III) in slightly acidic media, seven solutions were prepared with varying total concentrations of the components. The *p*H of the samples as well as their absorbance values (in the range of 200–900 nm) were registered frequently for two months and a further few times some months later. It has to be noted that the equilibrium was still not reached in the solutions over a year of reaction time. The initial composition of the solutions investigated are listed in Table 5.9, the ionic strength was adjusted to 1 M with $NaClO_4$.

**Table 5.9.** The initial total concentrations of the solutions investigated with both *p*H-metry and UV-vis spectrophotometry, side by side.

| No. | 1. | 2. | 3. | 4. | 5. | 6. | 7. |
|---|---|---|---|---|---|---|---|
| $T(Cr^{III})$ / M | 0.0420 | 0.0210 | 0.0105 | 0.0420 | 0.0420 | 0.0420 | 0.0210 |
| T(NaOH) / M | 0.0320 | 0.0163 | 0.0080 | 0.0240 | 0.0161 | 0.0079 | 0.0101 |

These seven samples can be divided into two sets, the first one is characterized by constant $T(OH^-)/T(Cr^{III})$ ratio (samples 1–3), while the second one is with varying $T(OH^-)/T(Cr^{III})$ ratio at a constant 0.042 M total chromium(III) concentration (samples 1, 4–6). The experimental curves are shown in Figure 5.28 and 5.29, respectively.

The initial measured *p*H values of the solutions at constant $T(OH^-)/T(Cr^{III})$ ratio were nearly the same regardless of the absolute values of the concentration, so the system can probably be considered as a buffer at the beginning. Further on, the *p*H decreased faster in the solutions as the absolute concentration was higher. The most interesting observation is that the higher the initial $T(OH^-)$ the lower the measured *p*H at the end of the reaction. It means that the more the initial hydroxide concentration in the solution the more the released $H^+$ during the reaction. On the other hand, the $H^+$ formed slows down the reaction. This auto-inhibition-like behavior is responsible for the uniform curve shape and also for the increasing separation of the kinetic curves with increasing total concentrations.

The initially measured *p*H values of the solutions at varying $T(OH^-)/T(Cr^{III})$ ratio were different, as it was expected. The most interesting feature of these curves is that the decrease rate of the *p*H was proportional with the increase of the total hydroxide concentration at the beginning of the reaction (Figure 5.29). Due to the above mentioned auto-inhibition effect, all four solutions reached the same *p*H value on the fifth day of the experiment, and decreased together until approximately the twelfth day, when they started to diverge again. This separation caused by the intermediates presenting in different absolute concentrations. Finally, the

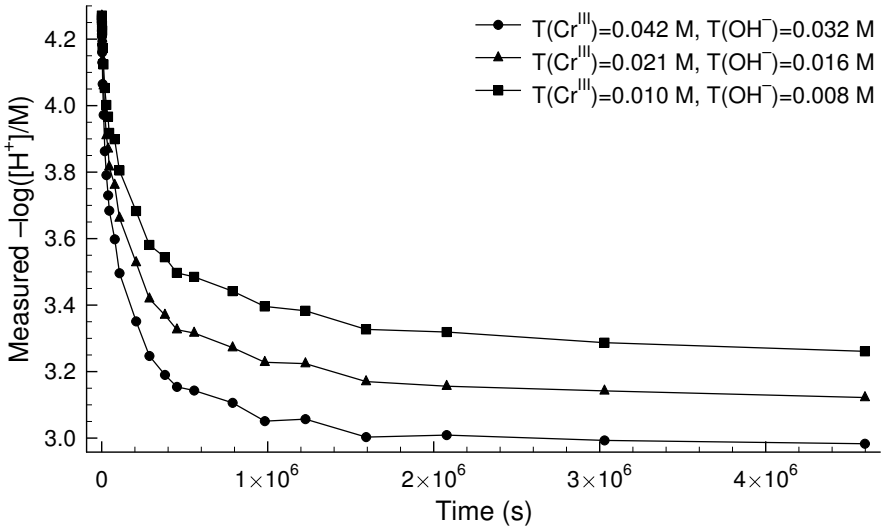


**Figure 5.28.** Measured $p$H-potentiometric data at constant $\mathrm{T(OH^-)/T(Cr^{III})} = 0.8$ ratio.

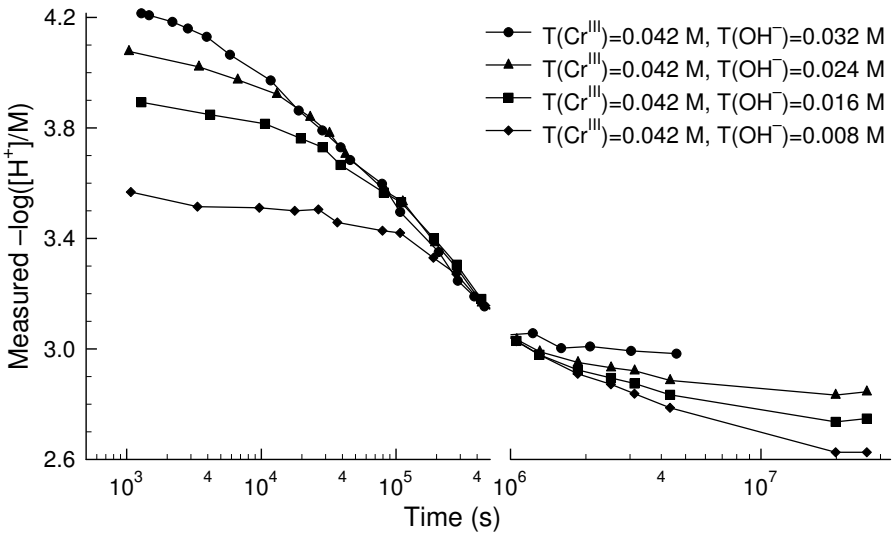


**Figure 5.29.** Measured $p$H-potentiometric data at varying $\mathrm{T(OH^-)/T(Cr^{III})}$ ratio. There is an $x$-axis break at around six days to make the initial changes more visible.

lowest $p$H could be measured in the solution having the smallest total hydroxide concentration. The similarities of these observations with those of Schaal and Faucherre (see Ref. 57, detailed on page 13) are remarkable.

The beginning of the hydrolysis reaction can be considered and treated as an equilibrium, therefore, the initial speciation can be determined by the PSEQUAD program[100] from the measured $p$H values and/or the ones extrapolated to the start of the reaction.

The first $p$H values were measured as soon as it was possible after the addition and homogenization of the reactive solution ($\sim$1000 s). The initial $p$H values belonging to $t = 0$ s were calculated by extrapolation, fitting an exponential curve for the first few measured values. During the evaluations both the primary measured and the extrapolated values were used. Since

**Table 5.10.** The fitted stability product and AR (average residual) values with the use of the measured and extrapolated initial $p$H values for the three possible initial compositions.

| $p$H measured | AR | $p$H extrapolated to $t = 0$ s | AR | Assumed hydroxo complex(es) |
|---|---|---|---|---|
| $\lg\beta_1 = -3.92 \pm 0.07$ | 0.19 | $\lg\beta_1 = -3.94 \pm 0.07$ | 0.17 | $Cr(OH)^{2+}$ |
| $\lg\beta_2 = -8.53 \pm 0.08$ | 0.11 | $\lg\beta_2 = -8.58 \pm 0.10$ | 0.13 | $Cr(OH)_2^{+}$ |
| $\lg\beta_1 = -4.277 \pm 0.026$<br>$\lg\beta_2 = -8.859 \pm 0.028$ | 0.018 | $\lg\beta_1 = -4.248 \pm 0.019$<br>$\lg\beta_2 = -8.967 \pm 0.026$ | 0.015 | $Cr(OH)^{2+}$, $Cr(OH)^{2+}$ |

$pK_w = 13.76$

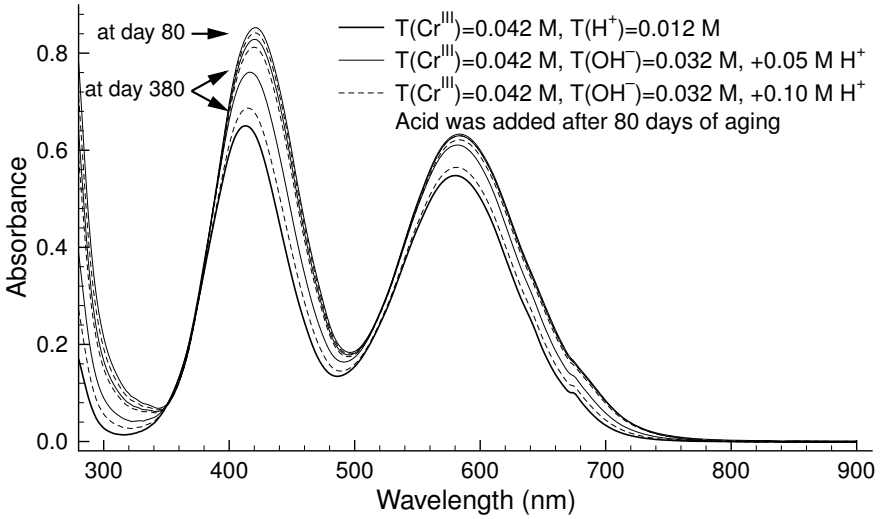


**Figure 5.30.** The UV-vis spectra of the solutions (originally $T(Cr^{III}) = 0.0420$ M, $T(OH^-) = 0.0320$ M) after adding excess acid to them on the $80^{th}$ day of the reaction and the spectrum of an acidic chromium(III) solution. (The two non-pointed spectra belong to day 88.)

result communicated in the literature are ambiguous on the existence of the $Cr(OH)_2^{+}$ complex, three different models were tested: one assumed only $Cr(OH)^{2+}$, the second one included only $Cr(OH)_2^{+}$ and the third one supposed both of them. The results are summarized in Table 5.10.

First of all, it can be concluded that the fitted values do not change significantly either the measured or the extrapolated data were used. For the third model (i.e. both the mono- and the dihydroxo complexes were assumed), the AR value of 0.018 is a little bit higher then the experimental uncertainty, and one order of magnitude lower than in cases of the other two models. The established $\log\beta_1 = -4.277$ and $\log\beta_2 = -8.859$ values are in good agreement with many ones reported in the literature.

To find out whether the overall reaction is an equilibrium one, excess perchloric acid was added to two portions of the solution 1 ($T(Cr^{III}) = 0.0420$ M, $T(OH^-) = 0.0320$ M) at the $80^{th}$ day of the reaction, and their UV-vis spectra were also registered over further 300 days. Some representative spectra (at days 80, 88 and 380) are shown in Figure 5.30. The concentration of

the excess $H^+$ was 0.05 M and 0.10 M in these two new samples without noticeable dilution of the original content.

It is seen that the spectra were changing very slowly but continuously, and they gradually approach the starting one containing only $[Cr(H_2O)_6]^{3+}$. The rate of the spectrum change is faster at higher acid excess. Thus, it can be concluded that this is an equilibrium reaction, but the large excess of acid is needed for measurable rate of the backward reaction.

In view of the the initial speciation and the quantitative description of the reaction at different absolute and/or relative chromium(III) and hydroxide concentrations, the following reaction mechanism is proposed after trying several dozens of different kinetic models (the rate equations belonging to each reaction are also listed below the reaction equation, and the coordinating water molecules are denoted with $w$ for simplicity) and its rate coefficients are summarized in Table 5.11.:

$$\mathrm{Cr}w_6{}^{3+} \underset{k_{11}^b}{\overset{k_{11}^f}{\rightleftharpoons}} \mathrm{Cr}w_5\mathrm{OH}^{2+} + \mathrm{H}^+ \qquad \text{(R5.11)}$$

$$r_{11}^f = k_{11}^f \cdot [\mathrm{Cr}w_6{}^{3+}]$$

$$r_{11}^b = k_{11}^b \cdot [\mathrm{Cr}w_5\mathrm{OH}^{2+}] \cdot [\mathrm{H}^+]$$

$$\mathrm{Cr}w_5\mathrm{OH}^{2+} \underset{k_{12}^b}{\overset{k_{12}^f}{\rightleftharpoons}} \mathrm{Cr}w_4(\mathrm{OH})_2{}^{+} + \mathrm{H}^+ \qquad \text{(R5.12)}$$

$$r_{12}^f = k_{12}^f \cdot [\mathrm{Cr}w_5\mathrm{OH}^{2+}]$$

$$r_{12}^b = k_{12}^b \cdot [\mathrm{Cr}w_4(\mathrm{OH})_2{}^{+}] \cdot [\mathrm{H}^+]$$

$$2\,\mathrm{Cr}w_5\mathrm{OH}^{2+} \underset{\text{too slow}}{\overset{k_{13}}{\rightleftharpoons}} w_5\mathrm{Cr{-}O{-}Cr}w_5{}^{4+} \qquad \text{(R5.13)}$$

$$r_{13} = k_{13} \cdot [\mathrm{Cr}w_5\mathrm{OH}^{2+}]^2$$

$$2\,\mathrm{Cr}w_4(\mathrm{OH})_2{}^{+} + \mathrm{H_2O} \underset{\text{too slow}}{\overset{k_{14}}{\rightleftharpoons}} w_5\mathrm{Cr{-}O{-}Cr}w_5{}^{4+} + 2\,\mathrm{OH}^- \qquad \text{(R5.14)}$$

$$r_{14} = k_{14} \cdot [\mathrm{Cr}w_4(\mathrm{OH})_2{+}]^2$$

$$2\,\mathrm{Cr}w_4(\mathrm{OH})_2{}^{+} \underset{\text{too slow}}{\overset{k_{15}}{\rightleftharpoons}} w_4\mathrm{Cr{-}O_2{-}Cr}w_4{}^{2+} \qquad \text{(R5.15)}$$

$$r_{15} = k_{15} \cdot [\mathrm{Cr}w_4(\mathrm{OH})_2{+}]^2$$

$$w_4\mathrm{Cr{-}O_2{-}H{-}Cr}w_4{}^{3+} \underset{k_{16}^b}{\overset{k_{16}^f}{\rightleftharpoons}} w_4\mathrm{Cr{-}O_2{-}Cr}w_4{}^{2+} + \mathrm{H}^+ \qquad \text{(R5.16)}$$

$$r_{16}^f = k_{16}^f \cdot [w_4\mathrm{Cr{-}O_2{-}H{-}Cr}w_4{}^{3+}]$$

$$r_{16}^b = k_{16}^b \cdot [w_4\mathrm{Cr{-}O_2{-}Cr}w_4{}^{2+}] \cdot [\mathrm{H}^+]$$

$$w_5\mathrm{Cr{-}O{-}Cr}w_5{}^{4+} \underset{k_{17}^b}{\overset{k_{17}^f}{\rightleftharpoons}} w_4\mathrm{Cr{-}O_2{-}Cr}w_4{}^{2+} + 2\,\mathrm{H}^+ + \mathrm{H_2O} \qquad \text{(R5.17)}$$

$$r_{17}^f = k_{17}^f \cdot [w_5\mathrm{Cr{-}O{-}Cr}w_4{}^{4+}]$$

$$r_{17}^b = k_{17}^b \cdot [w_4\mathrm{Cr{-}O_2{-}Cr}w_4{}^{2+}] \cdot [\mathrm{H}^+]^2$$

**Table 5.11.** The rate coefficients of the finally proposed mechanism.

| | Value | Note |
|---|---|---|
| $k_{11}^f$ | $5.75\times10^{-5}\,\mathrm{s}^{-1}\cdot k_{11}^b$ | $a$ |
| $k_{11}^b$ | $1.00\times10^{9}\,\mathrm{M}^{-1}\mathrm{s}^{-1}$ | $b$ |
| $k_{12}^f$ | $1.93\times10^{-5}\,\mathrm{s}^{-1}\cdot k_{12}^b$ | $a$ |
| $k_{12}^b$ | $1.00\times10^{9}\,\mathrm{M}^{-1}\mathrm{s}^{-1}$ | $b$ |
| $k_{13}$ | $(6.0\pm0.4)\times10^{-5}\,\mathrm{M}^{-1}\mathrm{s}^{-1}$ | $a$ |
| $k_{14}$ | $(1.1\pm0.2)\times10^{-2}\,\mathrm{M}^{-1}\mathrm{s}^{-1}$ | $a$ |
| $k_{15}$ | $(3.0\pm0.3)\times10^{-2}\,\mathrm{M}^{-1}\mathrm{s}^{-1}$ | $a$ |
| $k_{16}^f/k_{16}^b$ | $>10^{-3}\,\mathrm{M}$ | $a$ |
| $k_{17}^f/k_{17}^b$ | $>3\times10^{-3}\,\mathrm{M}$ | $a$ |

[a] These values were fitted.
[b] These values were held to be constant, but any value larger than $1\cdot10^{5}\,\mathrm{M}^{-1}\mathrm{s}^{-1}$ would be appropriate.

The first two reactions (R5.11 and R5.12) are the fast formation of the $Cr(OH)^{2+}$ and $Cr(OH)_2{}^{+}$ complexes, with lgK values of $-4.24$ and $-4.714$, respectively. These values are practically identical to the ones calculated from the initial measured $pH$ values by the PSEQUAD program package (see Table 5.10 on page 59). It also confirms that the formation of the $Cr(OH)_2{}^{+}$ cannot be neglected in slightly acidic media.

Reactions R5.13 and R5.14 describe the formation of a dimer complex bonding with a single oxigen ($w_5\mathrm{Cr}{-}\mathrm{O}{-}\mathrm{Cr}w_5{}^{4+}$) by the reaction of two monohydroxido or two dihydroxido complexes. The reaction between a monohydroxido and a dihydroxido complex also possible, but its rate coefficient cannot be determined, since this reaction is the combination of R5.13 and R5.14, and the simultaneous fitting of three parameters resulted in complete correlation. These reactions are certainly reversible, but the rate coefficients of the backward reactions could not be determined in the $p$H range of our measurements, since these reactions become significant only at higher $H^+$ concentrations, as it was clearly seen from those experiments, where excess acid was added to the aged solutions.

From the reaction of two dihydroxido complexes, the formation of a double-bonded dimer ($w_4\mathrm{Cr}{-}\mathrm{O}_2{-}\mathrm{Cr}w_4{}^{2+}$) is also possible according to the equation R5.15. Just as for the single-bonded dimer, the cleavage of the double-bonded one also does not play role under the experimental conditions applied, although they certainly take place at lower $p$H. The protonation-deprotonation equilibrium of this complex is also an important part of the reaction mechanism (R5.16).

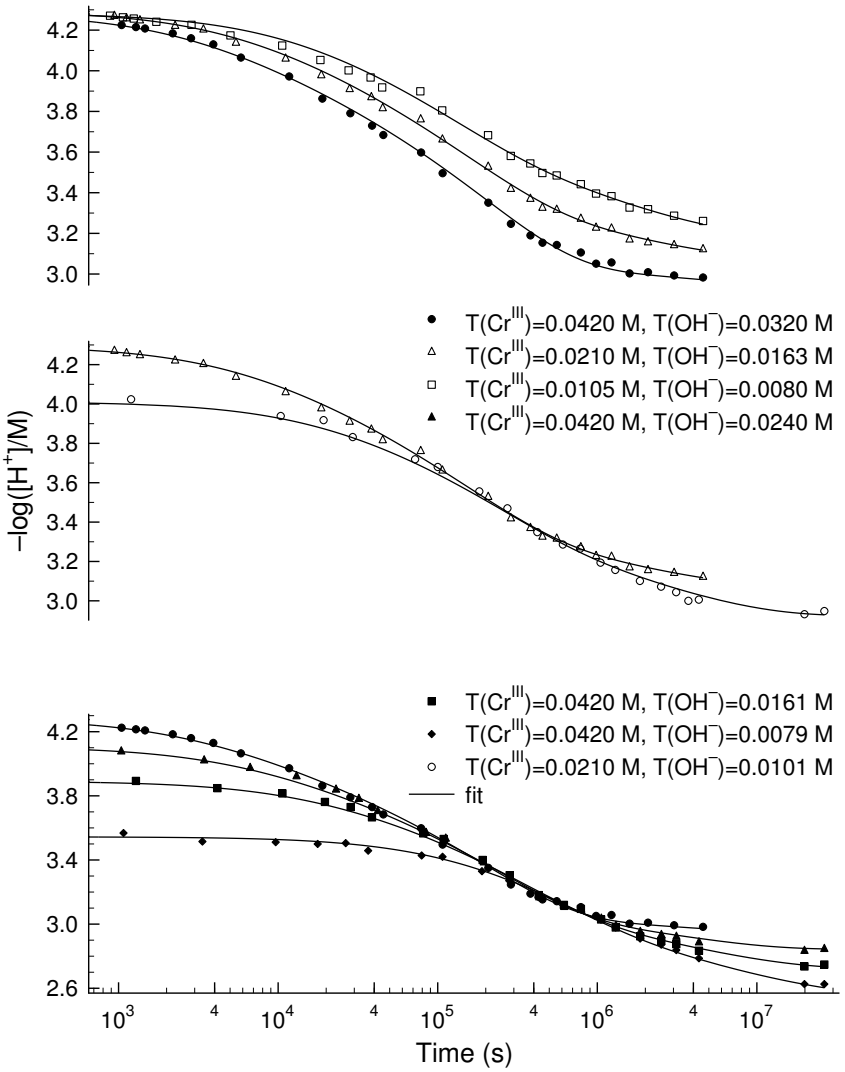


**Figure 5.31.** The measured absorbances (symbols) and the corresponding calculated curves (lines) using the finally proposed mechanism.

The double-bonded dimer can also be formed from the single-bonded one with releasing water and $H^+$ (R5.17). The last two reactions are not independent from the others, thus only relations for the ratio of their reaction coefficients could be estimated.

This mechanism describes the experimental data with an average residual of 0.017 $p$H unit, which is comparable to the experimental error. Both the experimental and the fitted data are collected in Figure 5.31.

Summing up all these, the kinetic curves of the pH-metric study strongly suggest that only dimer formation takes place and more complicated species should not be supposed.

To give structural confirmation of this statement, EXAFS measurements were performed on several solutions containing 0.2–0.5 M chromium(III) perchlorate prepared at different times before the measurements. The samples also included added sodium hydroxide with constant

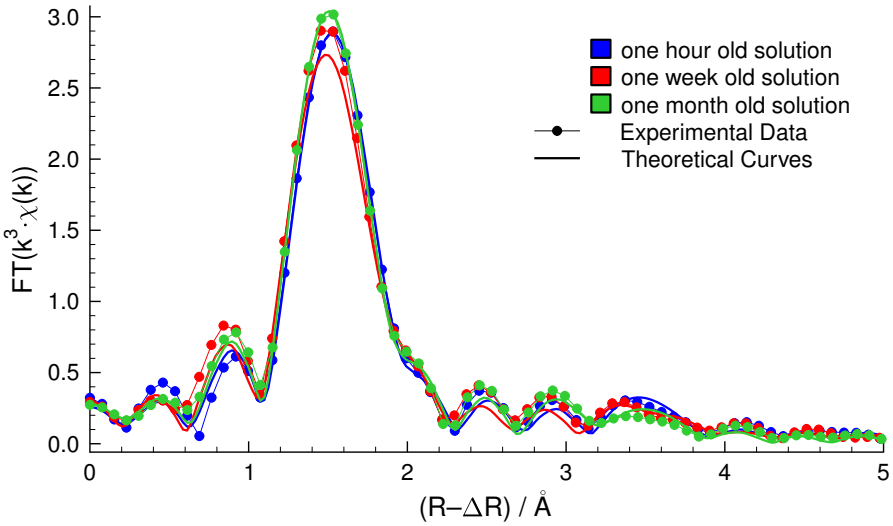


**Figure 5.32.** Fourier transforms of $k^3$-weighted EXAFS data of experimental and fitted curves of aqueous solutions initially containing 0.5 M chromium(III) perchlorate and 0.4 M sodium hydroxide after different aging time.

$T(OH^-)/T(Cr^{III}) = 0.8$ ratio. Finally, only the most concentrated solutions gave satisfactory results, the Fourier transform of their spectra are given in Figure 5.32.

The evaluation of these data clearly shows that no considerable changes happen even up to one month, which indicates that there are no significant changes in the structure around the chromium(III).

Assuming only a dimer is completely sufficient to back-calculate the measured data within the experimental uncertainties. In this dimer, the two chromium(III) ions are connected through either one or two oxygen bridge(s). In the primary octahedral coordination sphere of every chromium(III), there are two kinds of oxygen atoms, with 1.98 and 2.43 Å, and the distance between the two chromium(III) ions is 3.65 Å in the dimer (F% = 18.2). Due to the necessary large concentrations, the dimer is formed in reasonable concentration within one hour.

It should be noted that assuming only one dimer for EXAFS measurements may lead to a contradiction, since more forms of the dimer were assumed in the calculations. The EXAFS, however, in not able to distinguish Cr–O distances differing less than ∼0.2 Å so the single- and the double-bonded oxygen atoms provide an integral average sign.

The EXAFS measurements confirmed the results of the *p*H-metric data, since there were no need to include higher oligomers in the model to fit the measured data.

# 6 Conclusions

The available literature data is scarce and contradictory on the hydrolysis of tin(II), lead(II) and chromium(III) in strong alkaline media ($[OH^-]$>1 M). The composition, and the stability constants of the hydroxido complexes formed in these alkaline aqueous solutions are uncertain, and their structures are barely investigated in solutions. An additional difficulty arose especially for chromium(III), which unexpectedly showed a spontaneous oxidation to chromium(VI) under such highly alkaline conditions.

The overall aims of my doctoral studies was to clarify the composition and the structure of these complexes, and to investigate the spontaneous oxidation reaction of chromium(III) in alkaline solutions.

The composition of the tin(II) complexes were determined by potentiometric titrations using a $H_2$/Pt electrode operational in strong alkaline solutions (up to 5 M NaOH). The measurements confirmed that the tin(II):$OH^-$ ratio was 1:3, excluding the existence of $[Sn(OH)_4]^{2-}$ or higher hydroxido complexes. The structure of the complex was investigated by several methods. Both the XAS and Raman measurements suggested that the coordination number around tin(II) was three in the complex formed. The theoretical Raman spectra were also calculated for the possible species (i.e. $[Sn(OH)_3]^-$ and $[SnO(OH)]^-$), and the observation that the calculated and the experimental Raman bands showed exact match only for $[Sn(OH)_3]^-$ made this structure unambiguous. The intensity of the measured Raman spectra followed the Beer-Lambert law with the increasing tin(II) concentration, thus, it was confirmed that there was only one kind of species present under such conditions. This was also confirmed by $^{117}$Sn NMR spectroscopy. The $[Sn(OH)_3]^-$ complex was found to have a distorted trigonal pyramid structure with an average Sn–O distance of 2.078 Å and a Debye-Waller factor of 0.0038 Å$^2$ derived from the EXAFS spectra collected on strongly alkaline solutions containing tin(II). The local geometry around tin(II) was also aimed to be investigated by $^{119}$Sn Mössbauer spectroscopy both in quick frozen solutions and solutions at room temperature with the help of capillary Mössbauer spectroscopy. The latter was found to be impossible either in acidic or alkaline media due to the steep temperature dependence of Lamb-Mössbauer factor of tin(II), which results in the disappearance of the spectra below the melting point of the solutions. This was derived from a series of temperature dependent spectra of a quickly frozen, alkaline sample. The spectra

collected from these quick frozen strongly alkaline samples also confirmed the trigonal pyramid geometry for the complex.

Lead(II), similarly to tin(II), has $d^{10}s^2$ valence electron structure, was also systematically investigated. For lead(II), however, the composition could not be determined by potentiometry, due to its limited solubility under strongly alkaline conditions. The Raman spectra of lead(II)-containing solutions were recorded, and the theoretical spectra of the possible species, (i.e., $[PbO(OH)]^-$, $[Pb(OH)_3]^-$, $[Pb(OH)_4]^{2-}$ and more, lesser-likely species) were also calculated. The observed and calculated Raman peaks were found to be superimposable only for $[Pb(OH)_3]^-$. Just as for tin(II), the intensity of the measured Raman spectra followed the Beer-Lambert law with increasing lead(II) concentration, thus, it can be concluded that there was only one kind of species present in detectable quantity in concentrated hydroxide solutions. The lead $L_3$-edge XAS measurements further confirmed the above structure. According to the EXAFS spectra and the literature data, the coordination number around lead(II) was found to be three with an average Pb–O distance of 2.216 Å and a Debye-Waller factor of 0.0330 Å$^2$.

The recently discovered oxidation of chromium(III) to chromium(VI) was experimentally confirmed, as well as studied in detail during my doctoral work. The spectra of deoxygenated solutions with varying initial chromium(III) and hydroxide concentrations were monitored over more than a year. The reaction was found to be spontaneous, even without any traces of oxygen. The reaction is completed stoichiometrically; however, the process is very slow. Its kinetic curve can be divided into three distinct ranges. While the first two can formally be described by zeroth-order kinetics (but with different slopes), the final stage can be characterized by a simple exponential curve. The reaction rate passes through a maximum with the changing NaOH concentration at around 6–8 M, which can be explained qualitatively by assuming that the rate determining step is a second order one regarding the hydroxide and the $[Cr(OH)_4]^-$ ions. The apparent rate coefficient can be calculated with taking the extended Debye-Hückel theory (including the Davies correction) for interpreting the influence of ionic strength, as well as applying the Stokes-Einstein equation to account for the change in viscosity. Based on all these considerations and also on the fact that four independent colored species are needed to explain all the measured absorbances (according to the matrix rank analysis performed on the spectra collected), an eight-step mechanism was proposed. Its starting point is the reaction taking place between the hydroxide and $[Cr(OH)_4]^-$ ions, and it goes through intermediates containing chromium(IV) and chromium(V).

In the literature, chromium(III) was claimed to be present as oligo- and polymeric species above $p\mathrm{H} = 13$, analogous to some of the speciation models proposed for slightly acidic solutions. The UV-vis spectra of a series of solutions containing 8 M NaOH with varying chromium(III) were recorded right after the mixing. According to the matrix rank analysis performed, the initial number of the independent absorbing species is strictly one, which means only one kind

of species could be present in significant concentration. This result was also confirmed by using non-linear parameter estimation, where the best fit was obtained by a model assuming only $[Cr(OH)_4]^-$ in the chemical model, and it could not be improved with assuming any further species. XAS measurements were also carried out on such solutions, ranging from freshly prepared to 1 month aged. All the EXAFS spectra were found to be identical within the experimental error, wether it contained precipitation or not. The spectra could be fitted without assuming any oligomeric species, also indicating that the $[Cr(OH)_4]^-$ was the only dominant species in the solution phase.

The speciation, as well as the occurring reactions in slightly acidic chromium(III) solutions ($0 < T(OH^-)/T(Cr^{III} < 1$) were also investigated, since they served as analogy for the alkaline systems, however, its description is controversial in the literature. The $p$H and the UV-vis spectra of the solutions were monitored up to more than a year. The $p$H of these solutions decreased monotonously with time until the equilibrium was reached. In these reactive systems, the initially measured pH values can be explained via assuming the formation of $[Cr(OH)]^{2+}$ and $[Cr(OH)_2]^+$. Their stability products were found to be $\lg\beta_1 = -4.28 \pm 0.03$ and $\lg\beta_2 = -8.86 \pm 0.03$, respectively. Any other speciation yielded poor fits, and described our measurements with at least five-fold higher average residual. The $\lg\beta_1$ is practically identical with those reported, while our $\lg\beta_2$ points to the less significant presence of $[Cr(OH)_2]^+$ relative to previous reports in the literature. It was found that the reaction between $[Cr(OH)]^{2+}$ and $[Cr(OH)_2]^+$ was responsible for the kinetic changes observed. It was experimentally proven that all steps were equilibrium ones, and the final solution contained only dimers, consequently, the presence of more complicated oligomers is not supported by these measurements. We also proposed a seven-step mechanism for the dimerization reaction. The exclusion of the oligomer formation was further confirmed by EXAFS measurements. The spectra of our solutions could be fitted satisfactorily by assuming only one Cr–Cr distance, suggesting that only the dimeric species are present, and higher oligomers are absent.

# Összefoglalás

Az ón(II), az ólom(II) és a króm(III) ionok erősen lúgos közegű ($[OH^-]>1\,M$) hidrolízisére vonatkozó szakirodalom meglehetősen hiányos, ill. ellentmondásos. Az ilyen erősen lúgos, vizes oldatokban képződő hidroxido komplexek összetételei és stabilitási állandói nem egyértelműek, szerkezetüket oldatfázisban kevéssé vizsgálták. A króm(III) esetében még az oxidációs állapot stabilitása is kérdéses, mivel ilyen körülmények között felmerült a spontán króm(VI)-tá történő oxidálódás lehetősége is.

Doktori munkám során célul tűztem ki, hogy tisztázzam a képződő hidroxido komplexek összetételét és szerkezetét, valamint részletesen tanulmányozzam a króm(III) spontán oxidációját erősen lúgos közegben.

Az 1–5 M NaOH-ot tartalmazó vizes oldatokban az ón(II) komplex(ek) összetételét $H_2$/Pt elektróddal végzett *p*H-potenciometriás mérésekkel határoztuk meg. A mérések bizonyították, hogy az ón(II):$OH^-$ arány 1:3, ami kizárja az $[Sn(OH)_4]^{2-}$ vagy magasabb hidroxido komplexek képződését. A komplex szerkezetét számos módszerrel vizsgáltuk. Mind a röntgen abszorpciós, mind a Raman spektroszkópiás mérésekből arra következtethettünk, hogy az ón(II) koordinációs száma három. A lehetséges szerkezetekre ($[Sn(OH)_3]^-$, ill. $[SnO(OH)]^-$) elméleti úton is kiszámoltuk a Raman spektrumokat. A mért és számolt Raman sávok csak a $[Sn(OH)_3]^-$ komplex esetében mutattak pontos egyezést, ami szintén ezen komplex képződését támasztja alá. A mért Raman spektrumok intenzitása a növekvő ón(II) koncentrációval követi a Lambert-Beer törvényt, vagyis az adott körülmények között csak egyetlen féle komplex képződik. Az $^{117}$Sn NMR spektroszkópiás vizsgálatok ugyanerre az eredményre vezettek. Az $[Sn(OH)_3]^-$ komplex szerkezet trigonális piramis, amelyben az EXAFS spektrumok alapján az átlagos Sn–O interatomos távolság 2,078 Å a hozzátartozó Debye-Waller faktor pedig 0,0038 Å$^2$. Az ón(II) lokális környezetét $^{119}$Sn Mössbauer spektroszkópiával is szerettük volna megvizsgálni mind gyorsfagyasztott oldatokban, mind pedig szobahőmérsékleten, kapilláris Mössbauer spektroszkópia segítségével. Az utóbbit azonban nem lehetett kivitelezni sem savas, sem lúgos oldatokban az ón(II) Lamb-Mössbauer faktorának jelentős hőmérsékletfüggése miatt, melynek következtében a spektrum még jóval az oldat olvadáspontja alatt eltűnik. Mindezt egy gyorsfagyasztott lúgos mintán végzett hőmérsékletfüggő méréssorozat alapján állapítottuk meg. Ezeken a gyorsfa-

gyasztott oldatmintákon felvett spektrumok szintén megerősítették a trigonális piramisos szerkezetet.

Az ón(II)-höz hasonlóan $d^{10}s^2$ vegyérték elektronszerkezetű ólom(II)-t szintén szisztematikusan megvizsgáltam. Ólom(II) esetén a komplex szerkezete nem volt meghatározható potenciometriásan a lúgos közegben mutatott korlátozott oldhatóság miatt. Az ólom(II) esetében is felvettük a lúgos oldatok Raman spektrumát, valamint kiszámoltuk a lehetséges részecskék ($[PbO(OH)]^-$, $[Pb(OH)_3]^-$, $[Pb(OH)_4]^{2-}$, valamint más, kevésbé valószínű részecskék) elméleti spektrumát is. A mért és számolt Raman sávok csak az $[Pb(OH)_3]^-$ esetében mutattak jó egyezést. A Raman spektrumok intenzitása, az ón(II)-höz hasonlóan, követte a Lambert-Beer törvényt, tehát ebben az esetben is elmondható, hogy egyetlen féle részecske van jelen kimutatható mennyiségben az erősen lúgos oldatokban. Az ólom $L_3$ élén végzett röntgen abszorpciós mérések szintén az előbb említett szerkezetet erősítették meg. Az EXAFS spektrumok és irodalmi adatok alapján az ólom(II) hármas koordinációjú, az átlagos Pb–O távolság 2,216 Å , a hozzá tartozó Debye-Waller faktor pedig 0,0330 $Å^2$.

Doktori munkám során kísérletileg igazoltam, és részletesen tanulmányoztam a króm(III) króm(VI)-tá történő spontán oxidációját, amelyet nem rég javasoltak az irodalomban. Az oxigén menetesített, változó kiindulási króm(III) és hidroxid koncentrációjú oldatok UV-látható spektrumát több, mint egy éven keresztül mértem. Az oxidációs reakció még teljesen oxigén mentes körülmények között is spontánnak bizonyult. A folyamat nagyon lassú, de sztöchiometrikus. Az átalakulás kinetikai görbéje három elkülönülő részre osztható. Az első két szakasz formális nullad-renddel jellemezhető (különböző meredekséggel), míg a harmadik leírható egy egyszerű exponenciális görbével. A reakciósebesség 6–8 M NaOH koncentráció körül maximumon megy keresztül, ami kvalitatíven magyarázható, ha feltételezzük, hogy a hidroxid és a $[Cr(OH)_4]^-$ ionok közötti másodrendű reakció a sebességmeghatározó lépés. Az aktuális sebességi együttható közelítően számolható a Davies korrekciót is tartalmazó kiterjesztett Debye-Hückel egyenlet segítségével, amely az ionerősség változásának hatását veszi figyelembe, valamint a Stokes-Einstein egyenlet segítségével, amely a viszkozitás változását írja le. A fentiek, valamint annak figyelembe vételével, hogy a mátrix rang analízis értelmében a rendszer négy független színes részecskét tartalmaz, egy nyolc lépéses mechanizmust javasoltunk. A kezdő lépés a hidroxid ion és a $[Cr(OH)_4]^-$ közötti reakció, és króm(IV) és króm(V) tartalmú intermediereken keresztül megy végbe.

Irodalmi adatok alapján a króm(III) 13-as, vagy nagyobb *p*H-n oligo-, ill polimer részecskék formájában van jelen, amely állítást néhány, savas közegű speciációval való analógiára alapoznak. Egy 8 M NaOH-ot és változó kiindulási króm(III) koncentráció oldatsorozat UV-látható spektrumát vettük fel közvetlenül az összeöntés után. A mátrix rang analízis eredményének értelmében a független színes részecskék kezdeti száma egy, ami azt jelenti, hogy csak egyetlen féle részecske van jelen szignifikáns koncentrációban. A nem-lineáris paraméterbecslés is ezt

az eredményt erősítette meg, ugyanis a legjobb illeszkedést az a modell szolgáltatta, amelyben csak a $[Cr(OH)_4]^-$ jelenlétét feltételeztük. További részecskék figyelembe vételével az illesztés már nem volt javítható. A különböző ideig öregített oldatokon (frissen készítettől 1 hónapig) XAS méréseket is végeztünk. Az összes EXAFS spektrum megegyezett a kísérleti hibán belül, függetlenül attól, hogy az oldat tartalmazott-e csapadékot, vagy sem. Az EXAFS spektrumok oligomer részecskék feltételezése nélkül is megilleszthetőek voltak, megerősítve, hogy a $[Cr(OH)_4]^-$ az egyetlen domináns részecske az oldatfázisban.

Habár az irodalomban az enyhén savas közegű speciáció szolgált analógiául a lúgos közegek vizsgálatához, ennek irodalma sem egységes, ezért ilyen körülmények között is végeztünk vizsgálatokat ($0 < T(OH^-)/T(Cr^{III} < 1$). Az oldatok $p$H-ját és UV-látható spektrumát több, mint egy éven át mértük. Az oldatok $p$H-ja az egyensúly eléréséig monotonan csökkent. Ezekben a reaktív rendszerekben a kiindulási $p$H érték a $[Cr(OH)]^{2+}$ és $[Cr(OH)_2]^+$ részecskék feltételezésével magyarázható, melyek stabilitási állandói a következők: $\lg\beta_1 = -4{,}28 \pm 0{,}03$, $\lg\beta_2 = -8{,}86 \pm 0{,}03$. Minden más részecske feltételezése rosszabb illesztést eredményezett, legalább ötször nagyobb átlagos eltéréssel. Az általunk kapott $\lg\beta_1$ érték gyakorlatilag megegyezik az irodalomi értékekkel, míg a $\lg\beta_2$ érték a $[Cr(OH)_2]^+$ képződés kisebb mértékét mutatja az irodalomban közöltekhez képest. Megállapítottuk, hogy a kinetikai változásokért a $[Cr(OH)]^{2+}$ és a $[Cr(OH)_2]^+$ közötti reakció a felelős. Kísérletileg igazoltuk, hogy a reakció minden lépése egyensúlyi, valamint, hogy a reakció végén az oldatok csak dimer részecskéket tartalmaznak, vagyis magasabb tagszámú oligomerek képződése kizárható. A dimerizációs reakció leírására egy hét lépéses mechanizmust javasoltunk. Az oligomerek képződésének kizárását EXAFS mérésekkel is megerősítettük. Az oldatok spektruma megilleszthető volt egyetlen Cr–Cr távolság feltételezésével, ami szintén arra utal, hogy csak dimer részecskék vannak jelen az oldatban.

# Acknowledgment

First of all I would like to say thanks to my supervisor, Pál Sipos for giving me the opportunity to be a member of the Material and Solution Structure Research Group and also for his help and teaching that I have received from him since I have started my BSc thesis work with him. I also would like to thank my supervisor Gábor Peintler for his immense support; theoretical, as well as practical help and patience that I have received from him during the years of my PhD studies. I wish to express my sincere thanks to István Pálinkó for his detailed review and excellent advices during my work and the preparation of this thesis.

Let me gratefully acknowledge the great help and kindness of Ilona Halasiné Varga and Erika Mityókné Bíró technicians.

Let me also gratefully acknowledge the efforts of Prof. Ingmar Persson for his valuable insights and suggestions regarding X-ray absorption spectroscopy.

Special thank goes to Eszter Czeglédi for her valuable co-work and friendship.

I would like to say thanks to all of my colleagues, specially to my 'roommates': Krisztián Csankó, Zsolt Ferencz, Attila Gácsi, Gábor Varga and Márton Szabados for the unique and incomparable atmosphere :-) . Our morning coffees will remain unforgettable.

Many thanks are due to Balázs Endrődi for his precious friendship and support.

Finally, but not least many thanks to my parents and grandparents being a very supportive, helpful and warm family behind me during my studies as well as my whole life.

# Bibliography


[1] Prytz, M. *Z. Anorg. Allg. Chem.* **1928,** *174,* 355–375.

[2] Randall, M.; Murakami, S. *J. Chem. Soc.* **1930,** *51,* 3967–3971.

[3] Garrett, A. B.; Heiks, R. E. *J. Chem. Soc.* **1939,** *61,* 3342–3344.

[4] Garrett, A. B.; Heiks, R. E. *J. Chem. Soc.* **1941,** *63,* 562–567.

[5] Gorman, M.; Leighton, P. A. *J. Chem. Soc.* **1942,** *64,* 719–720.

[6] Vanderzee, C. E.; Rhodes, D. E. *J. Chem. Soc.* **1952,** *74,* 3552–3555.

[7] Tobias, R. S. *Acta Chem. Scand.* **1958,** *12,* 198–223.

[8] Chia-chang, L.; Yu-ming, T. *Russ. J. Inorg. Chem.* **1964,** *9,* 785–732.

[9] Davies, C. G.; Donaldson, J. D. *J. Chem. Soc. A* **1968,** 946–948.

[10] Johansson, G.; Ohtaki, H. *Acta. Chem. Scand.* **1973,** *27,* 643–660.

[11] Mark, W. *Acta. Chem. Scand.* **1977,** *31A,* 157–162.

[12] Smrz, S. J. *Recl. Trav. Chim. Pays-Bas* **1925,** *44,* 580–590.

[13] Pettine, M.; Milero, J.; Macchi, G. *Anal. Chim.* **1981,** *53,* 1039–1043.

[14] Yamaguchi, T.; Lindqvist, O.; Claeson, T.; Boyce, J. B. *Chem. Phys. Lett.* **1982,** *93,* 528–532.

[15] v. Schnering, V. H. G.; Nesper, R.; Pelshenke, H. *Z. Anorg. Allg. Chem.* **1983,** *499,* 117–129.

[16] Dokic, D.; Zubova, B.; Veselinovic, D.; Durdevic, P. *J. Serb. Chem. Soc.* **1991,** *56,* 661–669.

[17] P.Djurdjevic,; Zelic, R.; Veselinovic, D. *J. Serb. Chem. Soc.* **1995,** *60,* 785–795.

[18] Donaldson, J. D.; Grimes, S. M.; Johnston, S. R.; Abrahams, I. *J. Chem. Soc. Dalton Trans.* **1995,** 2273–2276.

[19] Sébi, F.; Potin-Gautier, M.; Giffaut, E.; Donard, O. F. X. *Geochim. Chosmochim. Acta* **2001,** *65,* 3041–3053.

[20] Cigala, R. M.; Crea, F.; Stefano, C. D.; Lando, G.; Milea, D.; Sammartano, S. *Geochim. Chosmochim. Acta* **2012,** *87,* 1–20.

[21] Gamsjäger, H.; Gajda, T.; Saangster, J.; Saxena, S. K.; Voigt, W. OECD Publishing: Chemical thermodynamics of tin, 2012.

[22] Randall, M.; Spencer, H. M. *J. Am. Chem. Soc.* **1928,** *50,* 1572–1583.

[23] Garrett, A. B.; Vellenga, S.; Fontana, C. M. *J. Am. Chem. Soc.* **1939,** *61,* 367–373.

[24] Vlcek, A. A. *Chem. Listy.* **1954,** *48,* 1474–????

[25] Akselrud, N. V. *Russ. J. Inorg. Chem.* **1958,** *3,* 23–??

[26] Olin, Å. *Acta. Chem. Scand.* **1960,** *14,* 126–150.

[27] Pedersen, K. J. *Kgl. Danske Videnskab. Selskab. Mat.-fys. Medd.* **1945,** *22,* 10–.

[28] Faucherre, J. *Bull. soc. chim France* **1954,** *128,*.

[29] Olin, Å. *Acta. Chem. Scand.* **1960,** *14,* 814–822.

[30] Carell, B.; Olin, A. *Acta. Chem. Scand.* **1960,** *14,* 1999–2008.

[31] Heyrovsky, J. *Trans. Faraday. Soc.* **1924,** *19,* 692.

[32] Lingane, J. J. *Chem. Rev.* **1941,** *29,* 1.

[33] Goward, G. W. Doctoral thesis, Princeton University, 1954.

[34] Pajdowski, L.; Olin, A. *Acta. Chem. Scand.* **1962,** *16,* 983–991.

[35] Carell, B.; Olin, A. *Acta. Chem. Scand.* **1962,** *16,* 2350–2356.

[36] Johansson, G.; Olin, A. *Acta. Chem. Scand.* **1968,** *22,* 3197–3201.

[37] Pokric, B.; Pucar, Z. *J. Inorg. Nucl. Chem.* **1973,** *35,* 1987–1993.

[38] Baes, C. F.; Mesmer, R. E. Wiley: Hydrolysis of Cations, 1976.

[39] Sylva, R. N.; Brown, P. L. *J. Chem. Soc., Dalton Trans.* **1980,** 1577–1581.

[40] Cruywagen, J. J.; van de Water, R. F. *Talanta* **1993,** *40,* 1091–1095.

[41] Ferry, D.; Salvatore, F. *Ann. Chim.* **1989,** *79,* 1–??

[42] Fiore, M.; Orecchio, S.; Romano, V.; Ruggirello, G.; Zingales, R. *J. Chem. Soc., Dalton Trans.* **1996,** 4597–4603.

[43] Perera, N.; Hefter, G. T.; Sipos, P. *Inorg. Chem.* **2001,** *40,* 3974–3978.

[44] von Fricke, R.; Windhausen, O. *Z. Anorg. Allg. Chem.* **1924,** *132,* 273–288.

[45] Bradley, S. M.; Lehr, C. R.; Kydd, R. A. *J. Chem. Soc., Dalton Trans.* **1993,** 2415–2420.

[46] Rai, D.; Sass, B. M.; Moore, D. A. *Inorg. Chem.* **1987,** *26,* 345–349.

[47] Zhao, Z.; Rush, J. D.; Holcman, J.; Bielski, B. H. J. *Radiat. Phys. Chem.* **1995,** *45,* 257–263.

[48] Beverskog, B.; Puigdomenech, I. *Corr. Sci.* **1997,** *39,* 43–57.

[49] Torapava, N.; Radkevich, A.; Davydov, D.; Titov, A.; Persson, I. *Inorg. Chem.* **2009,** *48,* 10383–10388.

[50] Drljaca, A.; Spiccia, L. *Polyhedron* **1996,** *15,* 4373–4385 and references therein.

[51] Zydorczak, B.; May, P. M.; Meyrick, D. P.; Bátka, D.; Hefter, G. *Ind. Eng. Chem. Res.* **2012,** *51,* 16537–16543.

[52] Baloga, M. R.; Earley, J. E. *J. Am. Chem. Soc.* **1961,** *83,* 4906–4909 see Figure 1 therein.

[53] Bamberger, C. E.; Richardson, D. M.; Breding, M. A.; Cheng, K. *Science* **1975,** *189,* 715–716.

[54] Pettine, M.; Campanella, L.; Millero, F. J. *Environ. Sci. Technol.* **2002,** *36,* 901–907.

[55] Bjerrum, N. *Z. physik. Chem.* **1907,** *59,* 581.

[56] Lamb, A.; Fonda, G. R. *J. Am. Chem. Soc.* **1921,** *43,* 1154–1178.

[57] Schaal, R.; Faucherre, J. *Bull. Soc. Chim. Frane* **1947,** 927–932.

[58] Charreton, B. *Compt. Rend.* **1957,** 1208–1210.

[59] Emerson, K.; Graven, W. M. *J. Inorg. Nucl. Chem.* **1959,** *11,* 309–313.

[60] Morrow, J. I.; Levy, J. *J. Phys. Chem.* **1968,** *72,* 885–890.

[61] Rich, L. D.; Cole, D. L.; Eyring, E. M. *J. Phys. Chem.* **1969,** *73,* 713–716.

[62] Finholt, J. E.; Thompson, M. E.; Connick, R. E. *Inorg. Chem.* **1981,** *20,* 4150–4155.

[63] Stünzi, H.; Marty, W. *Inorg. Chem.* **1983,** *22,* 2145–2150.

[64] Stünzi, H.; Rotzinger, F. P.; Marty, W. *Inorg. Chem.* **1984,** *23,* 2160–2164.

[65] Rotzinger, F. P.; Stünzi, H.; Marty, W. *Inorg. Chem.* **1986,** *25,* 489–495.

[66] Stünzi, H.; Spiccia, L.; Rotzinger, F. P.; Marty, W. *Inorg. Chem.* **1989,** *28,* 66–71.

[67] Merakis, T.; Spiccia, L. *Aust. J. Chem.* **1989,** *42,* 1579–1589.

[68] Spiccia, L.; Marty, W. *Polyhedron* **1991,** *10,* 619–628.

[69] Spiccia, L.; Marty, W. *Polyhedron* **1991,** *10,* 1865–1872.

[70] Grace, M. R.; Spiccia, L. *Polyhedron* **1991,** *10,* 2389–2397.

[71] Crimp, S. J.; Spiccia, L.; Krouse, H. R.; Swaddle, T. W. *Inorg. Chem.* **1994,** *33,* 465–470.

[72] Drljaca, A.; Spiccia, L. *Polyhedron* **1995,** *14,* 1653–1660.

[73] Drljaca, A.; Spiccia, L. *Polyhedron* **1995,** *14,* 1653–1660.

[74] Drljaca, A.; Spiccia, L. *Polyhedron* **1996,** *15,* 4373–4385.

[75] Sipos, P.; May, P. M.; Hefter, G. T. *Analyst* **2000,** *125,* 955–958.

[76] Sipos, P. M.; Hefter, G.; May, P. M. *J. Chem. Eng. Data* **2000,** *45,* 613–617.

[77] Erdey, L. Tankönyvkiadó: Bevezetés a kémiai analízisbe, 1955.

[78] Gajda, T.; Sipos, P.; Gamsjager, H. *Monatsch Chem.* **2009,** *140,* 1293–1303.

[79] Sipos, P.; Hefter, G.; May, P. M. *Aust. J. Chem.* **1998,** *51,* 445–453.

[80] Sipos, P.; Schibeci, M.; Peintler, G.; May, P. M.; Hefter, G. *Dalton. Trans.* **2006,** *6,* 1858–1866.

[81] Thompson, A. C.; Attwood, D. T.; Gullikson, E. M.; Howells, M. R.; Kortright, J. B.; Robinson, A. L.; Underwood, J. H.; Kim, K.-J.; Kirz, J.; Lindau, I.; Pianetta, P.; Winick, H.; Williams, G. P.; and, J. H. S. Lawrence Berkley National Laboratory, University of California: X-ray Data Booklet, 2009.

[82] George, G. N.; Pickering, I. F. **1995,** EXAFSPAK - A suite of Computer Programs for Analysis of X-ray absorption spectra, Stanford Synchrotron Radiation Laboratory, Stanford, CA, 1995. http://www-ssrl.slac.stanford.edu/exafspak.html.

[83] Zabinsky, S. I.; Rehr, J. J.; Ankudinov, A.; Albers, R. C.; Eller, M. J. *J. Phys. Rev. B* **1995,** *52,* 2995–3009.

[84] Jalilehvand, F. *Structure of Hydrated Ions ond Cyanide Complexes by X-ray absorption Spectroscopy,* Doctoral thesis, Royal Institute of Technology, 2000.

[85] Bunker, G. Cambridge University Press: Introduction to XAFS, 2010.

[86] Burger, K.; Vértes, A. *Nature* **1983,** *306,* 353–354.

[87] Burger, K.; Vértes, A.; Zay, I. *Inorg. Chim. Acta* **1983,** *76,* 247–250.

[88] Burger, K.; Vértes, A.; Suba, M.; Dékány, I. *Inorg. Chim. Acta* **1985,** *100,* 17–21.

[89] Burger, K. *Spektrochim. Acta* **1987,** *43,* 1105–1110.

[90] http://www.corning.com/docs/specialtymaterials/pisheets/Vycor%207930.pdf, last visit: 2014/09/16.

[91] Vértes, A.; Nagy, D. L., Eds.; Akadémiai Kiadó: Mössbauer spectroscopy of frozen solutions, 1990.

[92] Klencsár, Z.; Kuzman, E.; Vértes, A. *J. Radioanal. Nucl. Chem.* **1996,** *201,* 105–118.

[93] Mössbauer Effect Data Center, http://www.medc.dicp.ac.cn/index.php, last visit: 2014/09/16.

[94] Mössbauer, R. L. *Z. Physik.* **1958,** *151,* 124–143.

[95] Greenwood, N. N.; Gibb, T. C. Chapman and Hall Ltd.: Mössbauer Spectroscopy, 1971.

[96] Frisch, M. J. *et al.* "Gaussian09 Revision D.01", Gaussian Inc. Wallingford CT 2009.

[97] Barone, G.; Silvestri, A.; Ruisi, G.; Manna, G. L. *Chem. Eur. J.* **2005,** *11,* 6185–6191.

[98] Krogh, J. W.; Barone, G.; Lindh, R. *Chem. Eur. J.* **2006,** *12,* 5116–5121.

[99] Kárpáti, S.; Szalay, R.; Császár, A. G.; Süvegh, K.; Nagy, S. *J. Phys. Chem. A* **2007,** *111,* 13172–13181.

[100] Zékány, L.; Nagypál, I.; Peintler, G. PSEQUAD for Chemical Equilibria, Update 5-5.10 2000-2008 (1987-2012).

[101] Peintler, G.; Nagypál, I.; Jancsó, A.; I. R. Epstein, K. K. *J. Phys. Chem. A* **1995,** *101,* 8013–8020.

[102] Peintler, G. ZITA, A Comprehensive Program Package for Fitting Parameters of Chemical Reaction Mechanisms, Versions 2.1-5.0, Department of Physical Chemistry, University of Szeged, Szeged, Hungary (1989-2012).

[103] Ocana, M.; Serna, C. J.; Garcia-Ramos, J. V.; Matijevic, E. *Solid State Ionics* **1993,** *63–65,* 170–177.

[104] Zuo, J.; Xu, C.; Liu, X.; Wang, C.; Wang, C.; Hu, Y.; Qian, Y. *J. Appl. Phys.* **1994,** *75,* 1835–1836.

[105] Huang, B. X.; Tornatore, P.; Li, Y.-S. *Electrochim. Acta* **2000,** *46,* 671–679.

[106] Nakamoto, K. John Wiley and Sons: Infrared and Raman Spectra of Inorganic and Coordination Compounds, 1997.

[107] Sherman, D. M.; Ragnarsdottir, K. V.; Oelkers, E. H.; Collins, C. R. *Chem. Geol.* **2000,** *167,* 169–176.

[108] Aberola, N. *Polyhedron* **1985,** *4,* 1853–1857.

[109] Flinn, P. A. North-Holland Publishing Company: X-ray Data BookletMössbauer Isomer Shifts, 1978.

[110] Cusack, P. A.; Smith, P. J.; Kroenke, W. J. *Polym. Degr. Stab.* **1986,** *14,* 307–318.

[111] Ichiba, S.; Takeshita, M. *Bull. Chem. Soc. Jpn.* **1984,** *57,* 1087–1091.

[112] Lippens, P. E. *Phys. Rev. B* **1999,** *60,* 4576–4590.

[113] Cook, P. S.; Cashion, J. D.; Cassidy, P. J. *Fuel* **1985,** *64,* 1121–1126.

[114] Cook, P. S.; Cashion, J. D.; Cassidy, P. J. *J. Chem. Soc., Faraday Trans.* **1975,** *71,* 461–472.

[115] Paris, R. V. Plenum Press: Structure and Bonding in Tin Compounds, 1984 and references therein.

[116] Ballard, J. G.; Birchall, T. *Can. J. Chem.* **1975,** *53,* 3371–3373.

[117] McDonald, R. C.; Hau, H. H. K.; Eriks, K. *Inorg. Chem.* **1976,** *15,* 762–765.

[118] Persson, I.; Sandström, M.; Yokoyama, H.; Chaudhryn, M. *Z. Naturforsch. Sect. A* **1995,** *50,* 21–37.

[119] Shannon, R. D. *Acta Cryst. A* **1976,** *32,* 751–767.

[120] Lundberg, D.; Persson, I.; Eriksson, L.; D'angelo, P.; Panfilis, S. D. *Inorg. Chem.* **2010,** *49,* 4420–4432.

[121] *Inorganic Crystal Structure Database*; FIZ Karlsruhe, 2013.

[122] Allen, F. H. *Acta Cryst. B* **2002,** *58,* 380–388.

[123] Persson, I.; Lyczko, K.; Lundberg, D.; Eriksson, L.; Placzek, A. *Inorg. Chem.* **2011,** *50,* 1058–1072 and references therein.

[124] Mudring, A.-V. Wiley-VCH Verlag: Inorganic Chemistry in Focus, III. ed., 2006 pages 15–28.

[125] Mudring, A.-V.; Rieger, F. *Inorg. Chem.* **2005,** *44,* 6240–6243.

[126] Walsh, A.; Watson, G. W. *J. Solid State Chem.* **2005,** *178,* 1422–1428.

[127] Mudring, A.-V.; Rieger, F. *Eur. J. Inorg. Chem.* **2007,** *Vol. 2007,* 882–890.

[128] Gonzalez, M. C.; Martire, D. O. *J. Chem. Res. (S)* **1997,** 54–55.

[129] Sunaryo, G. R.; Katsumura, Y.; Ishigure, K. *Radiat. Phys. Chem.* **1995,** *45,* 703–714.